Predicting Soil Expansion Force in Static Pipe Bursting Using Cavity Expansion Solutions and Numerical Modeling

by

Ka Hou Ngan

A thesis submitted in partial fulfillment of the requirements for the degree of

Master of Science

in
Construction Engineering and Management

Department of Civil and Environmental Engineering
University of Alberta

© Ka Hou Ngan, 2015

Abstract

The prediction of total pull force is critical to the design of static pipe bursting installation and soil expansion is the major component of the total pull force. However, there are currently limited methods available for its prediction. In this thesis, three cavity expansion solutions, namely Carter, Delft solution, and Yu and Houlsby, as well as numerical modeling using ABAQUS software, were used to predict soil expansion pressure acting upon the expander (bursting head) during static pipe bursting installation. The determined soil expansion pressures were then used to calculate the expansion force required for static pipe bursting with or without consideration of soil collapse due to crack propagation in pipe during expander's forward advancement. Calculations were then compared to results from laboratory static pipe bursting experiments to evaluate the feasibility of the prediction methods.

The comparison indicated that numerical and Yu and Houlsby solutions reasonably predicted the soil expansion force. Carter solution significantly overestimated the soil expansion force due to its small-strain assumption, while Delft solution moderately underestimated the results, as soil dilation was not considered. There was no significant difference between the results from numerical modeling and Yu and Houlsby solution due to the small scale of the experiments. However, Yu and Houlsby solution cannot capture the effects of depth of cover, initial borehole radius (only the radius ratio), and coefficient of lateral earth pressure.

A parametric study for numerical and Yu and Houlsby solutions was also conducted to examine the influence of depth of cover as well as different initial and final borehole radii on the calculated expansion force using typical underground condition in Edmonton, Alberta, Canada. The results revealed that, although the soil expansion force obtained from Yu and Houlsby solution is higher than that obtained from numerical modeling, the difference decreases when the depth of cover increases. It was found that the Yu and Houlsby solution can provide a conservative prediction with a discrepancy of less than 30% for typical condition in Edmonton.

Preface

All of the work contained in Chapters 3 and 4 was co-authored by Ka Hou Ngan, Yaolin Yi, Ali Rostami, and Alireza Bayat. Additionally, all of the work contained in Appendix A was co-authored by Ka Hou Ngan, Somayeh Nassiri, Alireza Bayat, and Siri Fernando.

Acknowledgements

I would like to express my deepest gratitude and appreciation to my supervisor Dr. Alireza Bayat for his fully support and guidance throughout the research, which could not have taken place without him.

I want to extend my sincere gratitude to Dr. Yaolin Yi and Mr. Ali Rostami for sharing valuable knowledge and reviewing my papers throughout my graduate study.

I wish to thank Mr. Siri Fernando, Mr. Aruna Sugathadasa, and Mr. Max Mao from the City of Edmonton for their assistance in field study of pipe bursting and data collection.

I would like to thank the Natural Sciences and Engineering Research Council of Canada (NSERC) and the City of Edmonton for their financial support.

Additionally, I wish to express special thanks to Ms. Lauren Wozny at Consortium for Engineered Trenchless Technologies (CETT) for her help with editing my papers as well as this thesis.

Finally, my sincere appreciation and gratitude go to my parents and all my family members for their moral and financial support throughout my graduate study.

Table of Contents

List of Tables

List of Figures

List of Symbols

Symbols	Description
a	Current borehole radius
$a_{elastic}$	Borehole radius at onset of yield
a_n	Borehole radius at n
a_n/a_0	Radius (expansion) ratio
a_{n+1}	Borehole radius at n+1
a_0	Initial borehole radius
A	Function of material properties
A_n	Surface area between n and $n+1$
A_{se}	Area of soil expansion
b	Plastic radius
B	Function of material properties
c	Soil cohesion
C	Function of A and B
C_b	Correction factor of breaking force
C_f	Correction factor of friction force
C_{se}	Correction factor of soil expansion force
d_{in}	Inside diameter of new pipe
d_{io}	Inside diameter of original pipe
d_n	Distance between n and $n+1$
d_{on}	Outside diameter of new pipe
d_{oo}	Outside diameter of original pipe

D	Pipe outside diameter
D_n	Final borehole diameter
DR	Dimension ratio
E	Young's (elastic) modulus
f_{np}	Number of pieces factor
f_{sel}	Soil expansion limit factor
F_b	Breaking force
$F_{b.exp}$	Experimental breaking force
F_{bh}	Horizontal (parallel) breaking force
F_{bn}	Normal breaking force
F_f	Friction force
F_h	Hoop force
F_p	Pull force
F_{pipe}	Average measured friction force per unit length
$F_{p.exp}$	Experimental pull force
F_{seh}	Horizontal (parallel) soil expansion force
F_{sen}	Normal (parallel) soil expansion force
F_{se}	Soil expansion force
$F_{se,exp}$	Experimental soil expansion force
G	Shear modulus
h	Depth of cover
K_0	Coefficient of lateral earth pressure at rest
L_{pipe}	New pipe's length at each pull stage
L_{os}	Length of oversize
L_{se}	Length of soil expansion
m	Factor to differentiate between cylindrical (m = 1) and spherical (m = 2) analyses
p	Current internal pressure

p'	Effective internal pressure
p_0	Initial stress field
p'_0	Effective initial stress field
p'_{max}	Maximum allowable pressure
p_Y	Yield pressure
p'_Y	Effective yield pressure
$P_{avg,n}$	Average expansion pressure between n and $n+1$
P_n	Expansion pressure at n
r	Radius to the point of interest after applying internal pressure
r_0	Radius to the point of interest before applying internal pressure
R	Cavity expansion ratio
$R_{g,max}$	Maximum borehole radius
$R_{p,max}$	Maximum plastic radius
S_n	Surface area of the new pipe
t	Pipe wall thickness
t_{po}	Pipe thickness of original pipe
T	Function of material properties
p_u	Initial in-situ pore pressure
U	Displacement
U_x	Horizontal displacement
U_y	Vertical displacement
UT_{avg}	Average displacement around borehole
$UT1_{shoulder}$	Horizontal displacement on the shoulder of borehole
$UT2_{bottom}$	Vertical displacement on the bottom of borehole
$UT2_{crown}$	Vertical displacement on the crown of borehole
W_e	Expander’s weight
W_n	New pipe’s weight

Y	Function of cohesion and friction angle
Z	Function of material properties
α	Function of friction angle
α_L	Load uncertainty factor
β	Function of dilation angle
γ	Function of material properties
δ	Function of material properties
$\Delta u_{elastic}$	Elastic displacement
$\Delta u_{plastic}$	Plastic displacement
Δx	Breaking length
ε_b	Tangential strain at the plastic radius
η	Function of material properties
θ_e	Apex angle of expander
θ_p	Slope angle of the original pipe
Λ_1	Infinite power series
μ	Function of dilation angle and cavity type
μ_{se}	Friction factor in soil-expander interface
μ_{sp}	Friction factor in soil-new pipe interface
ξ	Function of material properties
ν	Poisson's ratio
σ_{1e}	Ultimate failure stress of original pipe
σ_b	Radial stress at the elastic-plastic interface
σ_r	Radial stress
σ_θ	Tangential stress
φ_p	Pull force reduction factor
Φ	Friction angle
Φ'	Drained friction angle

Φ_{s-s}	Interface friction angle between the expander and the surrounding soil
χ	Function of material properties
Ψ	Dilation angle
ω	Function of friction angle and cavity type

Chapter 1: Introduction

1.1 Background

Underground pipelines are essential components to society, allowing potable water, gas and internet access to businesses and residents through water mains, gas lines, and telecommunication conduits, as well as sending sewage and storm water for treatment using sanitary and storm sewers. In many North American cities, buried utilities including pipelines have been in place for more than a century, functioning well beyond their anticipated service life (Plastics Pipe Institute, 2007; IPBA, 2012). Common issues found in existing pipeline systems are corrosion, joint leakage, depositions of minerals and debris, pipe burst, and water leakage and contamination (Plastics Pipe Institute, 2007). The corresponding repair and maintenance of these issues is costly.

Trenchless technology refers to a group of alternative underground construction methods that provide installation, rehabilitation or replacement of underground pipelines with minimal excavation and disruption to the ground surface. This innovative technology includes cured-in-place pipe (CIPP), horizontal directional drilling (HDD), microtunneling, pipe bursting (trenchless pipe replacement), and pipe jacking. Pipe bursting can be further categorized into two main types: pneumatic (dynamic) and static (hydraulic) methods. This thesis focuses only on the study of static pipe bursting technology.

1.2 Research Impetus

Pipe bursting is a trenchless technology used for the replacement of structurally deteriorated, aging, and undersized pipes. At present, selection of the pulling machine (hydraulic unit) capacity significantly relies on the contractor's past experience, rules of thumb, and manufacturer specifications without the quantification of pull force (Ariaratnam and Hahn, 2007;

Lapos et al., 2007; Nkemitag, 2007; Nkemitag and Moore, 2007). These methods result in numerous uncertainties due to variation in soil type, depth of cover, and pipe strength and size at different project sites. In fact, failure to drag new pipe in place due to insufficient pull force can have significant impact on the project delivery date, equipment, cost, and safety. Thus, it is necessary to understand and estimate the resistance force components (friction, breaking, and soil expansion forces) in a pipe bursting project to choose the appropriate construction machinery. Furthermore, it is important to develop a practical approach in predicting the expansion force. Laboratory measurements revealed that the expansion force is the major resistance force in static pipe bursting operations, and current methods for calculating it are limited.

1.3 Objectives and Methodology

As discussed previously, soil expansion force is the critical resistance force component influencing the magnitude of pull force. The main objective of this thesis is to use cavity expansion solutions and numerical modeling to develop a feasible approach for soil expansion force prediction in static pipe bursting installation. The methodology is summarized as follows:

- Cavity expansion solutions including Carter et al. (1986), Delft solution (Luger and Hergarden, 1988; Keulen, 2001), and Yu and Houlsby (1991) are used to calculate the soil expansion forces during static pipe bursting installation and are then compared to measured results for validation.
- Numerical modeling adopting finite element software, ABAQUS, is used to calculate the soil expansion forces during pipe bursting, which are then compared to measured results for validation. Additionally, a parametric study on expansion force using numerical

modeling and Yu and Houlsby (1991) solution is conducted to examine the influence of depth of cover and borehole upsizing using typical underground conditions in Edmonton.

1.4 Thesis Structure

This thesis is presented as follows:

- Chapter 1 – Introduction: In this chapter, a brief background on pipe bursting and the importance of quantifying soil expansion force are provided. In addition, methods to calculate this force are also briefly introduced.
- Chapter 2 – Literature Review: In this chapter, a review of pipe bursting and other rehabilitation methods is conducted and methods are compared. Additionally, this chapter continues to review past and current approaches to measure and determine resistance force components in pipe bursting. Furthermore, review of cavity expansion solution is also provided.
- Chapter 3 – Predicting Soil Expansion Force during Static Pipe Bursting Using Cavity Expansion Solutions: In this chapter, Carter et al. (1986), Delft, and Yu and Houlsby (1991) solutions are employed to investigate their feasibility in expansion force prediction. Furthermore, a comparison between calculated and measured results is conducted for validation and analysis.
- Chapter 4 – Application of Numerical Modeling to Predict Soil Expansion Force in Static Pipe Bursting: In this chapter, soil expansion force during static pipe bursting is predicted using finite element software, ABAQUS. The expansion force obtained from numerical solution is compared to results from Yu and Houlsby (1991) solution and actual measurements for validation and analysis. Furthermore, a parametric study on expansion force between numerical and Yu and Houlsby (1991) solutions examines the influence of

different depths of cover and initial and final borehole radii in static pipe bursting projects with underground conditions typical to Edmonton.

- Chapter 5 – Summary, Conclusions, and Recommendations: In this chapter, results obtained from cavity expansion and numerical solutions are summarized and highlighted. Furthermore, this chapter also examines the limitations of the proposed methods for calculating expansion force, and further topics are proposed for future research.

Chapter 2: Literature Review

2.1 Pipe Bursting History

Pipe bursting technology was initially developed and performed by D. J. Ryan & Sons Ltd. and British Gas for the replacement of three- and four-inch (~76 and 102 mm) cast iron gas mains in England in the late 1970s (Howell, 1995). At the time, a pneumatic pipe bursting system was employed using compressed air to drive cone-shaped expander (bursting head) forward. This innovative trenchless technique was patented in the United Kingdom and the United States in the 1980s until 2005 (Plastics Pipe Institute, 2007; IPBA, 2012).

When pipe bursting technology was first introduced, it was adopted only as a rehabilitation method for cast iron gas distribution lines. Over time, replacement of the water and sewer lines was implemented with pipe bursting (Plastics Pipe Institute, 2007). By 2006, this technology had been used to install approximately 14,500 km of polyethylene pipe (Plastics Pipe Institute, 2007). To date, pipe bursting has been used worldwide to replace various pipeline systems, including water, gas, and sewer lines (Plastics Pipe Institute, 2007).

2.1.1 Pipe Bursting System

Pipe bursting is categorized into two main basic types according to the method used to break the original pipe and the source of energy applied on the expander (Simicevic and Sterling, 2001; Plastics Pipe Institute, 2007; IPBA, 2012; Kazi, 2013). They are pneumatic (dynamic) and static (hydraulic). Selection of the appropriate bursting method depends significantly on subsurface conditions, degree of pipe upsizing, material types of the original and new pipes, length and depth of the pipeline, and the contractor's past experience in pipe bursting operations. This thesis focuses on static pipe busting.

In static (hydraulic) pipe bursting, a pulling rod assembly or cable attached to the expander drags it forward through application of tensile force from a pulling machine (hydraulic unit), as illustrated in Fig. 2.1. Since the expander is typically conical in shape, it transfers a horizontal (axial) pull force into a radial force. The pull force consists of cracking the original pipe into pieces, expanding the surrounding soil with the mixture of debris, and overcoming the friction force. As the original pipe material is ductile, a splitting wheel or cutting knives attached to the expander are typically used to break the pipe through longitudinal slitting (Plastics Pipe Institute, 2007; IPBA, 2012).

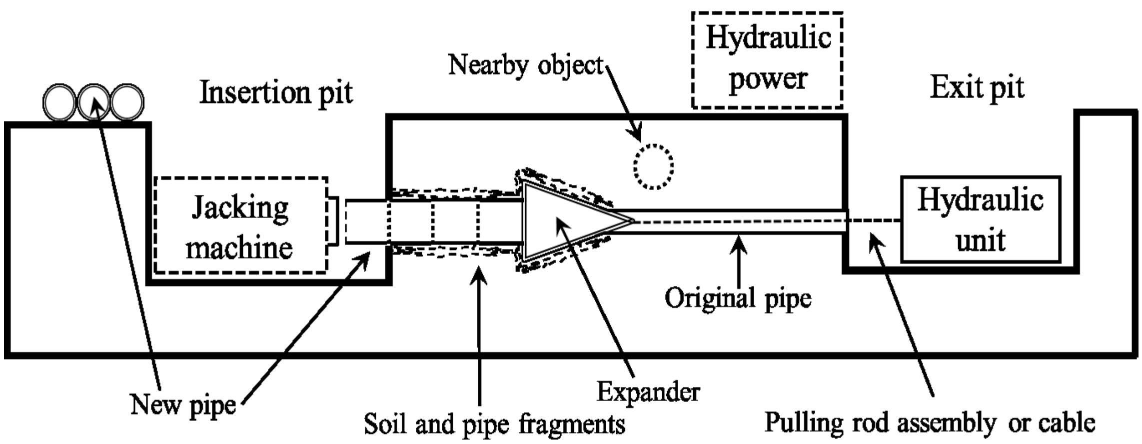

Fig. 2.1. Schematic layout of static pipe bursting

In static pipe bursting installation, sectional pipe is more practical for replacement in a limited or confined construction as opposed to continuous pipe. A hydraulic jacking machine located at the insertion pit is normally used to hold the sectional pipes and expander together during the pulling process, as shown in Fig. 2.1. Furthermore, the expander typically has a larger diameter compared to the original and new pipes to reduce friction between the new pipe and soil, creating a larger cavity for maneuvering the pipe.

2.1.2 Static Pipe Bursting Procedure

Static pipe bursting is the replacement of an original pipe through using a conical expander to fragment the pipe, and new pipe of equal or larger diameter is installed along in the original trajectory. To begin the procedure, an exit pit (machine pit) where the pulling machine is to be located and an insertion pit (entry pit) where new pipe is to be located require to excavation. A pulling rod assembly or cable passing through the original pipe makes a connection between the expander and pulling machine. As the conical expander is dragged by the machine through the original pipe, the expander shatters the pipe and forces its fragments out into the surrounding soil by means of radial force (Ariaratnam and Hahn, 2007). The process involves the initial cracking and fragmenting of the original pipe, with the expander pushing the surrounding soil and pipe fragments outwards to create a larger borehole. The new pipe attached to the expander is simultaneously installed as the expander advances along the same trajectory as the original pipe. This further reduces the potential for damage to nearby objects, such as adjacent utilities, during installation.

2.1.3 Comparison of Pipe Bursting to Other Rehabilitation Methods

Pipe bursting technology provides an economic pipe replacement alternative in place of traditional open cut methods and pipeline rehabilitation techniques. Specifically, pipe bursting is highly effective in deep depth of cover, replacement of low capacity pipeline, and pipe placed below groundwater table (Plastics Pipe Institute, 2007).

2.1.3.1 Pipe Bursting vs. Open Cut

Conventional open cut methods are typically the preferred option for pipe replacement or renewal when depth of cover is shallow and excavation does not have significant impacts on the surrounding environment. Issues associated with open cut projects such as road closures, restricted access to homes and businesses, and construction noise and dust make the method impractical and expensive, especially in urban areas.

Conversely, pipe bursting is advantageous in deep pipeline replacement. Deep open cut construction requires extra excavation, a larger lateral support system, and a greater dewatering system. During pipe bursting operations, full road closures are typically not required as the technology is "a type of subsurface construction work that requires little or no surface excavation and no continuous trenches" (IPBA, 2012). In open cut methods, the ground undergoes stress relief, which causes lateral ground movement and instability as excavation occurs. Furthermore, open cut construction typically cuts through road pavement structures, which requires new paving afterwards.

Studies conducted in the United States indicate that pipe bursting saves contractors an average of 25% on project costs, and has the potential of reaching cost-savings of up to 44% in comparison to open cut methods (Fraser et al., 1992). These findings were confirmed by Lee et al. (2007), who also found that the pipe bursting method is more cost-effective in comparison to open cut.

In conclusion, pipe bursting technology requires fewer indirect costs due to decreased traffic disturbance, shorter replacement duration, fewer interruptions to surrounding business/ residents, decreased environmental disturbance, and reduced surface paving costs (IPBA, 2012).

2.1.3.2 Pipe Bursting vs. Pipe Lining Method

Compared to pipe lining methods (i.e. cured-in-place pipe (CIPP) and slip lining), pipe bursting installation is a more favorable as the original pipe is structurally deteriorated and requires hydraulic capacity upgrade. Lining acts as an interior layer placed within the original pipeline to reduce further corrosion, to control leakage or spill, and to smooth fluid flow due to mineral and debris buildup in pipe, as illustrated in Fig. 2.2.

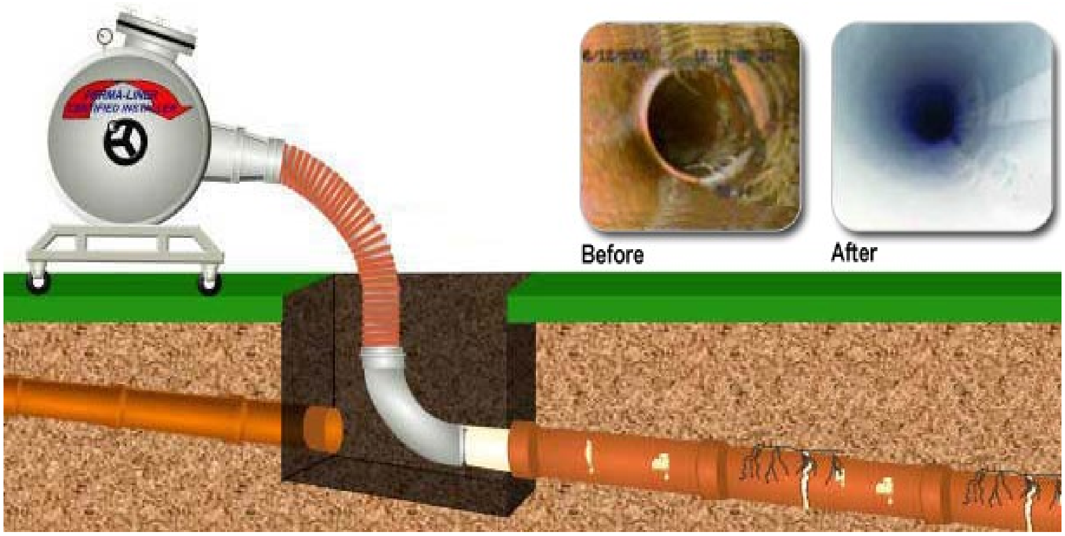

Fig. 2.2. Application of lining technology for pipe renewal (Express Plumbing & Rooter, 2013)

The main advantage of adopting lining technology over the pipe bursting method is that it requires limited to no access excavation to the pipeline. In fact, current lining technology does not have the ability to upsize existing underground pipelines and consequently cannot increase hydraulic capacity (Plastics Pipe Institute, 2007). Pipe bursting, in contrast, is practical in replacing an original pipe in size-for-size or upsizing projects with a new pipe in the original trajectory. This helps to increase the hydraulic capacity by replacing the old pipe with new pipe possessing a larger diameter. Furthermore, pipe bursting provides distinct cost advantage over pipe lining technology in two ways: 1) it addresses structural deterioration in the original pipe; and 2) it can accommodate additional hydraulic capacity.

2.1.4 Pipe Bursting Activity and Pipe Material

A survey of 886 pipe bursting projects conducted in North America from 2007 to 2010 indicate that pipe bursting was the most popular in the sanitary sewer market, followed by the potable water, storm sewer, and service laterals markets, as illustrated in Fig. 2.3 (Ariaratnam et al., 2014). The small percentage of service lateral projects can be attributed to the difficulty of funding and executing such projects, and the fact that lateral rehabilitation work is normally completed by plumbers rather than pipe bursting contractors (Ariaratnam et al., 2014).

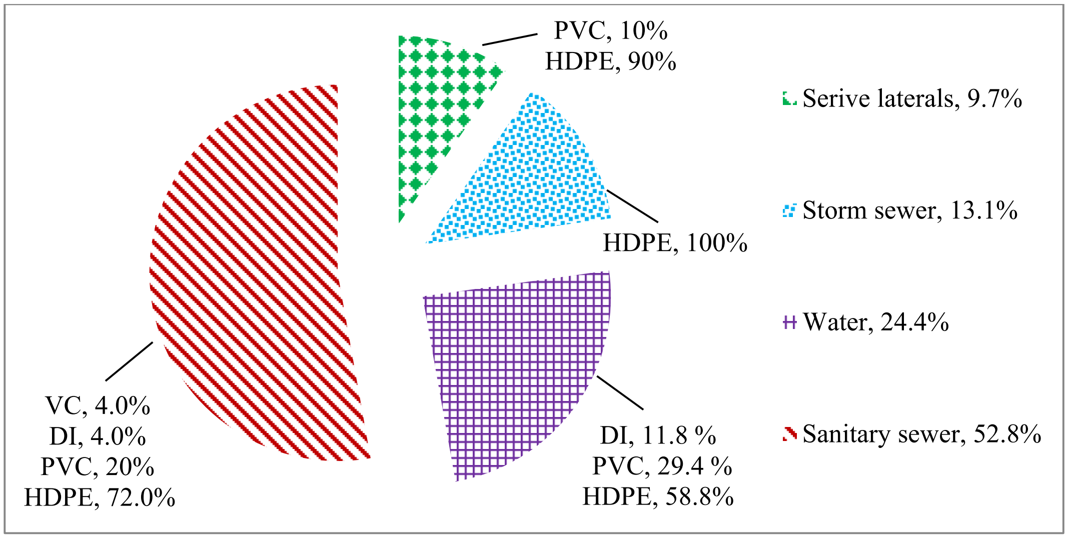

Fig. 2.3. Breakdown of pipe bursting activity by type of project and use of new pipe materials (reproduced from Ariaratnam et al., 2014)

For new pipe materials used in pipe bursting project, HDPE (high-density polyethylene) pipe was the most common material, followed by PVC (polyvinyl chloride), DI (ductile iron) and VC (vitrified clay) pipes, as depicted in Fig. 2.3. The high popularity of HDPE pipe can be attributed to its continuity, flexibility, and versatility over other pipe materials (Plastics Pipe Institute, 2007). HDPE pipe can be fused together in the field, is bendable for angled insertion, and is applicable to gas, water, and wastewater lines.

As indicated in a survey conducted by Ariaratnam et al. (2014), typical diameters of original and new pipes used in pipe bursting projects range from 150 to 300 mm and 200 to 375 mm respectively, as illustrated in Fig. 2.4. Additionally, pipe upsizing from 150 to 200 mm and 200 to 250 mm represents 70% of pipe bursting projects completed by the surveyed contractors.

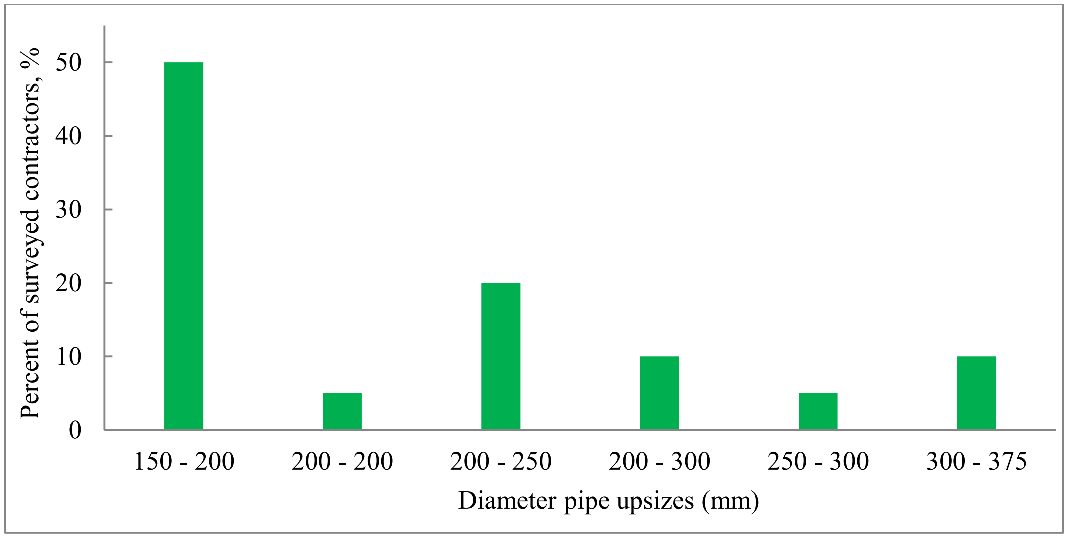

Fig. 2.4. Pipe upsizing in pipe bursting projects (reproduced from Ariaratnam et al., 2014)

2.1.5 Limitations of Pipe Bursting

IPBA (2012) has developed a system to classify the difficulty of pipe bursting projects. The rankings are A for routine, B for moderately difficult to challenging, and C for challenging to extremely challenging. A summary of the IPBA's pipe bursting classification system is shown in Table 2.1.

Table 2.1. IPBA pipe bursting classification (reproduced from IPBA, 2012)

Criteria	A - Routine	B - Moderately difficult to challenging	C - Challenging to extremely challenging
Burst depth (m)	< 3.7	3.7 - 5.5	> 5.5
Original pipe diameter (mm)	102 - 305	305 - 508	508 - 914
New pipe diameter	Size for size or one upsize in diameter	Two upsize in diameter	Three or more upsize in diameter
Burst length (m)	< 107	107 - 137	> 137
Soil	Compressible	Moderately compressible	Incompressible

The overall feasibility for a pipe bursting project depends significantly on the burst depth and length, diameters of the original and new pipes, and the subsurface soil conditions. As the burst depth increases, a larger lateral supporting system is necessary in insertion and exit pits to avoid soil collapse and improve trench stability. As sizes of the original and new pipes and burst length increase, the required pull force also increases as the friction force is proportional to the circumferential area and weight of the new pipe and installation length. Additionally, greater pipe upsizing requires greater soil expansion force to push soil and pipe fragments outwards. In Table 2.1, a size-for-size pipe replacement refers to replacing an original pipe with a new pipe having a similar inside diameter. A single-upsize, double-upsize and triple-upsize replacements refer to upsizing an original pipe with a new pipe by approximately one, two and three nominal sizes, respectively.

Most trenchless technologies, including pipe busting, are impractical when surrounding soil is impressible (i.e. hard clay, dense sand, and rock). These soil types hinder the expander's advancement, resulting in a significant increase in the required pull force and damages to the equipment and new pipe. In these situations, alternative rehabilitation methods, such as conventional open cut or lining technology, should be considered. Extra caution must also be taken during pipe bursting operations when any of the project's characteristics fall within category C of the IPBA's classification system.

Ariaratnam et al. (2014) conducted a survey of perceived risks associated with pipe bursting projects, as listed in Table 2.2. Pipe upsizing was found to have the highest perceived risk in pipe bursting operations. Meanwhile, change in original pipe conditions and adverse subsurface conditions were also identified as creating significant issues. Thus, a proper geotechnical investigation is the key in successful pipe bursting projects.

Table 2.2. Prioritization of perceived risks associated with pipe bursting projects (adapted from Ariaratnam et al., 2014)

Factors/conditions	Average rating (highest to lowest)
Upsizing more than 100% original diameter	9.7
Upsizing 50 - 100% original diameter	8.9
Bursting through bends in original pipe	7.4
Finding undocumented repairs to original pipe	6.3
Concrete encasement stalling bursting operation	5.9
Completing long burst lengths	5.4
Bursting through collapses of original pipe	5.1
Damaging adjacent utilities during the burst	5.1
Ground water affecting bursting operations	4.7
Surface heave damaging pavement/sidewalks	4.5
Changes in original pipe material affecting burst	4.4
Maintaining proper grade on gravity pipes	4.2
Original pipe originally installed in narrow trench	4.0
Bursting in clay or silt soils	3.9
Bursting in sand or gravel soils	3.5
Damaging new pipe during installation	3.4
Upsizing less than 50% original diameter	1.9

2.2 Pull Force during Pipe Bursting

2.2.1 Pull Force Components

Prediction of pull force is critical in pipe bursting design. Failure to install new pipe along the planned trajectory due to insufficient pull force from a pulling machine can cause significant impact to construction and safety. Pull force in static pipe bursting installation consists of three primary resistance force components, including breaking, friction, and soil (cavity) expansion forces (Ariaratnam and Hahn, 2007; Lapos et al., 2007; Nkemitag, 2007; Nkemitag and Moore, 2007; Bennett et al., 2011; Kazi, 2013). In order to successfully pull new pipe in place, the pull force must exceed all resistance force components.

Breaking force is the force required to fracture the original pipe into small pieces so that the expander and new pipe can pass through. This force magnitude, which is a function of hoop stress and internal pipe pressure for the original pipe, depends on the dimension and material strength and behaviour of the original pipe (Ariaratnam and Hahn, 2007; Nkemitag, 2007; Plastics Pipe Institute, 2007).

Friction force, which considers the weight of the new pipe and expander, is created from interfaces between the soil and new pipe, the soil and expander, and the pipe fragments and expander. It is also necessary to considering the arching effect in friction force at deep burial depths, where a further increase in the depth does not significantly affect the magnitude of overburden stress (Plastics Pipe Institute, 2007; Bennett et al., 2011).

Soil expansion force displaces the soil from the edge of the outside diameter of the original pipe to the edge of the outside diameter of the expander's tail end (Ariaratnam and Hahn, 2007; Nkemitag, 2007). This force expands the surrounding soil and pipe fragments outwards to create a larger borehole for the new pipe.

2.2.2 Experimental Studies

The majority of pipe bursting laboratory and field tests have been performed to examine and measure ground displacements associated with cavity expansion; however, a few tests have investigated resistance force components.

Lapos (2004) conducted six (only five included pull force measurements) static pipe bursting experiments in a 2-m wide, 2-m long and 1.6-m deep test cell filled with poorly graded sand with varying depths of cover and borehole sizes. Surface and transverse patterns of ground displacements, as well as forces of pull, breaking, and friction in the soil-new pipe interface were measured. Gaussian distribution adapting the work of Peck (1969) regarding tunneling was used to predict transverse patterns of ground displacements in static pipe bursting, presenting results agreeable to the experiments. A layout of one of the experiments and its schematic cross-section are illustrated in Figs. 2.5a and 2.5b, respectively.

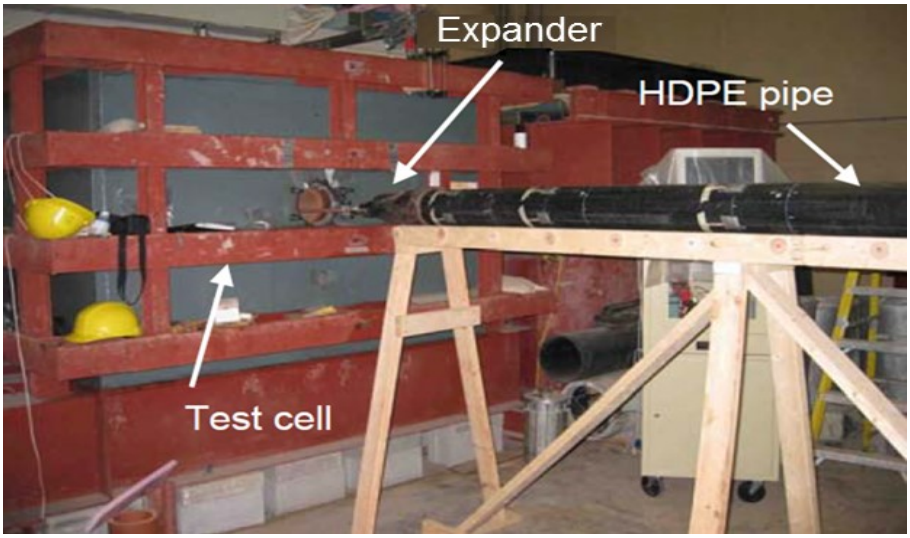

(a)

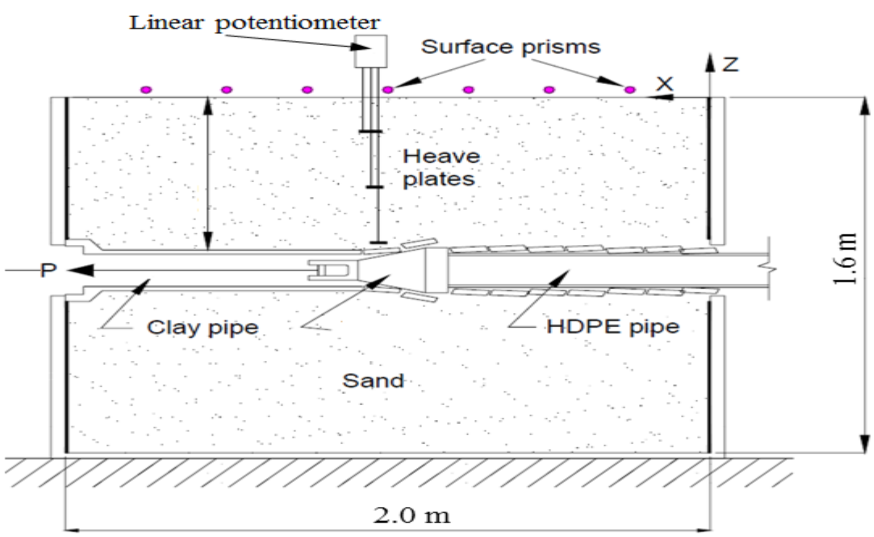

(b)

Fig. 2.5. Lapos' (2004) static pipe bursting experiment: (a) layout of the experiment; (b) schematic cross-section

In each experiment, a hydraulic pulling machine pulled the expander forward in 13 pull stages, each 250 mm in length. A load cell attached to a pulling rod was used to continuously record the pull force. The friction force developed along the soil-new pipe interface was recorded as the expander was completely pulled out of the test cell. The expander was supported by a steel bar in order to avoid inclusion of expander's weight in the friction measurement, as illustrated in Fig. 2.5a. The breaking force was measured aerially instead of in-soil.

Pull stages 1, 2, 8 and 9 should not be considered for comparison of the experimental and calculated soil expansion forces, since the expander entered the test cell during pull stage 2 and exited the test cell during pull stage 8. The average and maximum experimental pull forces for stages 3-7 ranging from 18.3 to 30.6 kN and 25.5 to 54.0 kN were recorded, respectively.

McLeod (2008) conducted two static pipe bursting field tests measuring the transvers and axial patterns of ground displacements in clayey soil. It was observed that ground displacements occurred vertically upward, lateral outwards, and axial forward as the expander advanced. The displacements diminished as the expander moved away from the point of interest.

Cholewa et al. (2009b) performed a static pipe bursting test in well graded sand and gravel within a test pit 8-m wide, 8-m long, and 3-m deep. The ground displacements and pull force were recorded. The maximum vertical ground displacement was observed to take place when the tail end of expander was advancing slightly beyond the point of interest. A layout and cross-section of the experiment are illustrated in Figs. 2.6a and 2.6b.

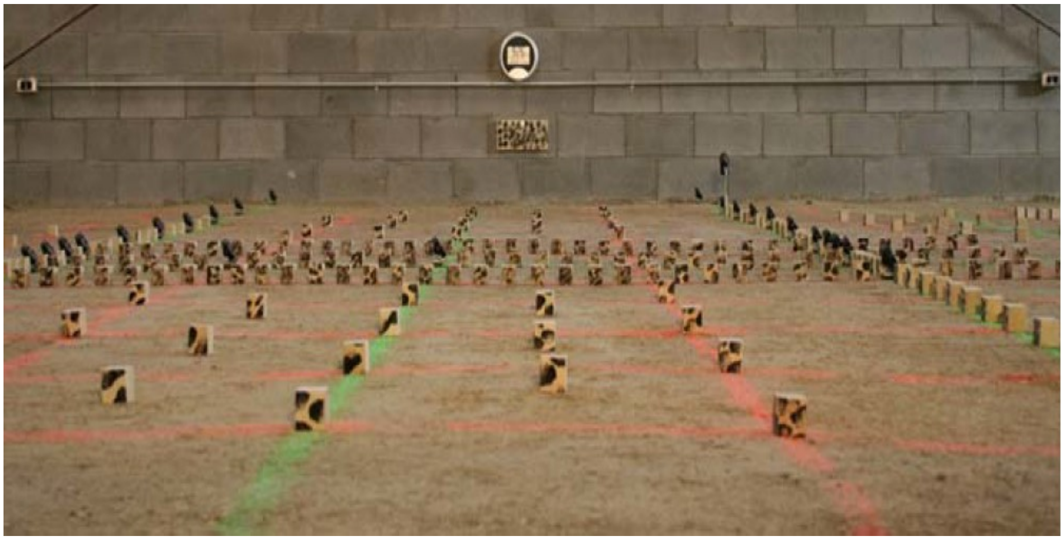

(a)

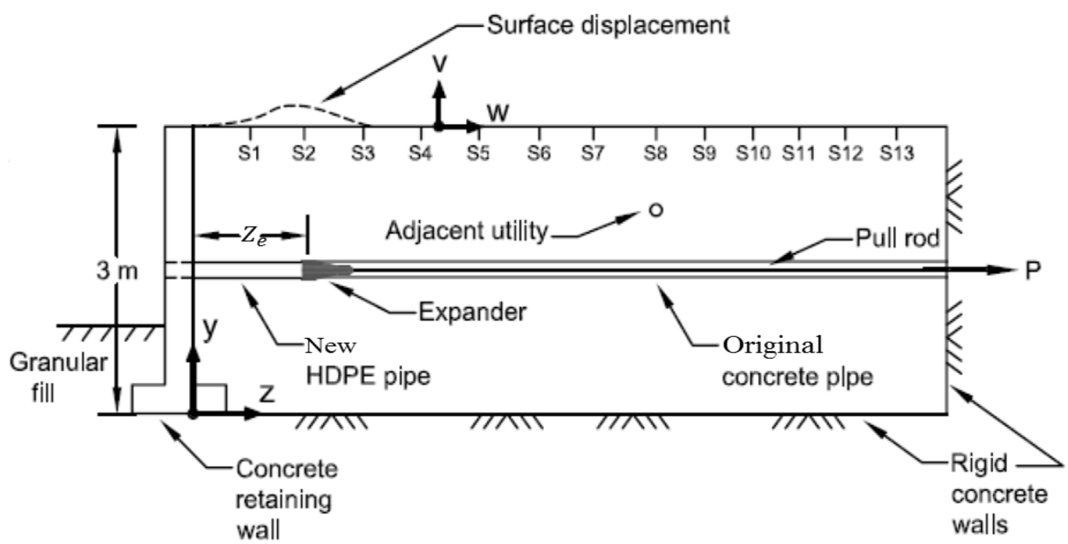

(b)

Fig. 2.6. Cholewa's et al. (2009b) static pipe bursting experiment: (a) layout of the experiment; (b) schematic cross-section

In Cholewa's et al. (2009b) test, a 0.202-m-diameter expander was used to break an unreinforced concrete pipe with an inside diameter of 0.153 m. This original pipe was buried 1.385 m below ground and was replaced with a high-density polyethylene pipe with an inside diameter of 0.168

m. Based on the measured pull force (F_p) versus expander location (Z_e) as illustrated in Fig. 2.7, the average and maximum pull forces were found to be 149 and 209 kN, respectively.

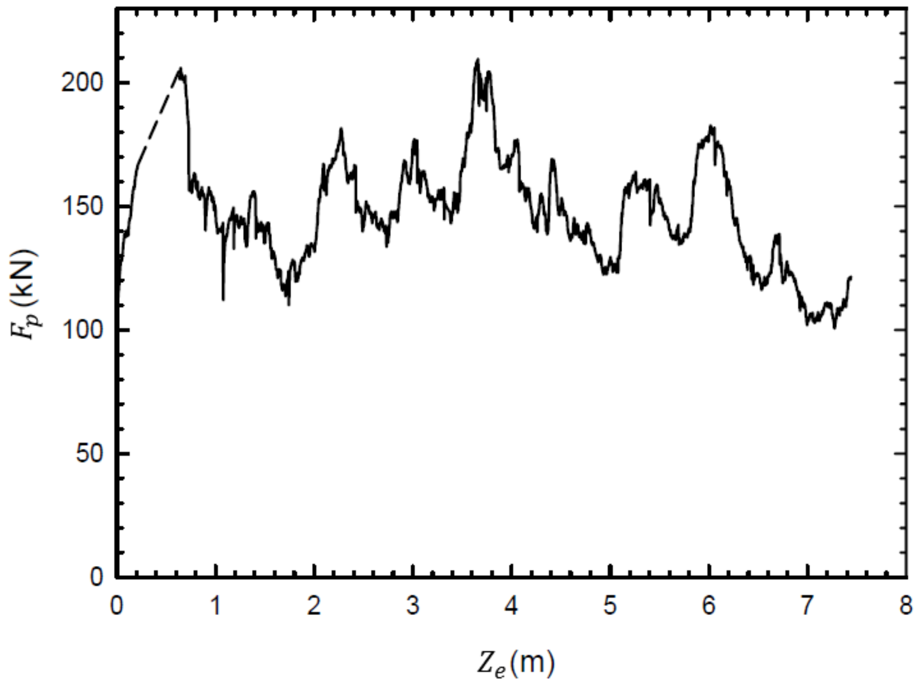

Fig. 2.7. Pull force versus expander location (Cholewa et al., 2009b)

The breaking force required to fracture the original pipe was approximately 20-50 kN due to fluctuation of the pull force caused by crack initiation and propagation in the pipe, as shown in Fig. 2.7. Furthermore, the friction force acting along the new pipe was measured to be 2 kN after the expander exited the porthole. Cholewa et al. (2009b) indicated that the largest resistance force component in their test was that required to create the cavity for the new pipe and expander and that required to move the expander forward.

Brachman et al. (2010) conducted a series of measurements on ground displacements for static pipe bursting experiments in stiff clay at varying depths. Axial forward, lateral, and vertical ground displacements as well as the impact of depth of cover on maximum surface displacement were measured and studied.

In 2012, the City of Edmonton conducted a static pipe bursting project for pipe replacement from 88th Street to the center of 90th and 91st Street along 127th Avenue in Edmonton, Alberta. The pipe bursting operation is illustrated below in Figs. 2.8a and 2.8b.

(a)

(b)

Fig. 2.8. The City of Edmonton pipe bursting project in 2012: (a) operation at insertion pit; (b) operation at exit pit

A 450-mm diameter vitrified clay pipe replaced a 300-mm diameter sanitary clay tile pipe along the same trajectory as the original pipe. The project length was appropriately 300 m with depth of cover varying from 4 to 6 m to accommodate glacial till. The project was divided into five different sections with various lengths. The maximum pull force was measured at 1900 kN with an average pull force of 1039 kN.

2.2.3 Numerical Modeling

Atalah et al. (1997) used FLAC3D to model ground displacements in a three-dimensional space through application of a uniform radial expansion within the borehole. The calculated ground displacements were not agreeable to the actual measurements. Greater downward movements below the pipe were obtained rather than higher upward movements due to free movements on the ground surface. Nkemitag (2007) and Nkemitag and Moore (2007) used two-dimensional finite software AFENA to model the longitudinal progression of the expander along the pipe axis in static pipe bursting. The details of numerical modeling are illustrated below in Fig. 2.9.

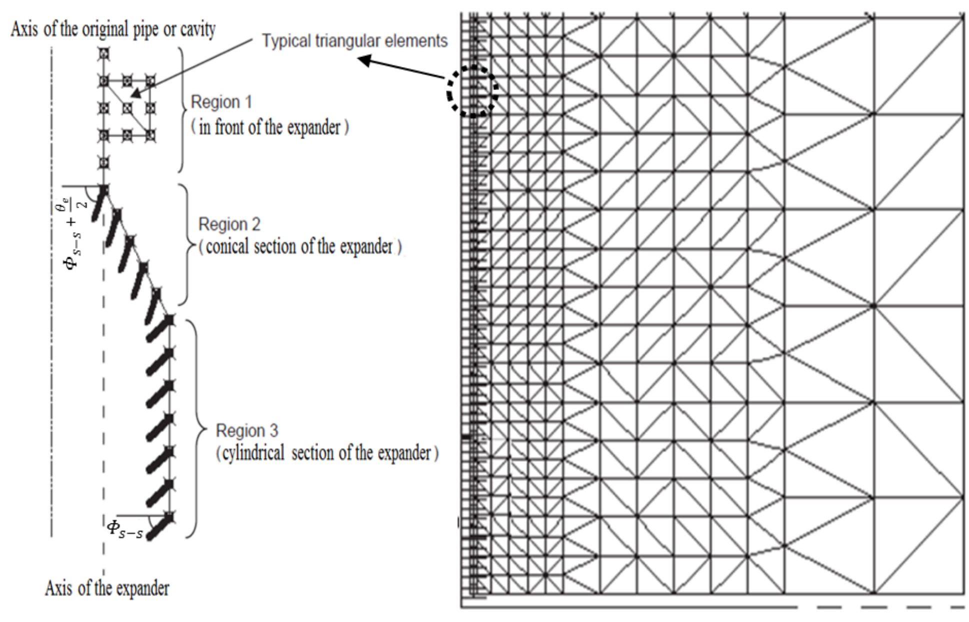

(a) (b)

Fig. 2.9. Details of numerical modeling: a) boundary conditions; b) mesh development (Φ_{s-s} and θ_e denote friction angle in steel-soil interface and expander's apex angle, respectively) (Nkemitag and Moore, 2007)

The soil properties used in numerical modeling were based on Lapos' (2004) tests. A mixed boundary condition using joint elements acting like linear spring was developed; the circle on Fig. 2.9b shows this boundary. Three regions were developed to consider the treatment of the moving boundary, as illustrated in Fig. 2.9a. As the expander advanced forward in the numerical model, the joint orientation changed to the appropriate angle considering an initial borehole radius of zero and a coefficient of lateral earth pressure of one, as illustrated in Fig. 2.9a. The boundary conditions and longitudinal progression of the expander in numerical modeling are illustrated in Fig. 2. 10.

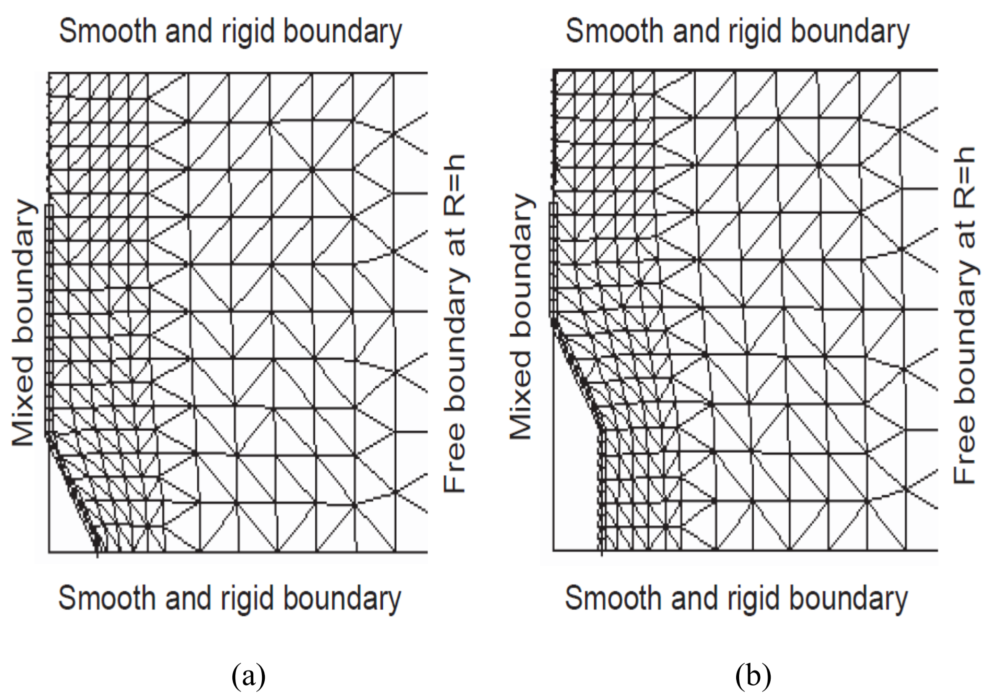

Fig. 2.10. Deformed mesh geometries illustrating longitudinal progression of expander: (a) conical part of expander within soil; (b) conical and cylindrical parts of expander within soil (Nkemitag and Moore, 2007)

Fig. 2.10a shows that the conical section of the expander was within the soil zone, meanwhile, Fig. 2.10b illustrates that the conical and cylindrical sections of expander were within the soil zone. This numerical simulation can be used to determine soil expansion as the expander advances. Furthermore, vertical ground displacements can be determined through application of a uniform radial internal pressure to the inner surface of an artificial stiff ring located within the borehole. The calculated soil expansion forces moderately overestimate the measured forces, with the calculated maximum displacements consistent with those measured.

Kazi (2013) used finite element software ABAQUS to estimate pull force and ground displacements for static pipe bursting in a three-dimensional space. Geometry, boundary conditions, and mesh size of the numerical model are illustrated in Fig. 2.11.

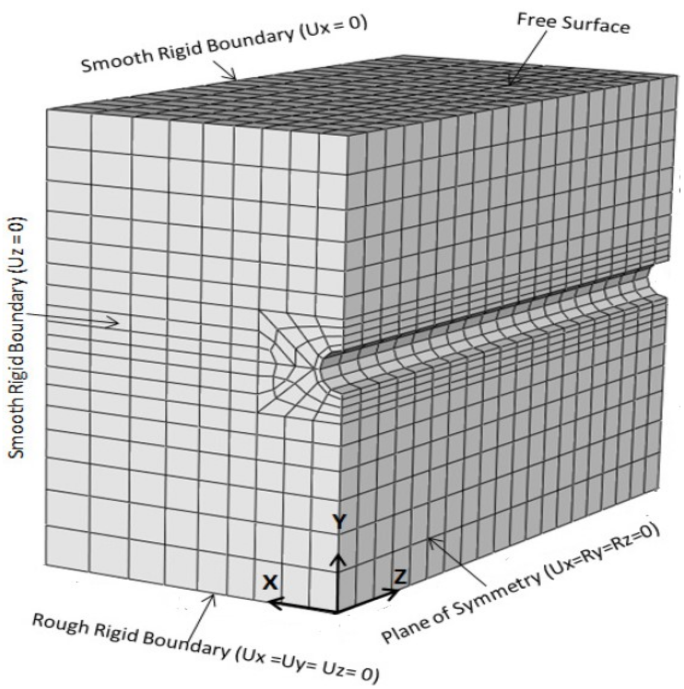

Fig. 2.11. Geometry, boundary conditions, and mesh size of the three-dimensional element model (Kazi, 2013)

The soil properties adopted in the numerical modeling and the size of numerical model were based on Lapos' (2004) tests. The master-slave interface model in ABAQUS was adopted to create a large body-to-body sliding movement in consideration of the expander-original pipe interaction during static pipe bursting. The expander, as well as the original and new pipe, was modeled as an analytical rigid body. The slope of the conical portion of the expander and the intersection between the expander and new pipe were modified differently than their actual geometries due to numerical instability. The axial displacements were set on the expander to simulate its longitudinal progression, and a coefficient of lateral earth pressure at rest was adopted to determine lateral earth pressure. This numerical modeling can stimulate pull force as well as axial, transverse, and maximum ground displacements in static pipe bursting. The calculated pull forces only reached to the lower bounds of the measured forces, with the calculated displacements consistent with those measured.

2.2.4 Pull Force Prediction

Ariaratnam and Hahn (2007) developed equations to determine resistance force components in static pipe bursting, namely friction, breaking, and soil expansion forces. A schematic layout of static pipe bursting with the corresponding resistance force components is illustrated in Fig. 2.12.

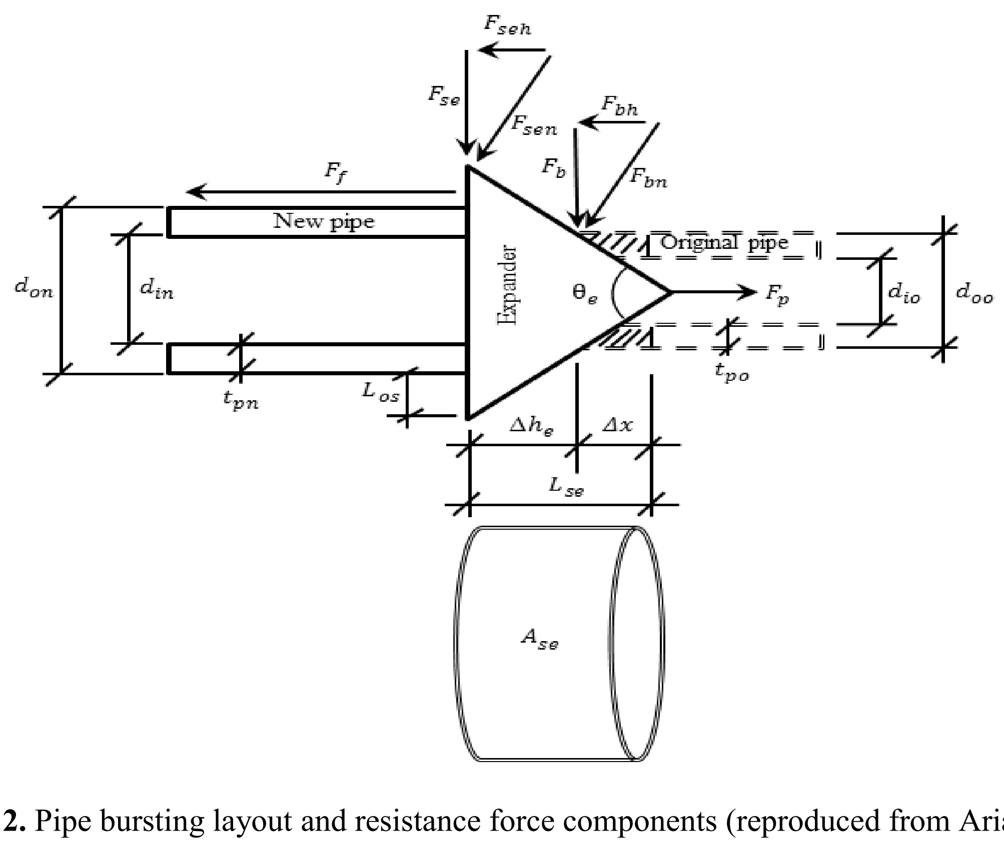

Fig. 2.12. Pipe bursting layout and resistance force components (reproduced from Ariaratnam and Hahn, 2007)

The friction force is primarily generated from the soil-new pipe interface considering the weight of the pipe and the overburden pressure acting on the pipe, neglecting the original pipe and expander in the calculation. In a lengthy installation, friction force typically governs the pull force due to the constructional length. Ariaratnam and Hahn (2007) proposed a theoretical model to estimate friction force (F_f) during static pipe bursting, see Equation 2.1.

$$F_f = \mu_{sp} \cos(\theta_p) (p_0 S_n + W_n) \tag{2.1}$$

Where μ_{sp} is the friction factor in the soil-new pipe interface, θ_p is the slope angle of the original pipe, p_0 is the soil pressure applied on the pipe, S_n is the outer surface area of the new pipe, and W_n is the weight of the new pipe.

The breaking force, which fragments the original pipe into smaller pieces, is a function of pipe hoop stress and internal pipe pressure. This force magnitude depends on the dimension, material strength, and behavior of the original pipe. The breaking force is:

$$F_{bh} = f_{np} \tan\left(\frac{\theta_e}{2}\right) F_h \tag{2.2}$$

where

$$F_h = \sigma_{1e} t_{po} \Delta x \tag{2.3}$$

Where F_{bh} is the horizontal breaking force, f_{np} is the number of pieces factor (which is equivalent to the number of cutting fins welded to the expander), θ_e is the angle of expander, F_h is the hoop force, σ_{1e} is the ultimate failure stress of original pipe, t_{po} is the pipe thickness of original pipe, and Δx is the breaking length (which is $10t_{po}$ based on suggestion from industry experience).

Soil expansion (compression) force enlarges the original borehole through pushing soil outwards during the expander's advancement. This equation is empirical due to the introduction of a soil expansion limit factor, which is applied to the expansion force to account for the extent of soil mobilization and parallel soil expansion force. This factor also considers that K_0 is not equivalent to one. This limit factor is obtained through comparison of measured soil expansion force to expansion equation. The force equation is expressed as follows:

$$F_{seh} = f_{sel}\, tan\left(\frac{\theta_e}{2}\right) cos\left(\theta_p\right) p_0 A_{se} \quad (2.4)$$

where

$$A_{se} = \pi(d_{on} + 2L_{os})L_{se} \quad (2.5a)$$

$$L_{se} = \Delta x + \Delta h_e \quad (2.5b)$$

$$\Delta h_e = [(d_{on}/2 + L_{os}) - (d_{oo}/2)]/\tan(\frac{\theta_e}{2}) \quad (2.5c)$$

Where F_{seh} is horizontal soil expansion force, f_{sel} is the soil expansion limit factor, A_{se} is the area of soil expansion, d_{on} is the outside diameter of the new pipe, L_{os} is the length of oversize, L_{se} is the length of soil expansion, and Δh_e is the exposed length of the expander.

Nkemitag (2007) defined a method to obtain experimental soil expansion force ($F_{se,exp}$) which was used to determine $F_{se,exp}$ in Lapos' (2004) tests. This expansion force is calculated by subtracting the experimental breaking force and friction force developed along the interfaces of soil-new pipe and soil-expander from the experimental pull force. The friction force developed between the soil and expander cannot be measured experimentally but can be estimated using the expander's weight and friction factor along the soil-expander interface. The formulae to determine $F_{se,exp}$ and the friction force are as follows:

$$F_{se.exp} = F_{p.exp} - F_f - F_{b.exp} \quad (2.6)$$

where

$$F_f = W_e(\mu_{se}) + L_{pipe}(F_{pipe}) \quad (2.7)$$

Where $F_{p.exp}$ is the experimental pull force, F_f is the friction force, $F_{b.exp}$ is the experimental breaking force, W_e is the expander's weight, μ_{se} is the friction factor in soil-expander interface, L_{pipe} is the length of new pipe at each pull stage, and F_{pipe} is the average measured friction force per unit length after the expander is completely out of test cell.

Bennett et al. (2011) indicated that pull force consists of the breaking force required to burst the original pipe, soil expansion force required to displace the surrounding soil, and friction force required to overcome friction between the soil and new pipe. A friction force equation for pipe bursting installations was proposed. In this equation, the force is a function of the size and length of the new pipe, the friction factor between the soil and pipe (μ_{sp}), and the overburden stress on the pipe. The equation is as follows:

$$F_f = \pi d_{on} L_{pipe} \mu_{sp} p_0 \tag{2.8}$$

The value of friction factor (μ_{sp}), which is dependent on soil type, pipe material, and presence of groundwater and lubrication, ranges from approximately 0.3 to 0.75 (Bennett et al., 2011). Coarse-grained soils (i.e. sand and gravel) typically have higher internal friction angles than fine-grained soils (i.e. clay and silt). Additionally, rough pipes (i.e. concrete and clay) have higher friction factors compared to smooth pipes (i.e. HDPE and PVC). This friction equation neglects to consider friction developed along the interfaces of soil-expander and soil-pipe fragments.

2.3 Cavity Expansion Solutions

Cavity expansion solution is a theoretical analysis and study to investigate the variations of stresses and deformations due to expansion and contraction in the cavity or borehole (Yu, 2000). Principally, the expansion process during pipe bursting can be simulated using cavity expansion solutions, such as those provided by Carter et al. (1986) and Yu and Houlsby (1991), as well as Delft solution. Fernando and Moore (2002) applied Yu and Houlsby (1991) solution to predict deformations within the plastic zone in pipe bursting and obtained result agreeable to experimental result. Hence, this indicates the possibility that cavity expansion solutions are applicable to soil expansion force prediction in static pipe bursting.

2.3.1 Introduction of Cavity Expansion Solutions

Cavity expansion solution was originally applied to metal indentation problems (Bishop et al., 1945; Hill, 1950). Hill (1950) provided a general solution for the finite expansion of a spherical cavity in a Tresca material. In his solution, the incremental velocity approach was adopted to consider time scale in the plastic radius and to determine the progress of deformations. Cavity expansion solution has been extensively used to solve geomechanics-related problems such as the explanation of cone penetration and pressuremeter tests, estimation of bearing capacity for driven piles, displacements for tunnels, and analysis of wellbore instability (Yu, 2000; Yu and Carter, 2002).

Small-strain definition in the plastic zone is applicable to interpretation of pressuremeter tests in sandy soils and determination of limit pressure solution for pile installation and bearing capacity of deep foundations (Carter et al., 1986). Vesic (1972) extended Hill (1950) solution to compressible soils by considering the volumetric strain as a finite value instead of zero, providing an approximate solution for limit pressures in spherical cavity expansion. Luger and Hergarden (1988) applied cavity expansion solution based on Vesic (1972) to evaluate the maximum allowable pressure in horizontal directional drilling (HDD) (Luger and Hergarden, 1988; Keulen, 2001; Bennett and Wallin, 2008; Staheli et al., 2010). Carter et al. (1986) derived an approximate solution to determine pressure-expansion relationships for cohesive-frictional and dilatant soils based on small-strain deformations in the plastic zone. It is widely used to apply the small- or engineering-strain assumption to traditional materials in which small deformations are allowed to occur. These analytical solutions mentioned above are based on small-strain analysis.

Large-strain definition in the plastic zone is a practical approach for prediction of pressure-expansion relation in dilatant soil (Yu and Houlsby, 1991). Chadwick (1959) proposed the total-strain approach in which plastic deformations consisted of elastic and plastic components, and stress-strain relationships can be represented between the Eulerian stresses and logarithmic strains in the plastic zone (Yu and Carter, 2002). This approach can be used to determine the spherical cavity expansion problems in Tresca and Mohr-Coulomb materials with the adoption of an associated flow rule. Bigoni and Laudiero (1989) solved the cavity expansion both analytically and by using numerical integration to address elastic deformations in the plastic zone. Yu and Houlsby (1991) extended Chadwick (1959) and considered the non-associated flow rule and Mohr-Coulomb criterion for dilatant behaviour in soils. The analytical solutions mentioned above are based on large-strain analysis.

2.3.2 Application of Cavity Expansion Solutions

Cavity expansion solution has been widely used to solve geomechanics-related problems such as in-situ soil testing, deep foundations, underground tunnels and excavations, and wellbore instability in the oil industry (Yu, 2000).

Pressuremeters, which are used to indirectly measure in-situ soil stiffness and strength, are installed in the ground through pushing, pre-boring, or self-boring methods. Self-boring pressuremeters are the least disruptive as a cutter on its tip creates a hole in the soil, similar to a tunneling machine, that fits the device exactly. Once a pressuremeter is in the soil, a uniform pressure is applied to the inside of the expandable flexible membrane, forcing it to press against the borehole wall. A curve of the cavity pressure-displacement relation can be obtained as a pressuremeter test is operated. The curve can then be used to back-calculate the mechanical soil properties such as soil stiffness and strength. The application of cylindrical cavity expansion solution has been considered to interpret self-boring pressuremeter tests (Clark, 1995). Cone penetrometers, which have a cone-shaped probe on the end of a series of rods, can be used to obtain soil profiles. As the probe is pushed into the ground at a constant speed, the sleeve friction on the outer surface of the rods and the cone tip resistance are measured. These measurements can be used to determine the type and strength properties of the soil. The application of spherical cavity expansion to predict the cone tip resistance in the cone penetration test is used commonly throughout the industry (Yu and Mitchell, 1998).

The applications of cavity expansion solution and the unloading of cavity from the initial stress field have been adopted to determine ground settlements caused by tunneling and to design tunnel support systems (Yu, 2000). The removal of soil and rock masses in underground excavation partially or totally affects the initial stresses in the soil medium, which reduces the normal stresses on the cavity. As internal pressure within the wall of the cavity is less than the shear or tensile strength of the surrounding soil, a failure zone develops around the cavity. Collapse of a tunnel in shallow excavations is assumed to happen as the plastic zone reaches the ground surface. At this point, the plastic flow becomes as it is no longer confined and restricted in movement (Caquot and Kerisel, 1966).

The cavity expansion and contraction solutions based on elastic, porous-elastic, and plastic models have been applied to consider wellbore instability. This involves reduction in borehole dimension due to the ductile yield of rock, enlargement in borehole dimension because of brittle rock rapture around the wellbore, and hydraulic fracture resulting from the presence of excessive mud pressure (Bradley, 1979; Santarelli et al., 1986; Wu and Hudson, 1991; Detournay and

Cheng, 1988; Woodland, 1990; Charlez and Heugas, 1991; Yu, 2000). Comparison of elastic stress field around the wellbore and the failure criterion for rock validates wellbore instability. The wellbore is considered unstable as the failure criterion is satisfied at any point in the rock (Yu, 2000).

Fernando and Moore (2002) applied cavity expansion solution developed by Yu and Houlsby (1991) to predict displacements within the plastic zone and compared the calculated result to experimental pipe bursting results obtained by Atalah et al. (1997). A 0.394-m-diameter expander was used to fracture a vitrified clay pipe with a diameter of 0.203 m. This original pipe was buried 1.829 m below ground and was replaced with a new HDPE pipe with a diameter of 0.324 m. An underground displacement at 0.305 m above the original pipe's centerline was measured using a heave plate. Experimental and calculated results were agreeable.

2.4 Research Motivations

As discussed previously, few studies have investigated the pull force in pipe bursting, especially in terms of the soil expansion force. The aforementioned friction and breaking equations can be used to evaluate the corresponding force components. The soil expansion force is particularly complicated to determine since it is not easily measureable as a separate value. Current methods used to obtain this force magnitude are completed through the subtraction of the breaking and friction forces from the measured pull force. In addition, expansion force has been found to have the greatest impact in static pipe bursting experiments compared to other resistance forces (Lapos, 2004; Cholewa et al., 2009b). Thus, it is important to develop a feasible approach to predict expansion force in order to properly estimate pull force in static pipe bursting. Cavity expansion solution has been applied to determine displacements within the plastic zone and has yielded agreeable results. It is worthwhile to investigate the practicability of using the solution to determine the soil expansion force. Furthermore, numerical modeling is also adopted to determine soil expansion force due to limitations in cavity expansion solutions, which includes assumptions of infinite soil medium, constant field stress, coefficient of lateral earth pressure of one, and no boundary conditions.

Chapter 3: Predicting Soil Expansion Force during Static Pipe Bursting Using Cavity Expansion Solutions[1]

3.1 Introduction

Static pipe bursting is a trenchless technology used to replace structurally deteriorated and undersized pipelines (Lueke et al., 2001; Chapman et al., 2007; Ariaratnam et al., 2014). This technology provides an economical pipe replacement alternative to traditional open cut method and other pipeline rehabilitation techniques; it decreases traffic intervention, leads to construction time-savings, reduces disruption to surrounding businesses and communities, and lowers environmental impact (Rogers and Chapman, 1995; Brachman et al., 2007; Lapos et al., 2007; Plastics Pipe Institute, 2007; Cholewa et al., 2009a, 2009b; Shi et al., 2013). Static pipe bursting replaces an original (old, existing, or host) pipe with a new (replacement) pipe of equal or larger diameter within the original trajectory through the application of a tensile force to a conical expander (bursting head). The expander is attached to a pulling cable or rod assembly that passes through the original pipe. It converts an axial (horizontal) pull force into a radial force to fragment the original pipe and create a cavity for the new pipe, as schematically shown in Fig. 3.1.

[1] A version of this chapter has been submitted to ASCE International Journal of Geomechanics. Authors: Ka Hou Ngan, Ali Rostami, Yaolin Yi, and Alireza Bayat.

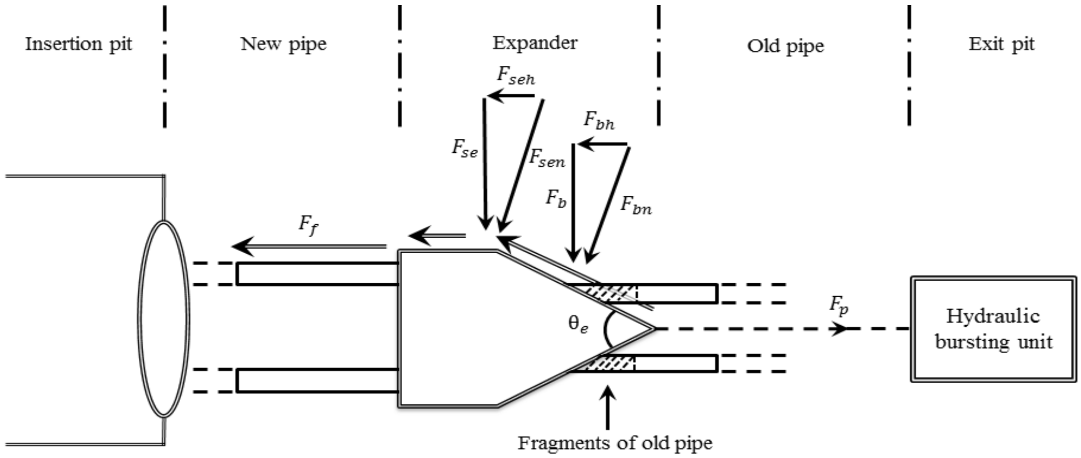

Fig. 3.1. Schematic layout of pipe bursting installation and the corresponding resistance force components (F_f, F_{se}, F_b, and F_p denote the forces of friction, soil expansion, breaking, and pull, respectively. The subscripts of h and n represent forces in horizontal and normal directions, respectively) (adapted from Ariaratnam and Hahn, 2007)

Failure to install a new pipe in the planned trajectory due to insufficient pull force from a pulling machine can significantly impact construction and safety. At present, selection of the capacity of pulling machine is mainly based on the contractor's past experience, rule of thumb, and manufacturer specifications without quantification of pull force (Ariaratnam and Hahn, 2007; Lapos et al., 2007; Nkemitag, 2007; Nkemitag and Moore, 2007). The pull force must exceed all resistance forces, which primarily consist of breaking, friction, and soil expansion forces, as illustrated in Fig. 3.1. The breaking force is the force required to fragment the original pipe, and its magnitude depends on the dimension, material strength, and behavior of the original pipe (Ariaratnam and Hahn, 2007; Nkemitag, 2007; Plastics Pipe Institute, 2007). Friction force is created from the interfaces between the soil and new pipe, the soil and expander, and the original pipe fragments and expander, considering the weights of the expander and new pipe, and the overburden pressure (Nkemitag, 2007; Chehab and Moore, 2010; Bennett et al., 2011). Soil expansion force is the force required to displace the soil from the edge of the outside diameter of the original pipe to the edge of the outside diameter of the expander (Lapos et al., 2004; Ariaratnam and Hahn, 2007; Nkemitag, 2007).

Previous laboratory tests have been conducted to investigate the resistance force components in static pipe bursting (Lapos, 2004; Cholewa et al., 2009b). Lapos (2004) conducted experiments in a 2-m wide, 2-m long and 1.6-m deep test cell filled with poorly graded sand, while Cholewa et al. (2009b) conducted a test in well graded sand and gravel within a test pit of 8-m wide, 8-m long, and 3-m deep. Results from these laboratory tests indicated that the largest resistance force component during static pipe bursting was the soil expansion force required to create a cavity for the expander. Ariaratnam and Hahn (2007) proposed an empirical method to estimate the soil expansion force considering the apex angle of the expander, overburden stress, and influence area of the soil expansion force. A soil expansion limit factor is used in this method; however, this factor must be obtained through comparison of experimental or field soil expansion forces to soil expansion equation. Additionally, this method does not consider soil characteristics. Numerical simulation has also been adopted to predict soil expansion force and pull force and in static pipe bursting, presenting results agreeable to experimental results (Nkemitag, 2007; Nkemitag and Moore, 2007; Kazi, 2013). However, numerical simulation is generally complicated for practical design.

Principally, the expansion process during pipe bursting can be simulated using cavity expansion solutions such as those provided by Carter et al. (1986) and Yu and Houlsby (1991), as well as Delft solution (Luger and Hergarden, 1988; Keulen, 2001). Fernando and Moore (2002) applied Yu and Houlsby (1991) solution to predict deformations within the plastic zone in pipe bursting and obtained results that were agreeable with experimental result. Hence, in this paper, three cavity expansion solutions, including Carter et al. (1986), Delft, and Yu and Houlsby (1991) solutions, were investigated to predict the internal (expansion) pressure acting upon the expander during static pipe bursting operation. The soil expansion pressure was then used to calculate the required expansion force. Finally, results from laboratory pipe bursting experiments conducted by Lapos (2004) were used to evaluate the feasibility of these methods.

3.2 Prediction of Soil Expansion Force during Pipe Bursting

The following section introduces Carter et al. (1986), Delft, and Yu and Houlsby (1991) cavity expansion solutions, as well as how the soil expansion pressure during pipe bursting is calculated. The cylindrical cavity expansion solution is used, as the transverse length of the borehole is relatively small compared to its longitudinal length. Internal pressure for the calculations is obtained based on the pressure needed to expand the borehole from the initial radius to a new radius. A consistent set of notations is adopted in the three solutions for comprehension and comparison.

3.2.1 Cavity Expansion Solutions

3.2.1.1 Carter et al. (1986) Solution

A small-strain analysis in dilatant elastic-plastic soils with the Mohr-Coulomb yield criterion considering non-associated flow rule are used in Carter et al. (1986) solution. The soil medium is assumed to have an infinite size to neglect boundary effects. The initial borehole radius is a_0, and geostatic pressure p_0 is considered isotropic, acting throughout the soil medium independent of gravity, as illustrated in Fig. 3.2. The internal pressure of the cavity increases to p slowly to avoid dynamic effects. The convected part of the stress rate is neglected in the solution. Plane-strain analysis is used to model cavity expansion, and, as a general assumption, compression positive is also adopted in the solution. Radial stress is the major principal stress, while tangential stress is the minor principal stress with a negative value. The soil is modelled as an elastic-perfectly plastic medium; therefore, it has an elastic behavior and complies with Hooke's law before yielding. As the internal pressure exceeds the yield pressure, the total displacement in the plastic zone is the summation of elastic displacement $\Delta u_{elastic}$ at onset of yield in the elastic zone and plastic displacement $\Delta u_{plastic}$ in the plastic zone. The total displacement in the plastic zone can be expressed as follows:

$$a = a_0 + \Delta u_{elastic} + \Delta u_{plastic} \tag{3.1}$$

Where a and a_0 are the current and initial borehole radii respectively.

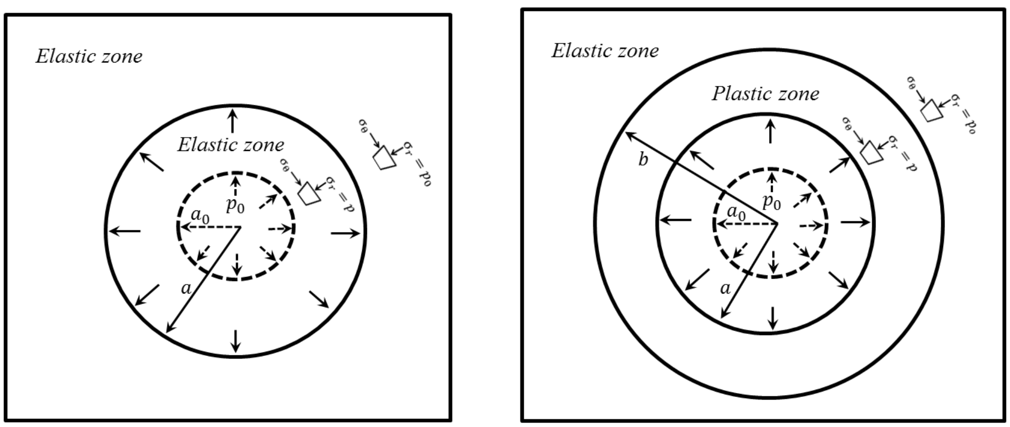

(a) (b)

Fig. 3.2. Cavity expansion in an infinite medium showing pressure-expansion relation: (a) pure elastic zone development ($p \leq p_Y$); (b) plastic zone development ($p > p_Y$)

Yield plastic stress takes place between the initial radius a_0 and the plastic radius b when the internal pressure exceeds the yield pressure. Based on Mohr-Coulomb yield criterion, the distribution of radial stress within the plastic zone is given by:

$$\frac{\sigma_r}{\sigma_b} = \left(\frac{r}{b}\right)^{\omega-1} \tag{3.2}$$

where

$$\omega = 1 - m\left(\frac{\alpha-1}{\alpha}\right) \tag{3.3a}$$

$$\sigma_b = \frac{1+m}{\alpha+m} \alpha(p_0 + c \ \cot \Phi) - c \ \cot \Phi \tag{3.3b}$$

$$\alpha = \frac{1+sin\,\phi}{1-sin\,\phi} \tag{3.3c}$$

where σ_r is the radial stress, σ_b is the radial stress at the elastic-plastic interface, r is the radius to the point of interest after applying internal pressure, ω is the function of friction angle and cavity type, m is the factor to differentiate between cylindrical (m = 1) and spherical (m = 2) analyses, α is the function of friction angle, p_0 is the initial stress field, c is the soil cohesion, and Φ is the friction angle.

Considering the distribution of radial stress, constitutive relation in the plastic zone, radial displacement in the outer elastic zone at the elastic-plastic interface, and boundary conditions, the expression of pressure-expansion for small deformations in the plastic zone is as follows:

$$\frac{\Delta u_{plastic}}{a_0} = \varepsilon_b [A(\frac{p+c\cot\phi}{\sigma_b+c\cot\phi})^{\gamma} + B\left(\frac{p+c\cot\phi}{\sigma_b+c\cot\phi}\right) + C] \tag{3.4}$$

where

$$\varepsilon_b = \frac{\alpha-1}{\alpha+m} \frac{p_0+c\ \cot\Phi}{2G} \tag{3.5a}$$

$$A = \frac{T}{1+\mu} \tag{3.5b}$$

$$\gamma = \frac{\alpha(\beta+m)}{m(\alpha-1)\beta} \tag{3.5c}$$

$$B = \frac{-Z}{1-\omega} \tag{3.5d}$$

$$C = 1 - A - B \tag{3.5e}$$

$$T = (m+1)(1 + \frac{m\chi}{\mu+\omega}) \tag{3.5f}$$

$$\chi = \frac{m(1-\mathrm{v}) - m\mathrm{v}(\alpha+\beta) + [(m-2)\mathrm{v}+1]\alpha\beta}{[(m-1)\mathrm{v}+1]\alpha\beta} \tag{3.5g}$$

$$\mu = \frac{m}{\beta} \tag{3.5h}$$

$$\beta = \frac{1+\sin\Psi}{1-\sin\Psi} \tag{3.5i}$$

$$Z = (m+1)\frac{m\chi}{\mu+\omega} \tag{3.5j}$$

where ε_b is the tangential strain at the plastic radius, A, B, γ, χ, and Z are the functions of material properties, C is the function of A and B. G is the shear modulus, T is the function of material properties, μ is the function of dilation angle and cavity type, v is the Poisson's ratio, β is the function of dilation angle, and Ψ is the dilation angle,

In Carter et al. (1986) solution, the stress and displacement before yield were not defined. In this case, cavity expansion of a thick-walled cylinder developed by Timoshenko et al. (1970) is used to consider stress and displacement in the elastic zone. The solutions of stress and displacement for a cylindrical cavity in an infinite medium before yield are:

$$\sigma_r = p_0 + (p - p_0)(\frac{a}{r})^2 \tag{3.6}$$

$$\sigma_\theta = p_0 - (p - p_0)(\frac{a}{r})^2 \tag{3.7}$$

$$u = \frac{p-p_0}{2G}(\frac{a}{r})^2 r \tag{3.8}$$

where p is the current internal pressure, σ_θ is the tangential stress, and u is the displacement.

Distribution of stresses and displacement at the onset of yield can be obtained from equations (3.6)–(3.8) by replacing r with the summation of a_0 and $\Delta u_{elastic}$ and replacing p with p_Y. Elastic displacement at the onset of yield $\Delta u_{elastic}$ and yield pressure p_Y can be expressed as follows:

$$\Delta u_{elastic} = \frac{(p_Y - p_0)}{2G}(a_0 + \Delta u_{elastic}) \tag{3.9}$$

$$p_Y = \frac{m[Y + (\alpha - 1)p_0]}{m+\alpha} + p_0 = 2mG\delta + p_0 \tag{3.10}$$

where

$$Y = \frac{2c\cos\phi}{1-\sin\phi} \tag{3.11a}$$

$$G = \frac{E}{2(1+\upsilon)} \tag{3.11b}$$

$$\delta = \frac{Y+(\alpha-1)p_0}{2(m+\alpha)G} \tag{3.11c}$$

where Y is the function of cohesion and friction angle, δ is the function of material properties, and E is the Young's modulus.

For pipe bursting operations, the total displacement is generally high compared to the elastic displacement for same-size or upsizing pipe replacements. This causes the internal pressure to expand the cavity greater than the yield pressure. The total displacement in the plastic zone is a cumulative displacement and consists of elastic and plastic displacement components as mentioned above. Therefore, it is necessary to first determine the elastic displacement at onset of yield from equation (3.9) and the plastic displacement from equation (3.1). The internal pressure p in the plastic zone can then be obtained from equation (3.4) after the plastic displacement is determined. As $\Delta u_{elastic}$ is higher than the radius difference between a_0 and a, it indicates that soil medium around the cavity wall undergoes elastic deformations and that the internal pressure does not exceed the yield pressure. In fact, the expansion does not necessarily initiate from the original pipe radius, since the soil collapses into the original pipe due to potential crack propagation during the advancement of expander. This demonstrates that initial borehole radius is not necessarily equivalent to the original pipe radius.

3.2.1.2 Delft Solution

Luger and Hergarden (1988) first introduced cavity expansion solution based on Vesic (1972) solution to evaluate maximum allowable pressure p'_{max} in the borehole during horizontal directional drilling. The method became widely accepted within the industry and was later named Delft solution. In industrial practice, internal pressure is typically controlled to stay below p'_{max} at any location along bore path to prevent hydraulic fracture. Delft solution adopts a small-strain analysis in the plastic zone, uses tension positive, and neglects soil dilatancy. As depicted in Fig. 3.3, p'_{max} in Delft solution is derived from the intersection of Lines A and B (Keulen, 2001).

Line B in Fig. 3.3 represents total radial stresses versus radial distance outside the borehole. When the expansion pressure reaches p'_{max}, the corresponding plastic radius is the maximum plastic radius $R_{p,max}$. Radial stress is the effective yield pressure p'_Y at the elastic-plastic interface $R_{p,max}$. Within the plastic zone, radial stress gradually decreases as distance from the borehole increases. As radial stress reaches to the boundary of the maximum borehole radius $R_{g,max}$, the corresponding stress is p'_{max}. This is why Line B slopes downward. Line A in Fig. 3.3 represents internal pressure in borehole versus borehole radius. For Line A, the increase in the effective internal pressure leads to an increases in the borehole radius. As the effective internal pressure reaches to the p'_{max}, the corresponding borehole radius is $R_{g,max}$ where Lines A and B intersect.

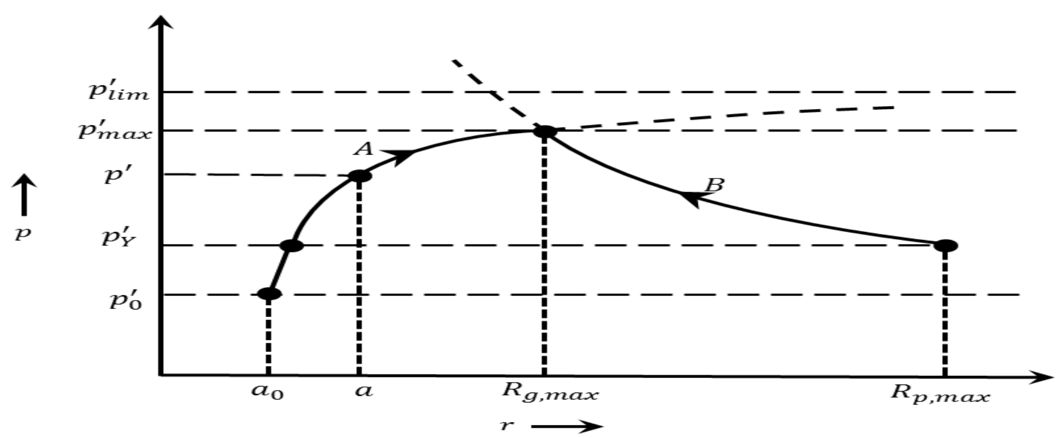

Fig. 3.3. Expansion pressure within borehole versus borehole radius (Line A) and total radial stresses versus radial distance outside borehole (Line B) (reproduced from Keulen, 2001)

The expression of pressure-expansion relation below p'_Y in Fig. 3.3 is as follows:

$$a^2 = a_0^2[1 - (\frac{p' - p'_0}{G})]^{-1} \quad (3.12)$$

The borehole radius before yield lies in between the initial borehole radius and the borehole radius at onset of yield, as shown in Fig. 3.3. The yield pressure is determined based on the Mohr-Coulomb failure criteria as follows:

$$p_Y = p'_0(1 + \sin\phi) + c\cos\phi + p_u \quad (3.13)$$

where p_u is the initial in-situ pore pressure.

With the substitution of yield pressure into equation (3.12), the consideration of no volume change in the plastic zone, and the use of volume circle ring, the new borehole radius can be expressed as a function of the initial borehole radius and the plastic radius:

$$a^2 = a_0^2 + b^2(\frac{p'_0 \sin\phi + c\cos\phi}{G}) \quad (3.14)$$

The equation of p'_{max} at the intersection of Lines A and B is shown as follows:

$$p'_{max} = [p'_0(1 + \sin\phi) + c\cos\phi + c\cot\phi] * [(\frac{a_0}{Rp,max})^2 + \frac{p'_0 \sin\phi + c\cos\phi}{G}]^{\frac{-\sin\phi}{1+\sin\phi}} - c\cot\phi$$

(3.15)

In order to use Delft solution for evaluation of expansion pressure in the plastic zone during pipe bursting, the plastic radius b must be replaced with $R_{p,max}$. The effective internal pressure requires for expanding soil in the plastic zone from initial to new boreholes, so equation (3.15) must be revised as follows:

$$p' = [\sigma'_0(1 + \sin\phi) + c\cos\phi + c\cot\phi] * [(\frac{a_0}{b})^2 + \frac{p'_0 \sin\phi + c\cos\phi}{G}]^{\frac{-\sin\phi}{1+\sin\phi}} - c\cot\phi$$

(3.16)

Equation (3.14) can be used to determine the plastic radius, while equation (3.16) is the final equation used to determinate effective internal pressure exceeding effective yield pressure during pipe bursting.

Deformations below the failure criterion are infinitesimal in Delft solution, since Hooke's Law is applied in the displacement equation of the elastic zone. During pipe bursting operations, cavity expansion due to the advancement of expander is typically high. This causes that effective internal pressure within the borehole to exceed the effective yield pressure, and a plastic zone forms around the cavity. As mentioned above, equation (3.16) calculates the effective internal pressure after the onset of yield. As effective internal pressure is below effective yield pressure, equation (3.13) can be used to confirm whether effective internal pressure exceeds effective yield pressure. If the effective internal pressure does not exceed effective yield pressure, the soil medium remains elastic and equation (3.12) can be used to find the effective internal pressure with known initial and new borehole radii.

3.2.1.3 Yu and Houlsby (1991) Solution

Large-strain analysis in the plastic zone and tension positive are adopted in Yu and Houlsby (1991) solution, and all other assumptions remain the same as those found in the Carter et al. (1986) solution. Internal pressure p exceeds yield pressure p_Y based on the Mohr-Coulomb yield criterion, which is shown in equation (3.10).

When the internal pressure does not exceed the yield pressure, the soil medium around the cavity wall is considered to be purely elastic. Equation (3.17) calculates the displacement between a point of interest before and after applying internal pressure, while equation (3.8) calculates the displacement in the elastic zone u. These equations can be used to determine the internal pressure in the elastic zone.

$$u = r - r_0 \tag{3.17}$$

where r_0 is the radius to the point of interest before applying internal pressure.

An expression for large-strain within the plastic zone can be reached by considering logarithmic strain and stress components. A solution for the pressure-expansion relation can be determined by integrating the large-strain expression in the plastic zone and considering initial and new borehole radii. The solution is as follows:

$$\frac{a}{a_0} = \left(\frac{R^{-\gamma}}{(1-\delta)^{\frac{\beta+m}{\beta}} - \frac{\gamma}{\eta} \Lambda_1(R,\xi)} \right)^{\frac{\beta}{\beta+m}} \tag{3.18}$$

$$\Lambda_1\,(R,\xi) = \textstyle\sum_{n=0}^{\infty} A_n^1 \tag{3.19}$$

$$A_n^1 = \begin{cases} \frac{\xi^n}{n!} ln(R) & if\ n = \gamma \\ \frac{\xi^n}{n!(n-\xi)} [R^{n-\gamma} - 1] & Otherwise \end{cases} \tag{3.20}$$

where

$$R = \frac{(m+\alpha)[Y+(\alpha-1)p]}{\alpha(1+m)[Y+(\alpha-1)p_0]} \tag{3.21a}$$

$$\eta = exp\{\frac{(\beta+m)(1-2\upsilon)[Y+(\alpha-1)p_0][1+(2-m)\mathrm{v}]}{E(\alpha-1)\beta}\} \tag{3.21b}$$

$$\xi = \frac{[1-\mathrm{v}^2(2-m)](1+m)\delta}{(1+\upsilon)(\alpha-1)\beta} \left[\alpha\beta + m(1-2\mathrm{v}) + 2\mathrm{v} - \frac{m\upsilon(\alpha+\beta)}{1-\upsilon(2-m)}\right] \tag{3.21c}$$

where R is the cavity expansion ratio, γ , η and ξ are the functions of material properties, and Λ_1 is the infinite power series.

When replacing r_0 with a_0 and r with a in equation (3.17) and substituting equations (3.10) and (3.17) into (3.8) as shown below in equation (3.22), borehole radius at onset of yield $a_{elastic}$ can be obtained to compare with the expander radius. For static pipe bursting, the expander typically has a higher diameter compared to original and new pipe diameters to reduce friction between new pipe and surrounding soil and create space for maneuvering the pipe (Plastics Pipe Institute, 2007). If the expander radius is larger than $a_{elastic}$ in equation (3.22), it implies that internal pressure exceeds yield pressure, and vice versa.

$$\frac{a_{elastic} - a_0}{a_{elastic}} = \frac{p_Y - p_0}{2G} \tag{3.22}$$

As the internal pressure exceeds the yield pressure, a plastic zone will develop around the cavity wall creating a plastic radius. With the use of equations (3.18) and (3.21a), the internal pressure p in the zone requiring expansion can be obtained.

3.2.2 Calculation of Expansion force for Static Pipe Bursting

Since the expander has a conical shape, the expansion pressure acting upon the expander varies longitudinally due to the varying of radius ratio (a_n/a_0). Hence, the expander is discretized into several sections, and the average expansion pressure acting upon each is calculated using cavity expansion solutions. Ideally, the initial cavity radius a_0 is the original pipe radius, and the greatest final radius is that of the expander. However, as the expander advances, cracks in the original pipe tend to propagate from the contact point between the expander and the pipe. This may cause soil collapse around the failure pieces (pipe fragments), especially in cohesionless soils, which alters the borehole of the original pipe to smaller dimensions. This study uses two expansion force calculation methods (Methods A and B) without and with consideration of soil collapse. In Method A, which does not consider soil collapse, the initial borehole radius a_0 is the original pipe radius and the expander is discretized longitudinally, as shown in Fig. 3.4a. For Method B, the soil collapse occurs and the length of the failure piece Δx shown in Fig. 3.4b represents the breaking length of the original pipe, which is highly dependent on pipe material, thickness, and condition, as well as overburden stress, soil type, and so on (Ariaratnam and Hahn, 2007). As determining the exact size of the collapse zone is complicated, Ariaratnam and

Hahn (2007) concluded that Δx is typically 10 times greater than the original pipe thickness according to industry experience; their conclusion has been adopted in this paper.

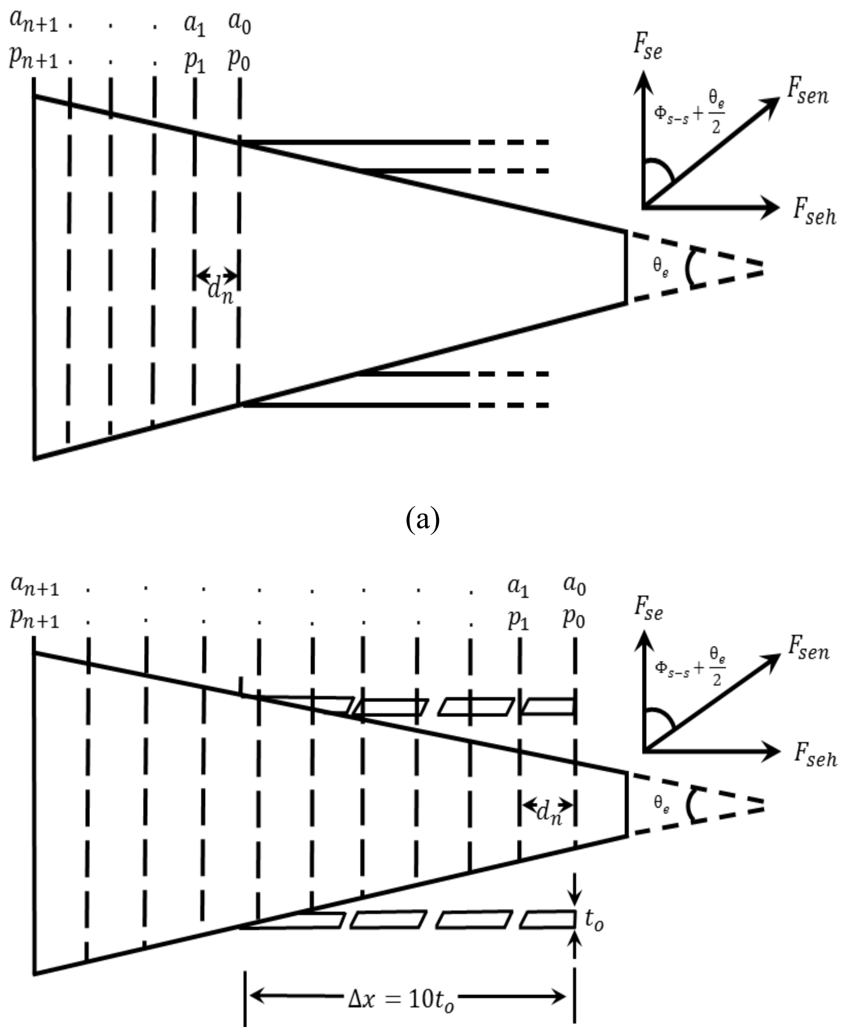

(a)

(b)

Fig. 3.4. Discretization of expander for calculation of soil expansion force: (a) Method A; (b) Method B. (a_n and P_n represent intermediate borehole radii and expansion pressures respectively, and Φ_{s-s} denotes friction angle in steel-soil interface)

As illustrated in Fig. 3.4, the contact area of the conical expander is discretized into equal sections beginning at the original pipe radius, or the tip of failure piece, to the largest radius of expander. The surface area of a conical frustum can be determined as follows:

$$A_n = \pi(a_n + a_{n+1})\sqrt{(a_{n+1} - a_n)^2 + d_n^2} \tag{3.23}$$

where A_n is the surface area between n and $n+1$, a_n is the borehole radius at n, a_{n+1} is the borehole radius at n+1, and $d_n$is the distance between n and $n+1$.

Instead of a gradient pressure, an average pressure is adopted for each section, and the vertical soil expansion forces are converted in horizontal direction, as shown in Fig. 3.4. The interface friction angle between the expander and the surrounding soil Φ_{s-s} is typically 20° for steel-granular backfill interface (Nkemitag, 2007). The general equation to determine horizontal soil expansion force is:

$$F_{seh} = \left(\sum_0^n P_{avg,n} \times A_n\right) \tan(\Phi_{s-s} + \frac{\theta_e}{2}) \tag{3.24}$$

where $P_{avg,n}$ is the average pressure between n and $n+1$.

For the cavity expansion solution, the mechanical interaction between the expander and original pipe is ignored. The soil properties change when soil collapse occurs as well as during the pipe bursting (expansion) process; however, the initial soil properties are used because it is hard to consider property changes. This assumption of neglecting the property changes results in Method A underestimating the expansion force, while Method B might overestimate.

3.3 Validation of the Calculation Methods

3.3.1 Laboratory Experiment for Pipe Bursting

Lapos (2004) performed five static pipe bursting tests (Tests #1- #5) in a 2-m wide, 2-m long and 1.6-m deep test cell filled with poorly-graded sand. The soil bulk density, depth of soil cover, and original pipe dimensions were treated as variables. The same expander and new pipe were used for all tests. The expander had an apex angle (θ_e) of 30° and the largest diameter of 202 mm, while the new pipe had an outside diameter of 150 mm. The soil had a friction angle (Φ) of

44°, a dilation angle (Ψ) of 30°, a cohesion (c) of 30 kPa, an elastic modulus (E) of 2 MPa, and a Poisson's ratio (v) of 0.25. Table 3.1 summarizes the variables for the five tests.

Table 3.1. Variables in Lapos' (2004) static pipe bursting tests

Parameters	Test #1	Test #2	Test #3	Test #4	Test #5
Soil bulk density (kg/m^3)	1541	1498	1515	1521	1503
Depth of soil cover (mm)	685	685	685	885	885
Outside diameter of original pipe (mm)	146	146	100	146	100
Thickness of original pipe (mm)	19	19	14	19	14

For each test, a hydraulic pulling machine dragged the expander forward in 13 pull stages, each 250 mm in length. A load cell attached to the pulling cable was used to continuously record the pull force in each pull stage. The friction force developed on the soil-new pipe interface was measured after the expander was completely pulled out of the test cell. In the friction measurement, the expander was mounted on a steel bar to avoid inclusion of its weight. Furthermore, the breaking force was measured aerially instead of in soil. The experimental soil expansion force was obtained by subtracting the experimental pull force from the experimental breaking and friction forces that developed between the soil and new pipe, as well as the expander and the soil. The maximum soil expansion force from each stage was used to calculate the average and standard deviation values, which were used as measured soil expansion force for comparison against calculated expansion force. It is noted that the data from the first two and last two pull stages were not used since the expander did not completely enter or partially pass the test cell. More detail on this experiment can be found in Lapos (2004) and Nkemitag (2007).

3.3.2 Expansion Pressure

The three cavity expansion solutions introduced were used to calculate the soil expansion pressure for pipe bursting tests in Lapos (2004). The entire expansion length was divided into 10 equal sections. The soil expansion pressures calculated using Methods A (without soil collapse) and B (with soil collapse) are presented against radius ratio (expansion ratio) a_n/a_0 in Figs. 3.5a and 3.5b, respectively. Since the result differences between Tests #1, #2, and #4 and between Tests #3 and #5 are insignificant, Figs. 3.5a and 3.5b include only the results for Tests #1 and #3.

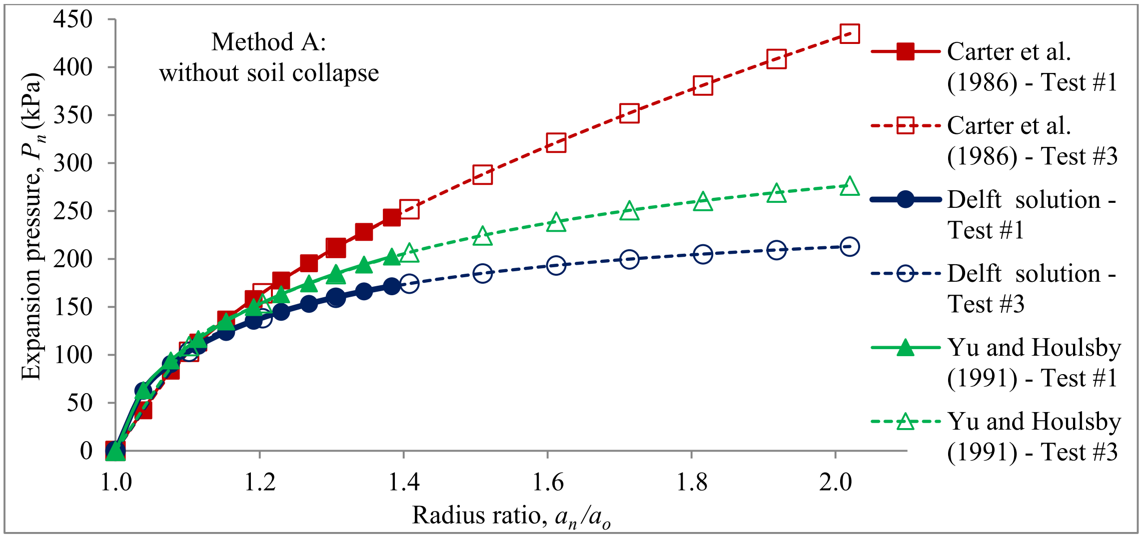

(a)

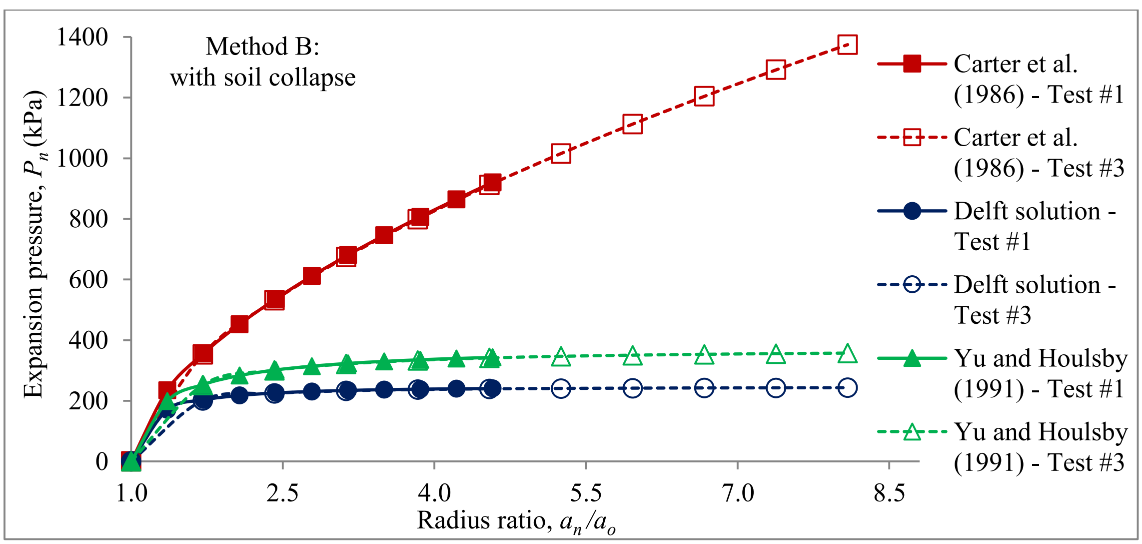

(b)

Fig. 3.5. Calculated soil expansion pressure versus radius ratio for Tests #1 and #3: (a) Method A; (b) Method B

Figs. 3.5a and 3.5b indicate that soil expansion pressure-radius ratio curves from each solution for Tests #1 and #3 overlap despite different initial radii. This is due to the radius ratios, as shown in equations (3.4), (3.16) and (3.18), which can be removed from pressure-expansion relations. The ratios increase with the expansion pressures for all three cavity expansion solutions. For relatively small radius ratios (i.e. <1.2), as shown in Fig. 3.5a, the expansion pressure-radius ratio curves are quite close, since expansion pressures based on small- and large-strain analyses in the plastic zone are similar under small displacements. For relatively large radius ratios (i.e. >2.5), as illustrated in Fig. 3.5b, expansion pressures for Yu and Houlsby (1991) and Delft solution reach plateaus , i.e. their corresponding limit pressures. Expansion pressure from Carter et al. (1986) continues to increase with radius ratio; however, it reaches its limit pressure for relatively large radius ratios.

Higher dilation angle results in higher expansion pressure (Houlsby, 1991; Yu and Houlsby, 1991). However, dilation is not considered in Delft solution, resulting in the lowest expansion pressures, as illustrated in Figs. 3.5a and 3.5b. In general, adopting large-strain analysis results in lower expansion pressure as propagation in the plastic zone is faster in comparison to that of small-strain analysis (Yu and Houlsby, 1991). Carter et al. (1986) does not consider the convected part of the stress rate in their derivation, so it can only be treated as an approximate solution to determine expansion pressure in the plastic zone (Yu and Houlsby, 1991; Yu and Carter, 2002). In contrast, Yu and Houlsby (1991) solution is applicable to small and large deformations in the plastic zone as well as stiff and soft soil types. Due to the defectiveness of applying Carter et al. (1986) to large deformed material in the plastic zone, an extraordinarily high expansion pressure is expected to be obtained for projects requiring a large upsize.

3.3.3 Comparison of Predicted and Measured Soil Expansion Forces

The number of discretized sections for the expander (Figs. 3.4a and 3.4b) affects the calculated soil expansion force, as indicated in Figs. 3.6a and 3.6b. However, the force calculated through Methods A and B becomes almost consistent when the number of discretized sections is greater than four; therefore, ten sections are used to calculate the expansion force for analysis and comparison.

As shown in Fig. 3.6a, the forces calculated via Method A for Test #1 based on the three solutions are relatively close due to small radius ratios. For Test #3, the force based on Carter et al. (1986) is considerably higher than that of the other two solutions. Fig. 3.6b illustrates that the difference of calculated expansion forces between Tests #1 and #3 from Yu and Houlsby (1991) and Delft solution is relatively small due to the internal pressures approaching to limit pressures, as indicated in Fig. 3.5b. The difference of calculated expansion forces between Tests #1 and #3 of Carter et al. (1986), in contrast, is relatively large due to dissimilar pressure distributions on the expander. Both Figs. 3.6a and 3.6b show that the expansion force based on Carter et al. (1986) is more sensitive to increase in radius ratio.

The expansion force ratios between Methods B and A (force calculated using Method B / force calculated using Method A) from Carter et al. (1986), Yu and Houlsby (1991), and Delft solution are 8.7, 4.3, and 3.5 for Test #1 and are 4.5, 2.0, and 1.7 for Test #3, respectively. This indicates that consideration of soil collapse has a significant impact on soil expansion force, especially for Test #1.

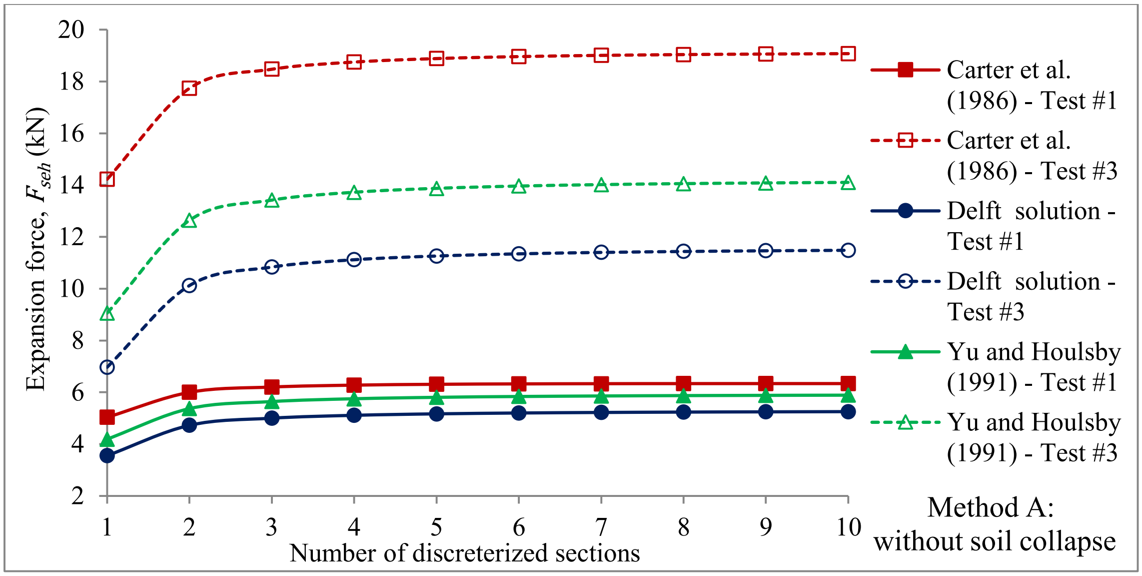

(a)

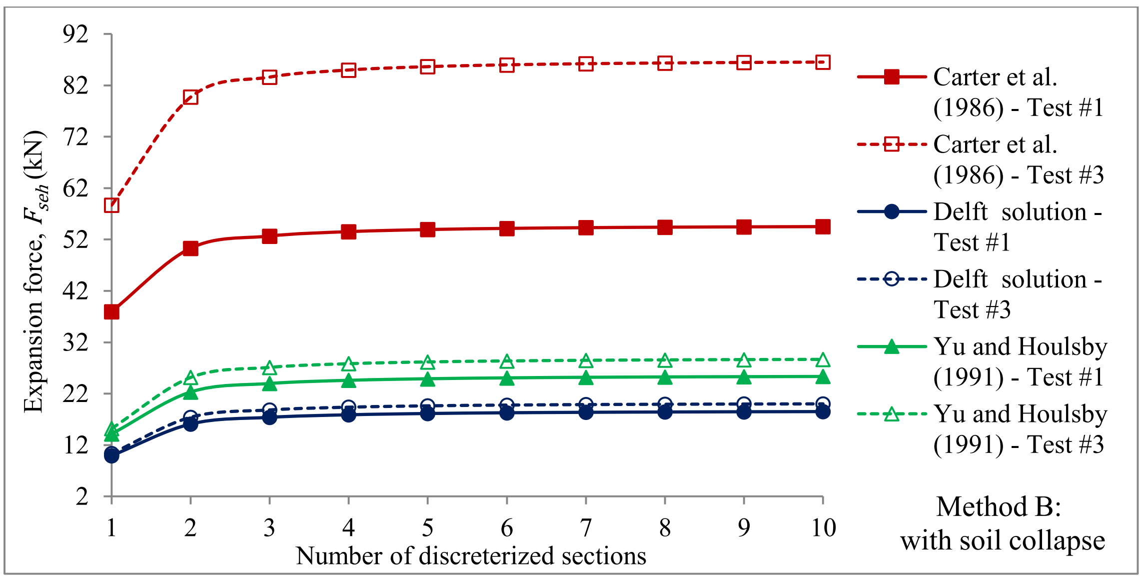

(b)

Fig. 3.6. Calculated expansion force versus the number of discretized sections of expander: (a) Method A; (b) Method B

Figs. 3.7a-c show the expansion forces based on Carter et al. (1986), Delft, and Yu and Houlsby (1991) solutions compared with the experimental results. As expected, the expansion forces calculated using Method A are significantly lower than the measured results, except for Test #3 based on Carter et al. (1986) solution. As shown in Fig. 3.7a, the calculated forces using Method B are 1.7-4.5 times higher than the average experimental forces, indicating Carter et al. (1986) significantly overestimates the soil expansion force during pipe bursting. As discussed previously, Cater et al. (1986) uses small-strain analysis; however, this assumption is not well-suited to the pipe bursting process, where large deformation often occurs. Consequently, the expansion force prediction based on Cater et al. (1986) is overestimated.

The calculated expansion forces based on Delft solution are illustrated in Fig. 3.7b, including comparison to experimental results. All forces calculated using Method A are lower than experimental results, while forces calculated using Method B for Tests #1, #2, and #3 are close to experimental results. In Tests #4 and #5, the measured expansion forces are remarkably higher than results calculated using Method B. These results indicate that Delft solution underestimates the soil expansion force during pipe busting because it does not consider soil dilation.

Fig. 3.7c presents the calculated soil expansion forces based on Yu and Houlsby (1991) compared to the measured results. For Tests #1, #2, and #3, forces calculated using Method B are 1.3-1.5 times higher than the average measured results. For Test #4, the average measured force is slightly higher than the force calculated using Method B. This is due to original pipe fragments potentially wedging in the expander as well as soil collapse that occurred during testing and inconsistent original pipe thickness, as reported by Lapos (2004) and Nkemitag (2007). The assumption of soil collapse for Method B is fulfilled; hence the measured result is close to that calculated using Method B. Similarly, high experimental expansion force close to the result calculated via Method B for Test #5 could be attributed to the same reasons. The above mentioned results indicate that the calculation method based on Yu and Houlsby (1991) is more accurate than both Carter et al. (1986) and Delft solutions.

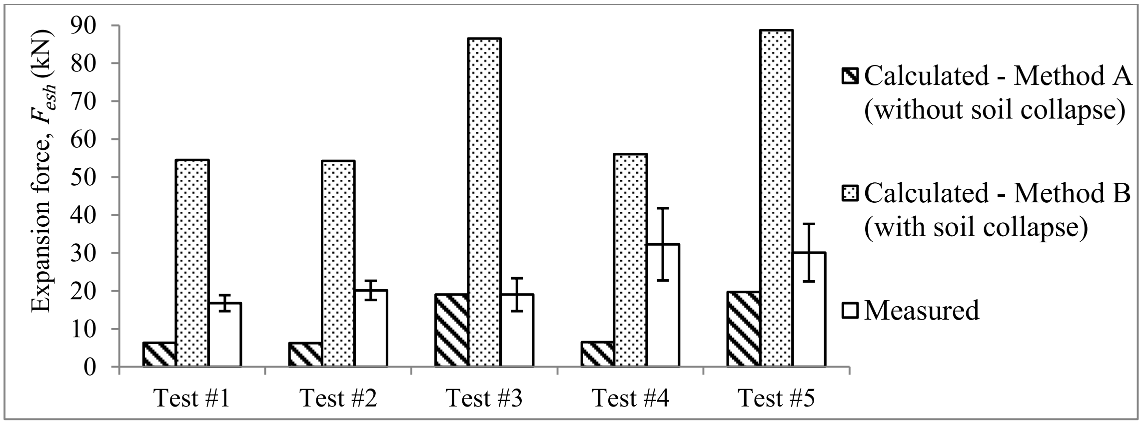

(a)

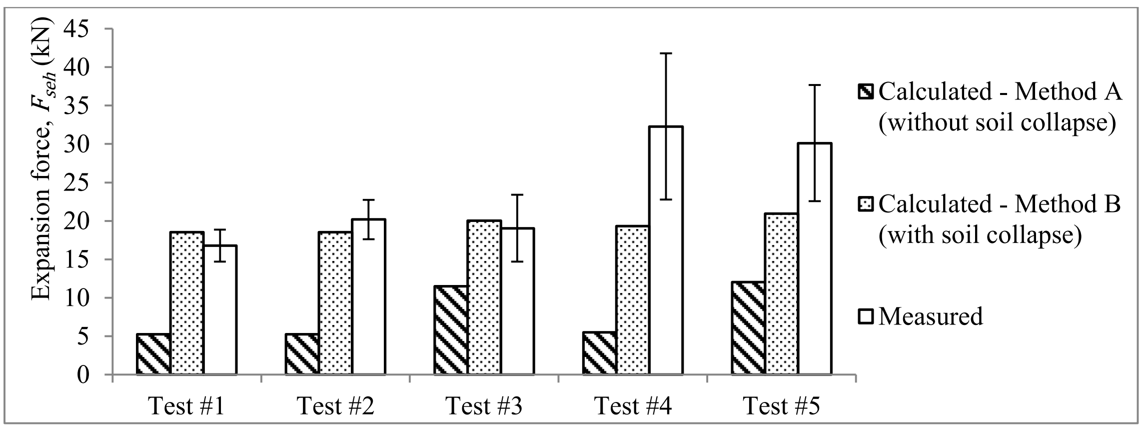

(b)

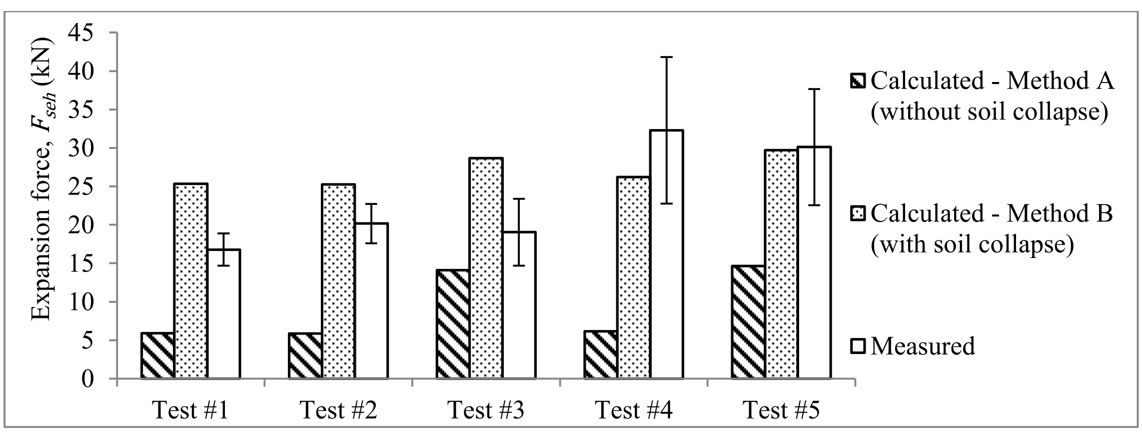

(c)

Fig. 3.7. Measured and calculated soil expansion forces based on: (a) Carter et al (1986); (b) Delft; (c) Yu and Houlsby (1991)

The advancement of the expander is a dynamic process. Soil surrounding the expander becomes denser as it is moved outwards by the expander. The propagation of cracks in original pipe leads to soil collapse, filling the gap between the expander and the pipe. When mixed with pipe fragments, the soil is typically looser than its native state. Furthermore, infinite and homogenous soil medium, coefficient of lateral earth pressure K of 1, and plane-strain analysis are adopted by the three cavity expansion solutions. Additionally, the breaking length suggested by Ariaratnam and Hahn (2007) is empirical. Despite the above mentioned simplifications, the calculation method based on Yu and Houlsby (1991) provides a useful range of soil expansion force, which can be used to estimate the total pull force to select the appropriate capacity of pulling machine.

3.4 Conclusions

Three cavity expansion solutions were used to predict expansion force for static pipe bursting installation, and their feasibilities were validated with laboratory experiments. Results indicate that the calculation method based on Yu and Houlsby (1991) provides a reasonable estimation of soil expansion force required. Conversely, expansion forces calculated based on Carter et al. (1986) and Delft solution are conservative and underestimated, respectively. Due to the complexity of the pipe bursting process and the simplifications adopted in expansion force calculation method, more experimental and field measurements are required to validate and improve the calculation method.

Chapter 4: Numerical Modeling to Prediction of Soil Expansion Force in Static Pipe Bursting[2]

4.1 Introduction

Static pipe bursting technology provides an effective underground replacement and rehabilitation solution for structurally deteriorated and undersized pipelines. Compared to the traditional open-cut method, pipe bursting can reduce the impact of socio-economic factors such as traffic interference, pollution, damage to adjacent infrastructure, business and community disruption, and construction time (Rogers and Chapman, 1995; Brachman et al., 2007; Lapos et al., 2007; Plastics Pipe Institute, 2007; Cholewa et al., 2009a, 2009b; Bennett et al., 2011; Kazi, 2013; Shi et al., 2013). Static pipe bursting replaces the original pipe by using a conical expander to fragment the pipe and installing a new pipe of equal or larger diameter in the original trajectory, as shown in Fig. 4.1. Pull force prediction is critical to the design of static pipe bursting projects, and there are three pull force components: breaking force fragments the original pipe into smaller pieces; friction force is created from soil-new pipe, soil-expander, and pipe fragments-expander interfaces; and soil (cavity) force expands the[3] surrounding soil and pipe fragments outwards to create a larger cavity for the new pipe (Ariaratnam and Hahn, 2007; Nkemitag, 2007; Nkemitag and Moore, 2007; Lapos et al., 2007; Bennett et al., 2011; Kazi, 2013).

[2] A version of this chapter has been submitted to Canadian Geotechnical Journal. Authors: Ka Hou Ngan, Yaolin Yi, Ali Rostami, and Alireza Bayat.

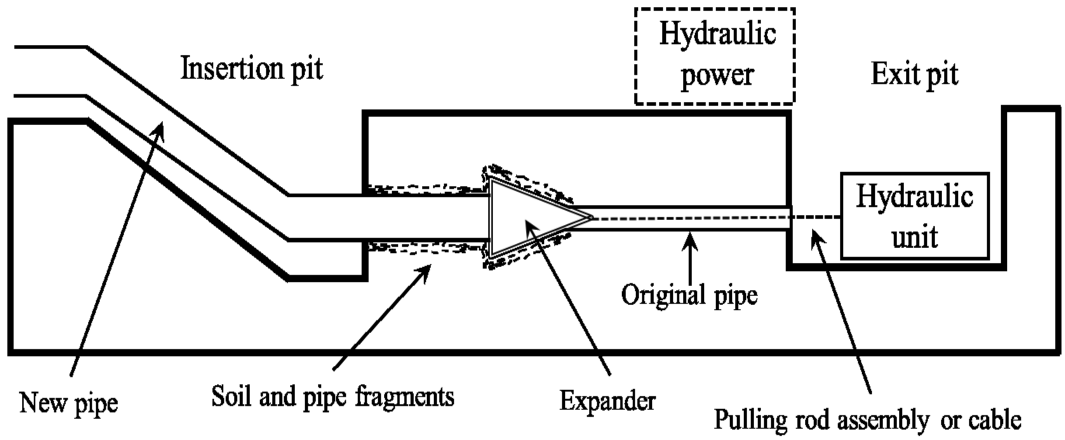

Fig. 4.1. Schematic layout of a static pipe bursting installation (adapted from Plastics Pipe Institute, 2007)

A number of laboratory and field experiments have been performed to investigate ground displacement associated with pipe bursting (Leach and Reed, 1989; Rogers and Chapman, 1995; Atalah et al., 1997; Lapos, 2004; Lapos et al., 2004; McLeod, 2008; Cholewa et al., 2009b; Brachman et al., 2010). However, only a few tests measured the pull forces in static pipe bursting, where the soil expansion force was found to have the greatest impact (Lapos, 2004; Lapos et al., 2004; Cholewa et al., 2009b). Ariaratnam and Hahn (2007) developed an empirical equation for expansion force calculation; however, this method requires a soil expansion limit factor obtained through comparison of the measured and calculated soil expansion forces. Subsequently, due to limited measured expansion forces available, application of this equation is restricted. Ngan et al. (2014) investigated the capability of cavity expansion solutions, including Carter et al. (1986), Delft solution (Luger and Hergarden, 1988; Keulen, 2001), and Yu and Houlsby (1991), for prediction of the soil expansion force during static pipe bursting installation. The comparison of predicted and experimental results indicated that Yu and Houlsby (1991) solution properly predicted the soil expansion force, while Carter et al. (1986) solution overestimated and Delft solution underestimated the results. However, there are some limitations associated with Yu and Houlsby's (1991) assumptions, such as infinite soil medium, which cannot consider the depth of soil cover above the pipe.

Numerical modeling was used to predict soil expansion force in an axisymmetric plane-strain analysis by Nkemitag (2007) and Nkemitag and Moore (2007) using AFENA, while to predict pull force in a three-dimensional analysis by Kazi (2013) using ABAQUS. All predictions used Lapos' (2004) tests for validation. In the work of Nkemitag (2007) and Nkemitag and Moore (2007), pipe bursting was assumed to start from an initial borehole radius of zero and the coefficient of lateral earth pressure was assumed to be one. Although three-dimensional numerical modeling (Kazi, 2013) was more accurate in comparison to the two-dimensional modeling (Nkemitag, 2007; Nkemitag and Moore, 2007), it was more complicated to conduct with long computing times and high occurrence of numerical instabilities. A comparison between two- and three-dimensional simulations for the maximum allowable pressure in horizontal directional drilling was conducted by Xia (2009) resulting in a difference of 4.5%, which indicates the feasibility of using two-dimensional simulation in determining soil expansion pressure.

In this paper, a two-dimensional numerical modeling with finite element software ABAQUS (Dassault Systèmes Simulia Corp 2013) was conducted to predict expansion pressure acting upon the borehole wall during static pipe bursting. The expansion forces, calculated based on numerical results, were compared to laboratory experiments conducted by Lapos (2004) and forces calculated based on Yu and Houlsby (1991). A parametric study was also performed using numerical modeling and cavity expansion solution to examine the influence of depth of cover as well as different initial and final borehole radii on the calculated expansion force during pipe bursting with typical underground conditions in Edmonton, Alberta, Canada.

4.2 Calculation of Soil Expansion Force during Pipe Bursting

4.2.1 Numerical Model Development

An axisymmetric plane-strain analysis was adopted in ABAQUS modeling considering the symmetrical arrangement of pipe bursting, as illustrated in Fig. 4.1. The geometrical model mesh was generated as a four-node bilinear plane strain quadrilateral (CPE4). The soil medium was developed according to the dimensions and soil properties in Lapos (2004), which will be introduced in the following section. The soil was assumed to be linearly elastic following Hooke's law until the onset of yield, while perfectly plastic after yielding following the Mohr-Coulomb yield criterion and non-associated flow rule. Soil properties changed during pipe bursting process; however, constant initial soil properties were used due to the complexity of considering property changes.

To begin, the equilibrium condition was created by applying geostatic stress and soil weight gradient to the entire soil medium. Afterwards, the borehole was excavated and a uniform radial internal pressure was established around the borehole in small increments beginning at 0 kPa. Pressure and gravity settings were entered into ABAQUS' load manager, while stress variation and lateral coefficient were entered into ABAQUS' predefined field manager. Jaky (1944) equation was used to estimate the coefficient of lateral earth pressure at rest for normally consolidated soils as follows:

$$K_o = 1 - \sin \Phi' \qquad (4.1)$$

where K_o is the coefficient of earth pressure at rest and Φ' is the drained friction angle.

The ground surface was free to movement and the bottom boundary was fixed in the soil medium. To reduce computing time, an axisymmetric boundary and free vertical displacement (U_y) were set at the left and right boundaries, respectively, as illustrated in Fig. 4.2.

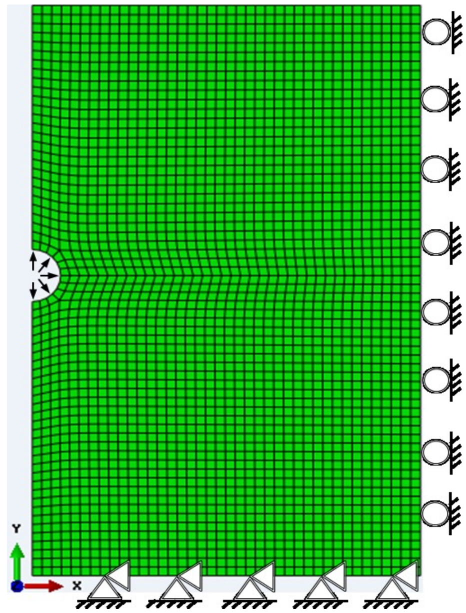

Fig. 4.2. The mesh and boundary conditions in numerical modeling

4.2.2 Soil Expansion Force Calculation Using Expansion Pressure

Expansion pressure acting upon the expander varies with borehole radius (expansion) ratio (a_n/a_0) due to the expander's conical shape. The expander was discretized into several equal sections in this study to determine the average expansion pressure in each section, as illustrated in Figs. 4.3a and 4.3b. The equation to calculate horizontal (longitudinal) soil expansion force F_{seh} is shown as follows:

$$F_{seh} = \left(\sum_0^n P_{avg,n} \times A_n\right) \tan(\Phi_{s-s} + \frac{\theta_e}{2}) \quad (4.2)$$

where

$$A_n = \pi(a_n + a_{n+1})\sqrt{(a_{n+1} - a_n)^2 + d_n^2} \quad (4.3)$$

where $P_{avg,n}$ is the average pressure between n and $n+1$, A_n is the surface area between n and $n+1$, a_n is the borehole radius at n, a_{n+1} is the borehole radius at $n+1$, and d_n is the distance between n and $n+1$.

During advancement of the expander, crack propagation in the original pipe may occur and result in soil collapse around the failure pieces or pipe fragments (Lapos 2004; Nkemitag, 2007). Therefore, two methods were used in this study to calculate the expansion force without (Method A) and with (Method B) consideration of soil collapse. The initial borehole radius a_0 in Method A was the original pipe radius, while the initial borehole radius a_0 in Method B had a smaller dimension considering the breaking length (Δx), as illustrated in Fig. 4.3b. Ariaratnam and Hahn (2007) suggested that the breaking length was typically ten times the original pipe's wall thickness based on industry experience; and this assumption was adopted in this study.

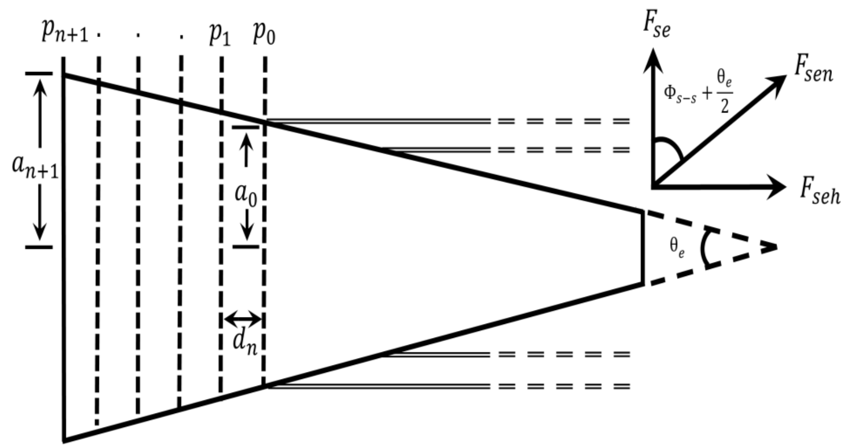

(a)

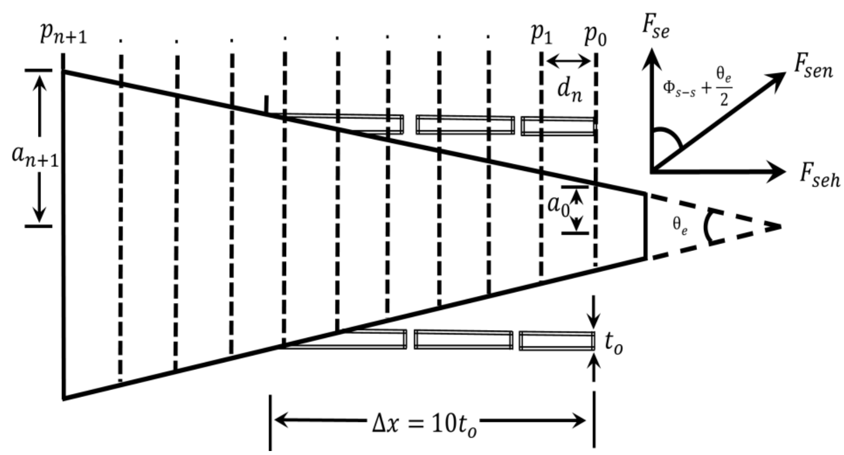

(b)

Fig. 4.3. Discretization of expander into equal sections: (a) Method A; (b) Method B

4.3 Validation of the Calculation Method

4.3.1 Pipe Bursting Laboratory Test for Validation

The five static pipe bursting laboratory experiments conducted by Lapos (2004) were used to verify numerical modeling in this study. The experiments were conducted in poorly graded sand within a test cell with 2-m width, 2-m length, and 1.6-m depth. The soil bulk densities in Tests #1-5 were 1541 kg/m^3, 1498 kg/m^3, 1515 kg/m^3, 1521 kg/m^3 and 1503 kg/m^3, respectively. The soil had a friction angle (Φ) of 44^o, dilation angle (Ψ) of 30^o, cohesion (c) of 30 kPa, elastic modulus (E) of 2 MPa, and Poisson's ratio (ν) of 0.25. The friction angle for soil-steel interface (Φ_{s-s}) was 20^o, and depths of cover were 685 mm for Tests #1-3 and 885 mm for Tests #4 and #5. An original pipe with an outside diameter of 146 mm and a thickness of 19 mm was used for Tests #1, #2 and #4, while an original pipe with a 100-mm outside diameter and 14-mm thickness was used for Tests #3 and #5. The same new pipe and expander were used for all tests; the expander had an apex angle (θ_e) of 30^o with the largest diameter of 202 mm, and the new pipe had an outside diameter of 150 mm.

The experimental soil expansion force was calculated by subtracting the measured breaking force and friction force from the pull force (Lapos 2004; Nkemitag, 2007). The maximum experimental soil expansion force at each pull stage was used to determine the average and standard deviation values (Ngan et al., 2014), which were then used as the measured soil expansion force for comparison and analysis. More details about the experiments can be found Lapos (2004) and Nkemitag (2007).

4.3.2 Expansion Pressure from Numerical Modeling

During numerical modeling, the ABAQUS typically aborted for one of two reasons: either the integral equation was not converged, or there was distortion in meshes, both resulting in numerical termination. The numerical results for pressure with respect to displacement can be obtained from the mesh node. The displacements were averaged around the borehole as follow:

$$UT_{avg} = \frac{UT2_{crown} + 2 * UT1_{shoulder} + UT2_{bottom}}{4} \tag{4.4}$$

where UT_{avg} is the average displacement around the borehole, $UT2_{crown}$ is the vertical displacement on the crown of the borehole, $UT1_{shoulder}$ is the horizontal displacement on the shoulder of the borehole, and $UT2_{bottom}$ is the vertical displacement on the bottom of the borehole.

The equation used to determine borehole radius during soil expansion is as follow:

$$a = a_0 + UT_{avg} \tag{4.5}$$

where a is the current borehole radius and a_0 is the initial borehole radius.

Knowing the borehole radius, the corresponding expansion pressure can be determined from the expansion pressure-borehole radius curves (e.g. Fig. 4.4). Figs. 4a and 4b illustrate expansion pressure versus borehole radius for all tests except Test #2, which had insignificant difference when compared to Test #1. With a higher depth of cover (e.g. Test #4 vs. Test #1 and Tests #5 vs. Test #3), a greater expansion pressure is required to move soil outward due to a higher overburden stress. Only Tests #1 and #4 using Method A reached the final borehole radius of 0.101 m (the largest expander), while the other tests reached their corresponding limit pressures as shown in Figs. 4a and 4b.

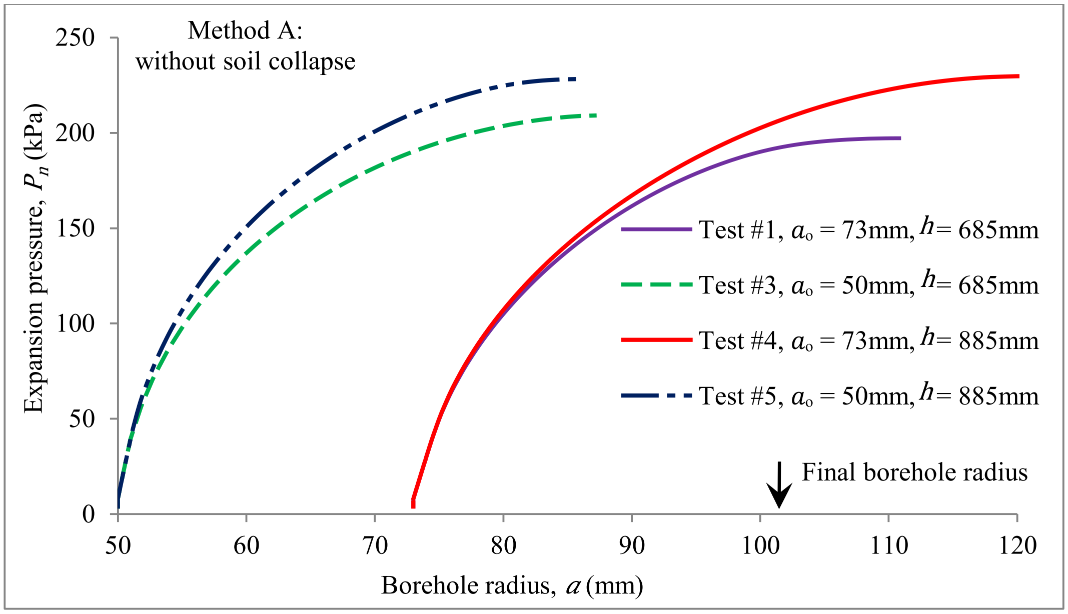

(a)

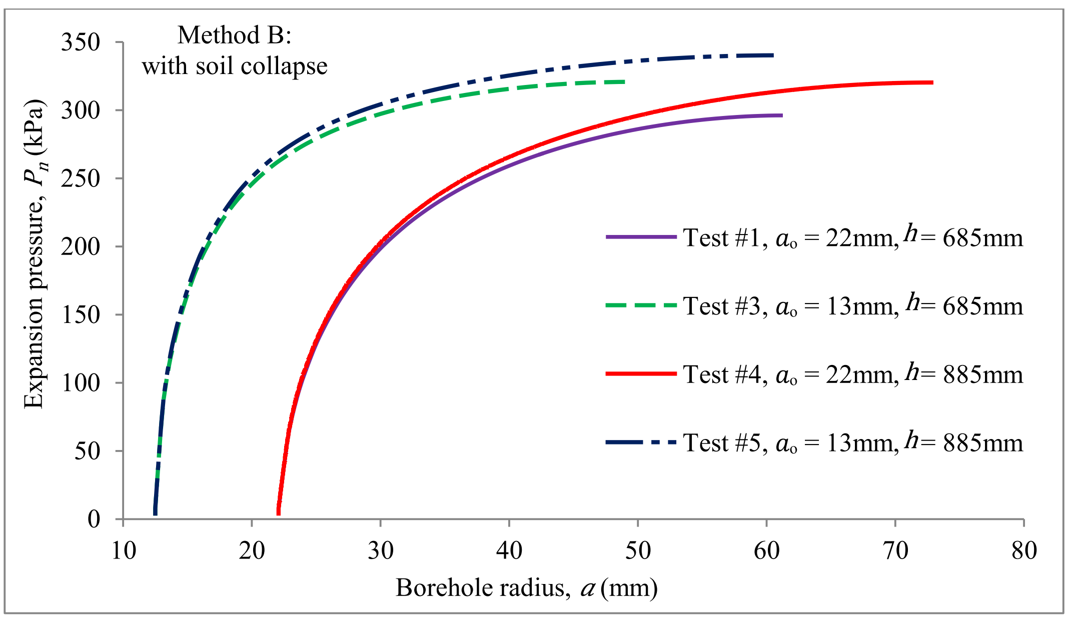

(b)

Fig. 4.4. Borehole radius versus expansion pressure obtained from numerical modeling: (a) Method A; (b) Method B

Soil expansion pressures at different sections of the pipe bursting tests (Lapos, 2004) obtained through numerical modeling using Methods A (without soil collapse) and B (with soil collapse) are presented against radius ratio (a_n/a_0) in Figs. 4.5a and 4.5b, respectively. For comparison, the soil expansion pressures calculated by Ngan et al. (2014) using analytical cavity expansion solution (Yu and Houlsby, 1991) are also presented in Figs. 4.5a and 4.5b. Only results for Tests #1 and #3 are presented due to insignificant differences between Tests #1, #2 and #4, and between #3 and #5.

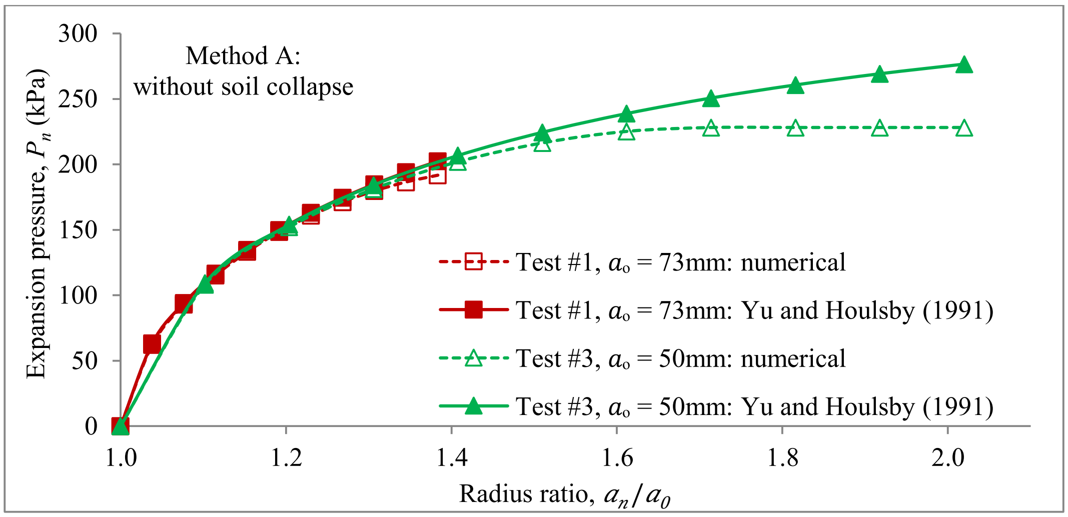

(a)

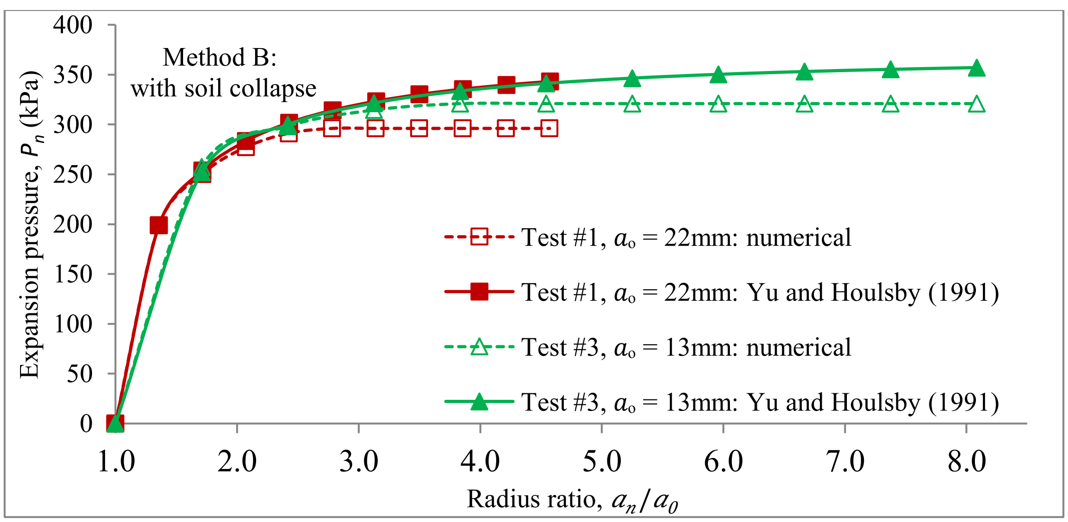

(b)

Fig. 4.5. Soil expansion pressure versus radius ratio from numerical and analytical solutions for Tests #1 and #3: (a) Method A; (b) Method B

Figs. 4.5a and 5b indicate that the soil expansion pressure-radius ratio curves nearly overlap when radius ratios are less than 1.5 and 2.5 for Methods A and B, respectively. In Fig. 4.5a, the curves for Test #3 obtained from the two solutions using Method A diverge after passing a radius ratio of 1.5, where the limit pressure is reached for the numerical modeling while expansion pressure for the analytical solution continues to increase. In Fig. 4.5b, curve divergences of the two solutions for Tests #1 and #3 initiate at radius ratios of 2.5 and 3.0, respectively. The radius ratio can be removed from the pressure-expansion relation in Yu and Houlsby (1991) solution, so that the same expansion pressure can be obtained from the same radius ratio. However, the numerical modeling results indicate that the initial borehole radius also affects the expansion pressure. For a smaller initial borehole radius with the same radius ratio (e.g. Tests #3 vs. #1 in Fig. 4.5b at a radius ratio higher than 3.0), a higher expansion pressure is needed due to a higher confinement in the borehole and greater borehole stability. For a smaller initial borehole radius (i.e. Test #3), the divergence of curves from the two solutions occurs at a higher radius ratio; when expanding from a smaller radius in numerical modeling, a higher expansion pressure is required, resulting in a greater limit pressure.

Both numerical modeling and analytical solution provide similar trends in curves due to that they both adopt Hooke's law, Mohr-Coulomb failure criterion, non-associated flow rule, and large-plane strain analysis. The soil medium in the analytical solution is considered to be infinite with use of constant field stress and a lateral earth pressure coefficient of one. These assumptions lead to a higher expansion pressure when compared to numerical modeling. However, the impact of these assumptions is insignificant due to the small Lapos' (2004) experimental scale.

4.3.3 Comparison of Predicted and Measured Soil Expansion Forces

Fig. 4.6 illustrates the soil expansion forces calculated based on numerical modeling compared to the measured forces from Lapos (2004). The soil expansion forces calculated by Ngan et al. (2014) using the same method introduced in Section 4.2.2 with the expansion pressures from the analytical solution (Yu and Houlsby, 1991) are also presented in Fig. 4.6 for comparison.

Expansion forces from numerical modeling and analytical solution are close, with slightly higher expansion pressures from the analytical solution for all tests, as illustrated in Fig. 4.6. Expansion forces from both solutions for Method A are significantly less than the lower bounds of the measured forces in all tests, since soil properties change and/or soil collapse were not considered. Expansion forces from both solutions using Method B are moderately higher than the upper bounds of measured forces in Tests #1-3, with numerical modeling results closer to the measured forces. Although constant soil properties were used in Method B, the effect of variation of the properties was partially considered, because the soil became loose when collapse occurred and dense when expansion occurred. Expansion forces for Test #4 from both solutions using Method B are moderately less than the average measured force. This is due to original pipe fragments potentially wedging in the expander as well as soil collapse that happened during testing and inconsistent original pipe thickness, as reported by Lapos (2004) and Nkemitag (2007). As the assumption of soil collapse for Method B is fulfilled, the measured result is close to that calculated using Method B. Likewise, high experimental expansion force close to the result calculated via Method B for Test #5 could be attributed to the same reason.

Nkemitag and Moore (2007) used AFENA software to model the forward movement of the expander, adopting mixed boundary condition at the interface between the expander and the surrounding soil, along which radial displacements were imposed to match the cavity expansion.

Their study also used Lapos' (2004) tests (Tests #1, 3, 4, and 5) for validation and their results are also close to the measurements as shown in Fig. 4.6. However, in the work of Nkemitag and Moore (2007), the cavity expansion started from an initial borehole radius of zero and the overburden pressure effect was not well considered due to adoption of the uniform and isotropic (K_o= 1) pre-existing earth pressure in numerical modeling.

The above results indicate that ABAQUS modeling can properly predict expansion force during pipe bursting through Method B. Although there is no significant difference between the results from numerical modeling and analytical solution, the latter cannot consider the effects of depth of cover, initial borehole radius (only the radius ratio), coefficient of lateral earth pressure, and boundary conditions; these effects are insignificant in Lapos' (2004) experiments, but could be significant in field applications. However, the analytical solution is simpler for industry design in comparison to numerical modeling. Hence, the following section will investigate the difference between the two solutions predicting expansion pressures for full-scale pipe bursting cases through a parametric study using typical underground parameters in Edmonton.

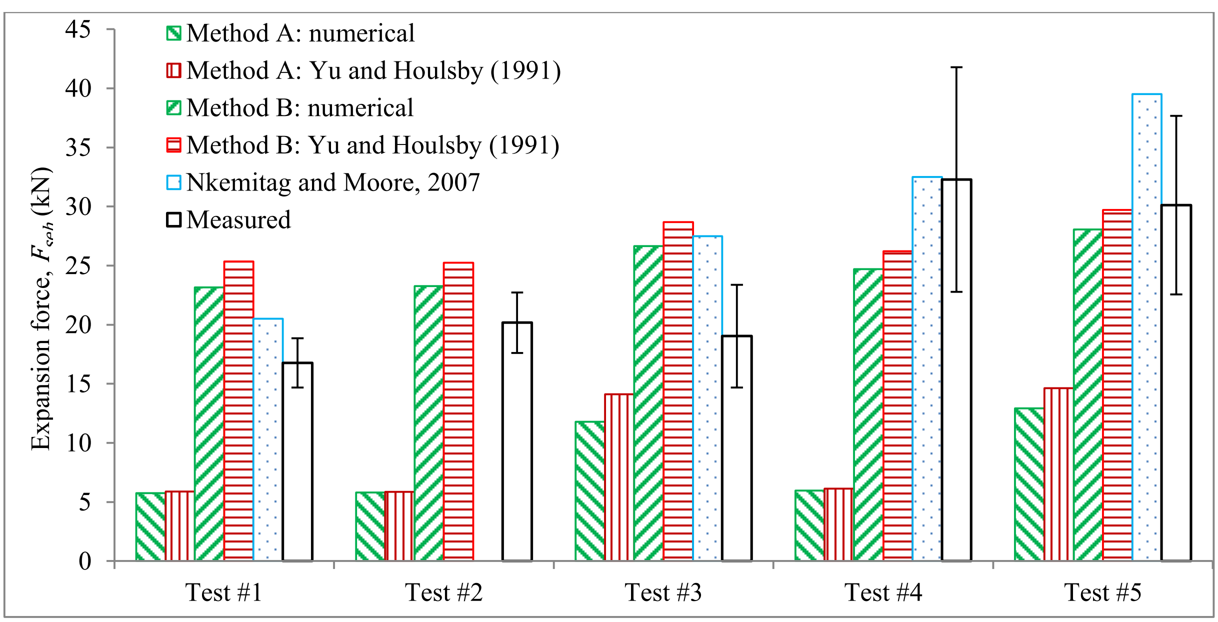

Fig. 4.6. Measured and calculated horizontal soil expansion forces

4.4 Parametric Study

4.4.1 Parameters

A parametric study was conducted using numerical modeling and the analytical solution (Yu and Houlsby, 1991) to investigate the effect of depth of cover as well as initial and final borehole radii on soil expansion pressure in pipe bursting. The typical glacial till in Edmonton, where a large number of pipelines are buried in this soil, was used as the surrounding soil in the parametric study. Glacial till in the region is generally several meters below ground surface and has a sufficiently high thickness that fluctuates moderately by location (Thomson and Yacyshyn, 1977; May and Thomson, 1978; Thomson and El-Nhhas, 1979). The till consists of 40-45% sand, 25-35% silt, 20-30% clay, and has a cohesive-frictional behaviour (Thomson and Yacyshyn, 1976). A typical bulk unit weight of 21 kN/m^3, elastic modulus of 200 MPa, friction angle of 33^o, dilation angle of 5^o, cohesion of 110 kPa, Poisson's ratio of 0.35, and coefficient of lateral earth of 0.85 (DeJong and Harris, 1971; El-Nahhas, 1977; Eisenstein and Thomson, 1978; May and Thomson, 1978; Medeiros and Eisenstein, 1982; Elwood et al., 2011) were used for the till in the parametric study.

According to Edmonton Sewer Design Standards and Guidelines (Epcor, 2013), Polyvinyl Chloride (PVC) water main installations should have a dimension ratio (outside diameter over pipe thickness) of 18 and minimum depth of cover of 2.5 m. The maximum depth of cover for pipe bursting may exceed 5.5 m according to the International Pipe Bursting Association (2012). In Edmonton, the depth of cover for underground pipeline can exceed 5.5 m due to the extreme cold weather. In the parametric study, a depth of cover ranging from 2.5 to 8.5 m was used. Geotechnical investigations in Edmonton have also revealed that groundwater only occasionally appears in the till (May and Thomson, 1978; Elwood et al., 2011). In this parametric study, it was assumed that the groundwater above the till was not considered and the underground soil only consists of a till soil layer to simplify calculations.

According to survey results from 886 pipe bursting projects in North America (Ariaratnam et al., 2012), the diameter of the original pipe typically ranges from 150 to 300 mm, the diameter of the new pipe ranges from 200 to 375 mm, and the diameter of the expander is 50 to 100 mm larger than the new pipe. The dimension ratio can be used to estimate the pipe wall thickness and then to determine the breaking length considering soil collapse (Method B) as suggested by Ariaratnam and Hahn (2007). The initial and final borehole radii for Methods A and B used in the parametric study are determined (Table 4.1) considering a fixed apex angle of 30° for the expander. In Table 4.1, the initial radii for Methods A and B are based on Ariaratnam's et al. (2014) survey and dimension ratio calculation. The final radii chosen are based on combinations of the minimum or maximum new pipe radius (100 or 187.5 mm) and the minimum or maximum new pipe-expander upsizing (25 or 50 mm) (Ariaratnam et al., 2014). This selection of initial and final radii covers the possible upsize range in pipe bursting.

Table 4.1. Variables in initial and final borehole radii for Methods A and B

	Parameters	Case 1 (C1)	Case 2 (C2)	Case 3 (C3)	Case 4 (C4)
	Final radius, a (mm)	125	150	212.5	237.5
Method A	Initial radius, a_o (mm)	75	75	150	150
	Radius ratio, a_n/a_o	1.7	2.0	1.4	1.6
Method B	Initial radius, a_o(mm)	50	50	100	100
	Radius ratio, a_n/a_o	2.5	3.0	2.1	2.4

The numerical modeling method used in the parametric study is the same as that introduced in Section 4.2.1. The depth of cover ($2.5\text{m} \leq h \leq 8.5\text{m}$) varied with each case as mentioned previously, while the medium width and depth from the borehole to the bottom boundary were set to 20 m. It was found that the boundary effect occurred when the depth was set at a small value, leading to higher expansion pressure. For a high depth (i.e. 20 m), the boundary effect can be neglected in numerical modeling. Ten discretized sections were used to calculate the expansion force as introduced in Section 4.2.2. The analytical solution (Yu and Houlsby, 1991) was also used to calculate the expansion pressure, which was then used to calculate the expansion force with the same method introduced in Section 4.2.2.

4.4.2 Result Analysis

Figs. 4.7a and 4.7b illustrate the calculated expansion force from numerical modeling and analytical solution for different depths of cover as well as initial and final borehole radii using Methods A and B, respectively. For both solutions, the expansion forces increase with depth of cover due to increase in overburden stress. The slope of expansion force versus depth of cover in the analytical solution increases linearly as overburden stress is linearly proportional to expansion pressure, as discussed previously. Similar to the results in Fig. 4.6, the expansion force obtained from the analytical solution is higher than the corresponding result from the numerical modeling due to assumptions of an infinite medium and constant stress field in the analytical solution. However, the difference decreases as the depth of cover increases, and, in some cases, the results from the two solutions are almost the same when the depth of cover is 8.5 m. This is because, as the depth of cover increases, the medium becomes closer to being infinite. Table 4.2 shows that depth of cover is normalized with respect to final borehole diameter. With a greater value of h/D_n, the result difference between numerical and analytical solutions gets closer as illustrated in Fig. 4.7.

Table 4.2. Normalization of depth of cover with respect to final borehole diameter

Depth of cover, h	2.5	4.0	5.5	7.0	8.5
C1: Depth over final dia., h/D_n	10.0	16.0	22.0	28.0	34.0
C2: Depth over final dia., h/D_n	8.3	13.3	18.3	23.3	28.3
C3: Depth over final dia., h/D_n	5.9	9.4	12.9	16.5	20.0
C4: Depth over final dia., h/D_n	5.3	8.4	11.6	14.7	17.9

Fig. 4.7 confirms that both the radius ratio and initial radius affect the calculated expansion force from either solution. For the same initial radius but different radius ratios (i.e. C1 vs. C2 and C3 vs. C4 in Figs.4.7a and 4.7b), a small increase in the radius ratio results in a high increase in the expansion force. For a similar radius ratios but different initial radii (i.e. C1 vs. C4 in Fig.4.7a or 4.7b) the expansion force with the greater initial radius is significantly higher even though its radius ratio is slightly lower. As discussed for Fig. 4.5b, a higher expansion pressure is needed for a smaller initial borehole radius with the same radius ratio; in Fig. 4.7, the higher expansion force for the greater initial radius is attributed to the larger surface area of the conical expander. For the same reason, although the radius ratio in C2 is considerably greater than that in C3, the latter results in a higher expansion force, as shown in Fig. 4.7.

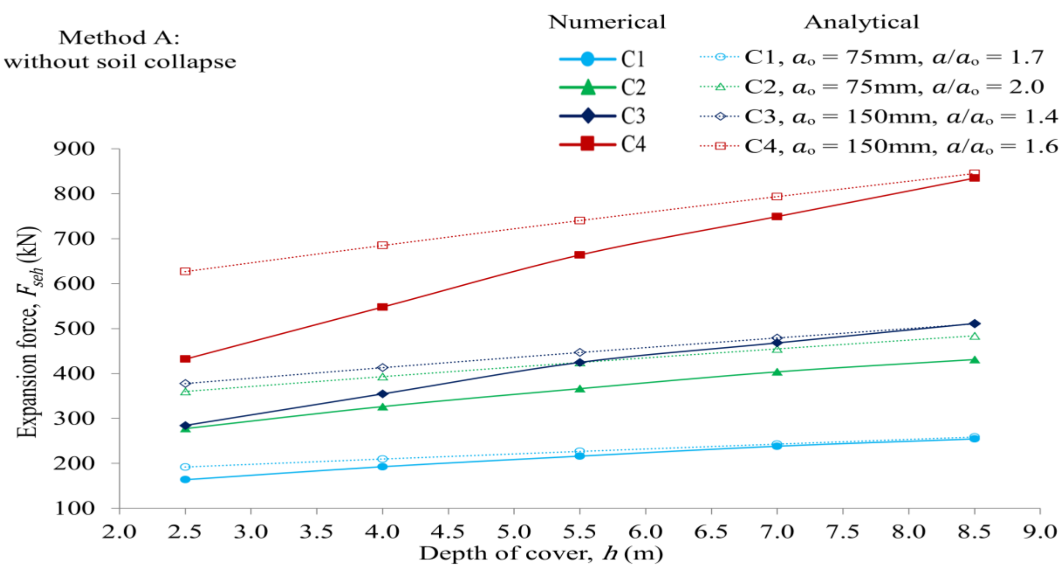

(a)

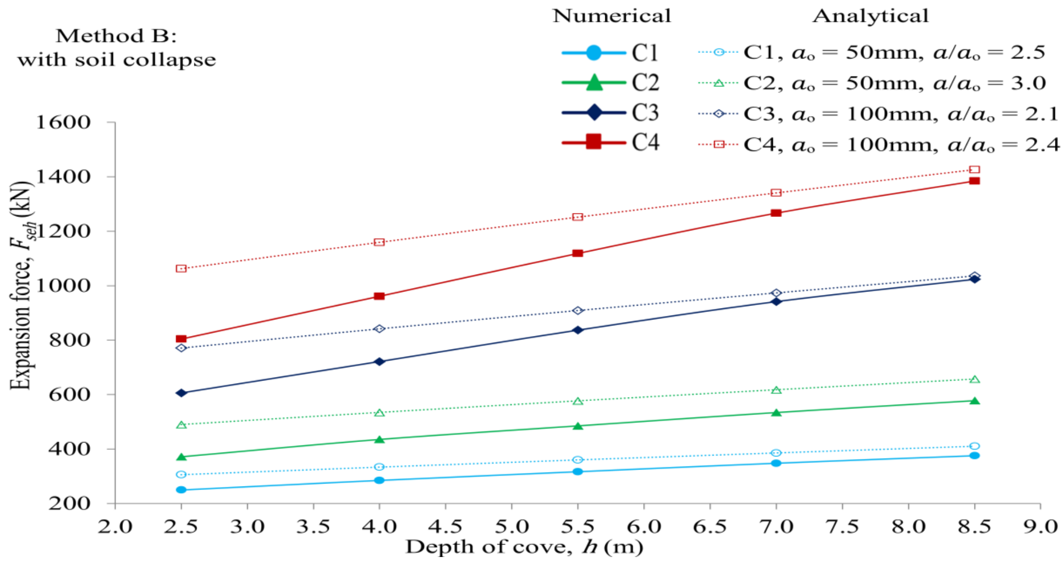

(b)

Fig. 4.7. Comparison of numerical and analytical solutions for expansion force in different depths of cover and pipe upsizing: a) Method A; b) Method B

The percentage discrepancy between analytical modeling and numerical solution for the same depth of cover and pipe upsizing is illustrated in Fig. 4.8. As expected, the discrepancy decreases when the depth of cover increases. The discrepancy is also larger for greater radius ratios with the same initial radius. The maximum discrepancy is approximately 30%, which occurs in C4 with a 2.5 m depth of cover calculated using Method A. The discrepancies are less than 25% for all results calculated using Method B, which is more accurate than Method A, as discussed in Section 4.3.3. Based on the findings in Fig. 4.8, it is suggested that the analytical cavity expansion solution (Yu and Houlsby, 1991) can be used to predict the soil expansion force in pipe bursting due to its simplicity in comparison to numerical modeling; however, it should be noted that it provides a conservative prediction, which is less than 30% for typical underground conditions in Edmonton.

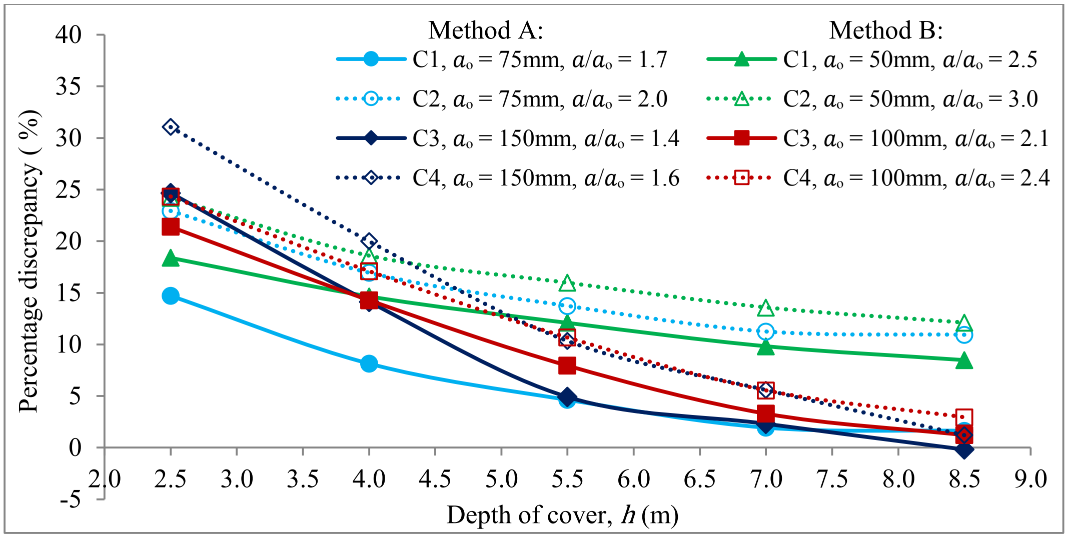

Fig. 4.8. Comparison of percentage discrepancy of expansion force between analytical and numerical solutions for the same depth of cover and pipe upsizing

4.5 Conclusions

The comparison of calculated and experimental results indicated that numerical modeling could properly predict the soil expansion force during pipe bursting by considering soil collapse. For small-scale laboratory experiment, there was no significant difference between the results from numerical modeling and analytical cavity expansion solution (Yu and Houlsby, 1991); however, the analytical solution cannot capture the effects of depth of cover, initial borehole radius (only the radius ratio), coefficient of lateral earth pressure, and boundary conditions. The parametric study results reveal that, although the soil expansion force obtained from analytical solution is higher than that from numerical modeling, the difference decreases when the depth of cover increases. Since the analytical solution is more simplistic for industry design compared to numerical modeling, it is suggested that the former can be used for conservative prediction with a discrepancy less than 30% for typical underground conditions in Edmonton. However, more experimental and field measurements are encouraged to validate and improve the calculation method. Additionally, the breaking length used in this study is based on an empirical estimation

(Ariaratnam and Hahn, 2007), which is only related to the original pipe thickness; hence, further study is also suggested for improvement.

Chapter 5: Summary, Conclusions, and Recommendations

5.1 Summary

Three cavity expansion solutions (Carter et al., 1986, Delft solution, and Yu and Houlsby, 1991) and numerical modeling via finite element software ABAQUS were used to determine soil expansion pressure acting upon the expander in static pipe bursting operations. The calculated pressures from expansion and numerical solutions were then used to calculate soil expansion forces without or with consideration of soil falling into the borehole due to crack propagation in original pipe during the expander's advancement. A comparison of calculated and measured soil expansion forces was conducted to investigate the feasibility of the calculation methods. Furthermore, a parametric study using numerical modeling and Yu and Houlsby (1991) solution was applied to glacial till typically found in Edmonton, Alberta to investigate the influence of different depths of cover and initial and final borehole radii on expansion force in static pipe bursting.

5.2 Conclusions

The conclusions for this thesis can be summarized as follows:

- Among the three cavity expansion solutions, Yu and Houlsby (1991) solution provided the most accurate prediction. The results obtained from Carter et al. (1986) solution significantly overestimated the soil expansion force as a small-strain analysis was adopted in the plastic displacement. Delft solution moderately underestimated the results as dilation angle was neglected. In static pipe bursting, borehole expansion occurs under large-strain deformations, and Yu and Houlsby (1991) solution fulfils this critical assumption as it presents calculated results agreeable to those measured.

- When comparing numerical modeling and Yu and Houlsby (1991) solutions, results obtained from both were approximate to experimental results with minor differences. This is because both solutions adopted Hooke's law, Mohr-Coulomb failure criterion, non-associated flow rule, large-plane strain analysis, as well as application both methods to small-scale experiments. However, Yu and Houlsby (1991) solution cannot capture the effects of depth of cover, initial borehole radius (only the radius ratio), and the coefficient of lateral earth pressure.
- The parametric study results indicated that expansion pressure in Yu and Houlsby (1991) solution increased linearly with depth of cover. The expansion force magnitude was also greater for higher borehole radius (expansion) ratios. Meanwhile, the force magnitude in numerical solution was less than that of Yu and Houlsby (1991) solution due to assumptions of infinite medium, constant field stress, and coefficient of lateral earth pressure.
- Since Yu and Houlsby (1991) solution is more simplistic for industry design compared to numerical modeling, it is suggested that the former can be used for conservative prediction with a discrepancy of less than 30% for typical underground conditions in Edmonton.

5.3 Limitations

The main limitations in the proposed methods for soil expansion force prediction are listed as follows:

- In the three cavity expansion solutions, the assumptions of infinite soil medium and a coefficient of lateral earth pressure (K_0) of one were adopted, neglecting boundary conditions. Soil-strain softening and hardening behaviors after yielding were not considered.

- In the cavity expansion and numerical solutions, plane-strain analysis, homogenous soil properties, and elastic-perfectly plastic medium were also adopted. All conditions where soil becomes dense during expansion and loose during collapse were neglected.
- The breaking length suggested by Ariaratnam and Hahn (2007) is empirical primarily based on industry experience.

5.4 Future Work

Future work should be conducted to improve the assumptions listed above. For numerical modeling, a three-dimensional space considering property change during pipe bursting process should be accommodated. Furthermore, a thorough study of the breaking length in different pipe sizes and materials is necessary to accurately predict the length. Additional field and experimental expansion force measurements, especially in large-scale tests, are necessary to validate and improve the proposed methods for the calculation of soil expansion force.

Appendix A: Evaluation of Pull Force Field Data for a Deep Pipe Bursting Project in Edmonton, Alberta

A version of this Appendix has been published as a conference paper in North American Society for Trenchless Technology in 2013. This paper was co-authored by Ka Hou Ngan, Somayeh Nassiri, Alireza Bayat, and Siri Fernando.

Abstract: A field study was conducted in collaboration with the City of Edmonton to further understand required pull forces during the pipe bursting process in cold climates with a high overburden. The project included replacing approximately 300 meters of a defective 300-mm diameter sanitary clay tile pipe, with a 450-mm diameter vitrified clay pipe at the original alignment and grade, using pipe bursting method. Pull forces required to burst the pipe during the construction were measured on site. The majority of measured pull forces followed the anticipated increasing trend by the increase in length of new pipe. Simplified theoretical model for numerical calculation of pull forces in static pipe bursting operations developed by Ariaratnam and Hahn in 2007 was used to estimate the required pull forces, using the geotechnical information, pipe specifics and other site-specific information available for the project. The model's predictions were evaluated using the field measurements. It was found that the model provides a good estimation for maximum pull forces, especially for lengthy installation of new pipe.

A1 Introduction

Static pipe bursting is a trenchless technology used mainly to replace buried undersized and/or structurally deteriorated pipelines. This rehabilitation technology has substantial benefits for underground construction. It effectively reduces the amount of required construction area, thereby limiting surface disruption during the pipe bursting operation. Pipe bursting in comparison to an open-cut project can significantly reduce traffic, business, pedestrian and environmental disturbance.

This paper presents the pullback forces measurements taken at the site for a 300-m pipe bursting project in Edmonton, Alberta. The project is unique in the sense that it's located in a cold region, where pipes are buried as deep as six meters, hence dealing with high overburden. Failure for the pipe to withstand the vertical overburden and traffic pressures will damage the entire pipe bursting project, since the excessive pressures can easily compress and break the pipe into pieces. Furthermore, the high overburden pressures require higher pull force which generates high tensile stresses on the new pipe (Plastics Pipe Institute, 2007). The theoretical model developed by Ariaratnam and Hahn (2007) was used to predict the pullback force measurements for five different pipe replacement sections. The purpose is to show the agreement between the theoretical model's predictions and the field measurements, thereby identifying the strengths and deficiencies of the theoretical model. The study intends to help the underground construction industry to effectively estimate the required pull forces during the pipe bursting process.

A2 Project Description

The Static pipe bursting project was conducted from 88th Street to the center of 90th and 91st Street along 127th Avenue in Edmonton, Alberta. An approximately 300-m original pipe was replaced as deep as 4.5 and 7.3 meters below ground surface at an average gradient of 0.46%. The project was the last portion of 127th Avenue Opportunistic Sewer Separation project, which separated existing combined sewer system into storm and sanitary sewer systems and it conveys the sanitary sewer from the adjacent neighborhoods into a 900 mm sanitary trunk. Due to the deterioration of the existing pipe and the requirement of additional capacity, a 450-mm diameter vitrified clay pipe was utilized to replace the 300-mm diameter sanitary clay tile pipe along the same trajectory as the original pipe. Two lengths of sectional pipe, rather than continuous pipe, were used. Two-meter pipes were pulled in place from 88th street to the center of 89th and 90th street, and one-meter pipes were placed from the center of 89th and 90th street to the center of 90th and 91st Street. A stainless iron ring was attached to the tailing end of the front pipe and leading end of the rear pipe to hold the pipes together. Lubricant was applied to the surface of the new pipeline to reduce friction between the surrounding soil and the pipeline to reduce the coefficient to friction of less than 0.3.

A2.1 Site Layout

A schematic plan view of the construction site is presented in Fig. A1. A total of four insertion pits, each 9.1 m by 2.4 m, as well as two 6.1 m by 1.8 m machine pits were excavated along 127th Avenue. As seen in Fig. A1, the first machine pit was located midway between 88th and 89th Street and the second machine pit was located midway between 90th and 91st Street. As illustrated in Fig. A1, the first, second, third and fourth insertion pits were located at 88th, 89th, the center of 89th and 90th, and 90th Street, respectively.

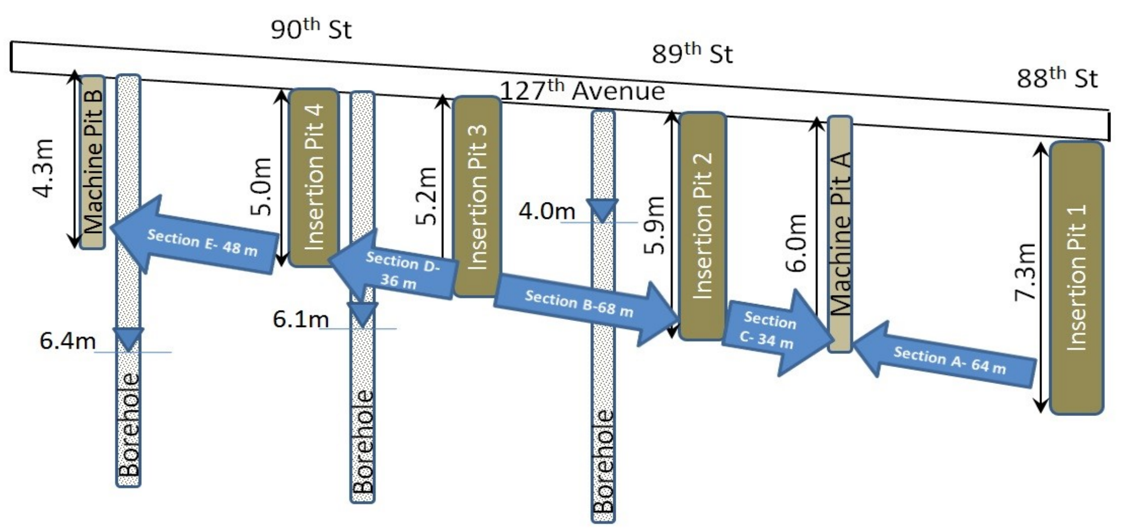

Fig. A1. Schematic layout of five pipe bursting sections along 127th Avenue, Edmonton

127th Avenue is a four lane undivided arterial roadway. The north side of 127th Avenue is mainly bounded by single-family residential housing and various commercial uses on the south. The project was conducted between June 8 and August 24, 2012 with a total of five sets of bursting operations. The first set of pipe bursting (Section A in Fig. A1) with a 64 m length was pulled from the first insertion pit towards the first machine pit. The second set, (Section B) with a 68 m length, was from the third insertion pit towards the first machine pit, and the pulling was stopped when new pipe reached the second insertion pit. The third set (Section C) was from the second insertion pit towards the first machine pit and was 34-m long. The fourth set (Section D) was from the third insertion pit towards the second machine pit, and the pulling was stopped when the new pipeline reached the fourth insertion pit. Section D was 36 m in length. The fifth set (Section E) was from the fourth insertion pit towards the second insertion pit and was 52 m long. Three boreholes located between 88th and the centers of 90th and 91st Streets were drilled and one borehole was drilled in 2005. The pavement structure on 127th Avenue is composed of an asphalt layer with a thickness of approximately 250 mm and a concrete base with a thickness of 150 mm. Based on extrapolation between borings, clay fill ranging from 0.3 to 1.2 m is located below the pavement structure. Glacio-lacustrine clay ranging from 1.4 to 4.3 m is present below the clay fill. Glacial clay till, which commences at a depth between 4.7 to 6.2 m, is situated below the Glacio-lacustrine clay.

A2.2 Description of Equipment and Installation Procedure

The operation of static pipe bursting mainly consists of five essential pieces of equipment: a pulling machine, a hydraulic power unit, an expander, squeezer, and pulling rods. The pulling machine used for the project was Grundoburst 1900G, with a maximum pull force of 1900 kN. The external hydraulic power unit TT B110 supplied the pulling machine with power. The expander was a conical shaped with four cutting fins attached, where its widest diameter is larger than that of the original pipe and the new pipeline by 340 and 200 mm, respectively. The pulling rods were 2.25 m long with a pilot sleeve attached to the leading end of the rod for the purpose of guiding the rod string through the original pipe. Initially, pipe bursting was conducted by pushing pulling rods through the original pipe. A squeezer or cylinder pack with pressure plate located at insertion pit was utilized to facilitate pushing sectional new pipes into the entrance of the original pipe. Squeezer also helped keep the assembled pipe sections under compression to keep the pipe joints tight, when the expander was pulled forward through the original pipe. The reason of using the squeezer is that the joints were not restrained. The pulling machine dragged pulling rods, with expander attached, towards the machine pit from insertion pit, while a hose connected to a lubrication tank injected lubricant onto the surface of the new pipeline to reduce the friction force between the surrounding soil and the pipeline during the pipe bursting process. The expander shattered the original pipe and forced its fragments out into the surrounding soil by the radial force applied to the pipe wall from the expander within the pipe. The new pipeline was attached to the rear of the expander and was pulled or dragged into place at the original alignment and grade simultaneously, as the expander displaced the surrounding soil for creating a cavity for the new pipe.

A3 Analysis of Field Data

During the pipe bursting operation, the maximum pull back force and duration of pulling the new product pipe into place were recorded for each section of replacement. Before and after the completion of pipe bursting for each section, permanent vertical ground displacements were recorded for each section of new pipes with a total of three measurements taken at different spots using a Total Station. One measurement was taken at the centerline of the pipeline, and the other two were taken at 0.5 m offset north and 0.5 m offset south of the centerline.

A3.1 Analysis of Pull Forces Data

As described previously, the pipe bursting project was conducted in five sections. Each corresponding sectional length varied from 34 to 68 m. To advance the new pipe, the pull force must be large enough to overcome all the frictional forces and the horizontal component of the breaking force. Maximum pull forces for a total of 123 pipe segments were recorded in the field for the five sections, using a force gage embedded in the pulling machine. The pull force measurements for each section are presented in Fig. A2. As seen in Fig. A2, the magnitude of the measured pull force increases with the increase in pipe segment number for Sections A, B, C and E. Section D is an exception from this behaviour and shows a relatively flat trend with peak pull force occurring at approximately the middle of the new pipeline. The soil in the middle was harder than other locations based on the geotechnical report and observation. According to the geotechnical report, the soil in Section D was identified as stiff clay, and wet sand in Section A, B and C, and very thin sand and clay fill in Section E at the location of the existing pipeline. Short distance and no frame in the middle pit may cause the flat trend. The initial pull force for each section, is approximately 855 ± 95 kN, and is relatively consistent, except for Section D, which shows an initial pull force of 608 kN.

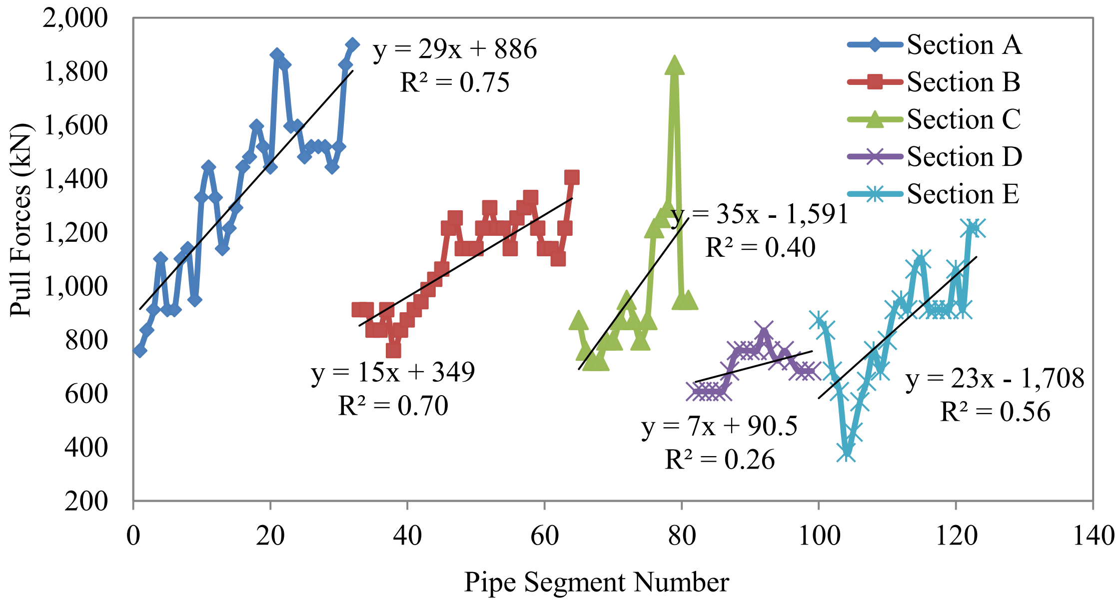

Fig. A2. Pull force measurements during replacement for each section along the project

The highest pull force of 1,900 kN was recorded at the final segment of new pipe in section A, and is located 64 m away from its insertion pit. Two exceptionally high and low peaks are noticed in Sections C at the end of each run in Fig. A2. For Section C, at the machine pit, a steel plate with a small opening was installed between the soil and the bursting frame. The small opening in the steel plate was intended to prevent excess soil from being pulled out of the machine pit and therefore to minimize the ground movement. For Section C, due to the lack of experience of the operation crew, the expander actually cut into the steel plate so that the pull force peaked at this time. After the steel plate was pulled out, the pull force was substantially lowered. The reason for the sudden drop of pullback force at early stage in Section E is not clear.

A4 Theoretical Prediction of Pull Force and Comparison with Field Data

Selection of the appropriate pulling machine is critical during a pipe bursting process. Failure to pull new pipeline in place due to insufficient pull force can have significant impact on project delivery date, cost, equipment, and safety of personnel. For most cases, the selection of pulling machine is based on past experiences and rules of thumb. This method of decision making creates numerous uncertainties due to variations of soil properties, depth of cover, and pipe material strength and size at different sites.

A theoretical model can be implemented to accurately predict pull forces. For a successful pipe bursting operation, the pull force generated from the pulling machine must be large enough to overcome all resistance forces. Resistance forces primarily include three components: friction, breaking, and soil expansion (compression) force.

During the pipe bursting process for replacing pipe, the friction force is primarily developed between the surface of new pipeline and the surrounding soil. For the pipe bursting project completed by the City of Edmonton, the resistance force was significantly reduced by lubricating the surface of new pipe and by using an expander larger than the pipe. Lubrication can reduce the friction between the soil and pipe interfaces. When the expander is moving forwards from the insertion pit, the cavity will be automatically developed through the advancement of the oversize tail end of the expander. The friction force will frequently govern the pull force in lengthy installation of new pipe due to the long constructional length. Ariaratnam and Hahn (2007) proposed a theoretical model for estimating friction force during static pipe bursting, see Equation A1.

$$F_f = \mu_{sp} \cos(\theta_p) (p_0 S_n + W_n) \tag{A1}$$

Where μ_{sp} is the coefficient of friction, θ_p is the slope angle of the original pipe, which is used to convert p_0 and W_n in the direction parallel to the original pipe, $p_0$is the effective soil pressure applied on the pipe, S_n is the outside surface area of the new pipe, and W_n is the weight of the new pipe. Normal force for this project is a function of the effective soil stress at the centerline of the existing pipe and the weight of the new pipe. The coefficient of lateral earth pressure, K_0, is assumed to be equal to one. Force due to soil pressure can be obtained by multiplying soil pressure to the outside area of new pipe. The magnitude of soil pressure is also influenced by the level of existing groundwater. Groundwater above the original pipe can reduce the normal force applied on the pipe due to the decrease of effective stress and vice versa.

The breaking force is the force required to break the original pipeline into fragments during a pipe bursting operation. These pieces are then pushed outwards into the surrounding soil during the advancement of the expander. The magnitude of breaking force is a function of the original pipeline dimension and wall thickness and the pipeline material strength and behaviour.

In pipe bursting projects, the primary resistance of fracturing the pipeline arises from cylinder stress, which consists of hoop and longitudinal stresses. Hoop stress, is the principal normal stress in the surface of thin-walled pressure vessels, which tends to make the pipe diameter expand outwards. The breaking force must exceed the hoop stress in order to break the pipeline into pieces or cut it into strips. The breaking force is determined using the following equation developed by Ariaratnam and Hahn (2007).

$$F_h = \sigma_{1e} t_{po} \Delta x \tag{A2}$$

$$F_{bh} = f_{np} \tan\left(\frac{\theta_e}{2}\right) F_h \tag{A3}$$

Where F_h is the hoop force, σ_{1e} is the ultimate tensile strength of original pipe, t_{po} is the wall thickness of original pipe, Δx is the breaking length, which is $10 \times t_{po}$ based on suggestions from industry experience as stated by Ariaratnam and Hahn (2007), F_{bh} is the breaking force parallel to pull force, f_{np} is the number of pieces factor, which is equivalent to the number of cutting fins welded to the expander for ductile material of original pipe, θ_e is the angle of expander, which converts the breaking force in the direction parallel to the pull force.

Soil expansion force, as defined by Ariaratnam and Hahn (2007) and Nkemitag (2007), is the force that is necessary to displace or shift the soil from the edge of the outside diameter of the original pipe to the edge of the outside diameter of the expander at tail end. For the calculation of soil expansion force, it is assumed that the soil is only displaced outwards or perpendicular to the pipe and parallel soil expansion does not occur. The soil expansion (compression) limit factor is an uncertainty factor applied into the equation of soil expansion force to account for the extent of soil mobilization, to account for the fact that K_0 is not equal to one in reality, and for the existence of parallel soil expansion force. The breaking force is determined using the following equations proposed by Ariaratnam and Hahn (2007).

$$A_{se} = \pi(d_{on} + 2L_{os})L_{se} \tag{A4}$$

$$L_{se} = \Delta x + \Delta h_e \tag{A5}$$

$$\Delta h_e = [(d_{on}/2 + L_{os}) - (d_{oo}/2)]/\tan(\frac{\theta_e}{2}) \tag{A6}$$

$$F_{seh} = f_{sel}\, tan\left(\frac{\theta_e}{2}\right) cos\left(\theta_p\right) p_0 A_{se} \tag{A7}$$

Where A_{se} is the area of soil expansion, d_{on} is the outside diameter of new pipe, L_{os} is the length of oversize, which is half length difference between outside diameter of expander at tail end and outside diameter of new pipe, $L_{se}$is the length of soil expansion, Δh_e is the exposed length of expander, d_{on} is the outside diameter of original pipe, F_{seh} is the horizontal component of soil expansion force, and f_{sel} is the soil expansion limit factor.

The magnitude of theoretical pull force is the sum of friction force (F_f), breaking force (F_{bh}), and soil expansion force (F_{seh}). The theoretical pull force is determined as follows:

$$F_p = \left(\alpha_L/\varphi_p\right) * (C_f * F_f + C_b * F_{bp} + C_{se} * F_{seh}) \tag{A8}$$

Where α_L is the load uncertainty factor to imply that resistance forces encountered during pipe bursting process are larger than those evaluated, which is set at 1.1, φ_p is the pull force reduction factor for attempting to avoid pulling machine from running at maximum power output, which is set at 0.9, C_f is the correction factor of friction force, C_b is the correction factor of breaking force, and C_{se} is the correction factor of soil expansion force.

A sensitivity analysis was developed due to unavailability of precise values for the coefficient of friction. A comparison of the theoretical and experimental pull forces for all sections with different values for the coefficient of friction was conducted. Section D was removed from the analysis due to the abnormal trend compared to the trends observed for the other sections. In addition, one outlier from Section C was also discarded because of human error during operation for Section C as mentioned earlier. Coefficient of determination (R^2) between the predicted and measured forces for all sections is shown in Table A1. Coefficient of friction at soil/pipe interface is typically within 0.3 - 0.5 range without lubrication (Peng, 1978). Since no suggested values were found for the coefficient of friction when lubrication is used, a wide range of 0.05-0.5 was used in a sensitivity analysis to predict the pull force for each section. A comparison between the predicted and measure pull forces can be used to identify the best value for the coefficient of friction. As seen in Table A1, the best prediction for Section A is obtained for coefficients of 0.2 and 0.25 at coefficient of determination (squared-R) of 72% between the pull forces predicted by the theoretical model and the forces measured. This value is 0.175 for Section B with R^2 of 65%, 0.25 for Section C with R^2 of 64%, and 0.175 for Section E with R^2 of 68%. Fig. A3 shows the best predicted pull forces for each section in comparison to the field measurements.

Table A1. Summary of coefficients of determination for pull force predictions for Sections A, B, C and E

Coefficient of Friction	Coefficient of Determination, R^2 (%)				
	Section A	Section B	Section C	Section E	Average
0.05	49	50	49	47	49
0.1	53	55	50	52	53
0.15	61	63	53	65	61
0.175	67	65	55	68	65
0.2	72	64	59	67	67
0.225	72	62	62	65	66
0.25	70	60	64	62	64
0.3	64	56	63	59	60
0.35	60	55	61	56	57
0.4	57	54	58	55	55
0.45	56	53	56	54	54
0.5	55	52	55	54	54

Coefficient of determination can be used to determine the ability of the theoretical model in predicting the actual measurements. The value of R^2 ranges from 0 to 100, and a large value of R^2 typically manifests that the model has a high and accurate goodness of fit with experimental data. For the theoretical model developed by Ariaratnam and Hahn (2007), almost all values of R^2 for various coefficients of friction are well above 50 percent in Table A1, with a minimum R^2 of 47 percent and a maximum R^2 of 72 percent. Accordingly, the theoretical model can be classified as good for estimating the measured pull force during pipe bursting operation.

As seen in Fig. A3, the theoretical model can predict the middle and upper portions of pull force for all sections. A large discrepancy is however evident at lower forces between the theoretical and experimental pull forces for all sections. According to Pipe Bursting Good Practices Guidelines 2011 (Bennett et al., 2011), there are two reasons for poor model predications at the start of pipe bursting. First, the annulus at the entrance of original pipe in most real cases remains open initially; hence very low vertical effective stress (p_0) exists. However, as the expander and new pipe progress, the annulus may progressively close for soft clays and loose to medium dense sand, with a corresponding increase in p_0. Second, buoyancy of pipe due to the existence of groundwater reduces and affects the magnitude of p_0. This in turn also lowers the friction force. However, only a small amount of groundwater leakage was observed during pipe bursting operation and the buoyancy of pipe was not considered in predicting the pull forces.

At the start of pipe bursting operation, breaking and soil expansion forces are the primary resistance force. After reaching a certain point such as passing the second segment of replacing pipe in this project, the magnitude of friction force eventually outweighs the other force components. Fig. A4 shows that the magnitude of pull force at the early stage is significantly influenced by breaking and soil expansion forces. The occurrence of large discrepancy primarily results from low soil expansion force (F_{seh}) when comparing experimental F_{seh} measured by Lapos (2004) in their project and the theoretical F_{seh} we calculated using the theoretical model for 127th Avenue project. He conducted pipe bursting experiments covering four different combinations of initial pipe diameter and burial depth in a 2 m wide by 2 m long by 1.6 m deep steel tank. Poorly-graded sand was used as a backfill material and an expander with a maximum outside diameter of 202 mm was used to break the clay pipe. Table A2 summaries the material type and dimension for existing and replacing pipeline, burial depth, and average experimental $F_{seh.}$ As seen in Table A2, burial depth has the highest influence on the magnitude of soil expansion force. When comparing these two project scopes, burial depth for 127th Avenue project is within 4.3 – 7.3 m range which is deeper than that of Lapos' (2004) test (685 – 885 mm). However, the theoretical F_{seh} we calculated is within 36.2 - 40.8 kN range which is not significantly different to the experimental soil expansion force (17.4 – 36.0 kN) measured by Lapos (2004).

Table A2. Summary of Lapos' (2004) static pipe bursting experiments

Original pipeline	Material Type	Inside Diameter (mm)	Wall Thickness (mm)
1	Clay Pipe	100	14
2	Clay Pipe	146	19

New Pipeline	Material Type	Inside Diameter (mm)	Wall Thickness (mm)
A	High Density Polyethylene (HDPE)	145	10

	Type of Replacement	Burial Depth (mm)	Average Experimental Soil expansion Force (kN)
Test #1	Same-size (2->A)	685	17.4
Test #2	Upsize (1->A)	685	21.5
Test #3	Same-size (2->A)	885	33.1
Test #4	Upsize (1->A)	885	36.0

There are three primary factors that influence the magnitude of soil expansion force. First, lateral earth pressure (K_0) in the theoretical model was assumed to be one for the purpose of simplifying calculation on the model. In practice, the K_0 value should be refined and adjusted based on different types of soil. Second, the model presumed that the soil is only compressed purely perpendicular to the centerline of the original pipe axis as indicated by Ariaratnam and Hahn (2007). Second assumption implies the inexistence of parallel soil expansion in the direction parallel to the slope of original pipe. In fact, the existence of parallel soil expansion has been proved through observation that some soil is dragged out when the expander is leaving the exit hole at the machine pit. Third, soil displacement, whether the soil surface heave or settlement occurs, during pipe bursting operation has strong influence on the magnitude of soil expansion force. For modeling this force, the soil displacement or extent of soil mobilization was not considered. In fact, soil expansion limit factor must be adjusted to consider possible uncertain soil factors instead of assigning the limit factor to one, and further research is needed to come up with a more realistic value and range for the limit factor in different site situations. Furthermore, experimental pull force for Section B at upper portion is relatively flat with minor fluctuations. In reality, the pull force is expected to increase with increase of pulling stages due to the fact that friction force is depending on the length of replacing pipe in contact with the surrounding soil.

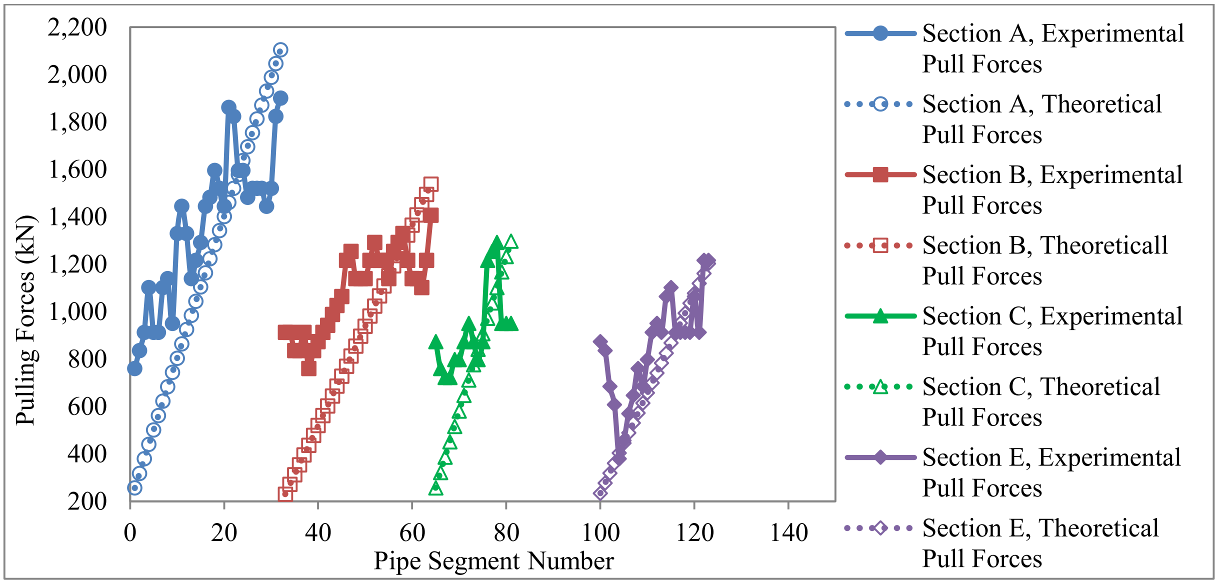

Fig. A3. Comparison of theoretical and experimental pull force with coefficients of friction of 0.2 for Section A, 0.175 for Section B, 0.25 for Section C, and 0.175 for Section E

From Table A1, the maximum average coefficient of determination occurs for coefficient of friction of 0.2 and its value is 67 percent, at which the optimal model for theoretical pull force can be obtained for all the sections. A decomposition of theoretical pull force into friction, bursting and soil expansion forces with coefficient of friction of 0.2 for all sections is presented in Fig. A4. Once the expander passes the second segment of new pipe for each section, the theoretical friction force governs the pull force with significant fluctuations and rapidly increases with increase of segment number for all sections. The maximum theoretical friction force of approximately 1564 kN occurs at the last new pipe's segment in Section A. This is due to the fact that the length of replacement is almost the longest in Section A. In contrast, theoretical bursting and soil expansion forces are flat trends with no obvious fluctuations. For the theoretical breaking force, its values are constant with the magnitude of 119 kN for all sections. In fact, it is expected a higher breaking force at the start of breaking original pipe due to initial crack and a lower breaking force during crack propagation only if cracking is continuous. The fragments of broken original pipe would also affect the magnitude of required breaking force through impeding the advancement of new pipeline. For the theoretical soil expansion force, it shows minor fluctuations with the peak value of 41 kN. Minor fluctuations were caused by uneven depth of cover along the length of pipe bursting operation since vertical effective stress is a function of burial depth and assumption of uniform soil pressure applied on the surface of the original pipe. As stated earlier, the soil expansion limit factor is an important factor that accounts for uncertain soil behavior. This factor was set at one due to insufficient information for determining this parameter.

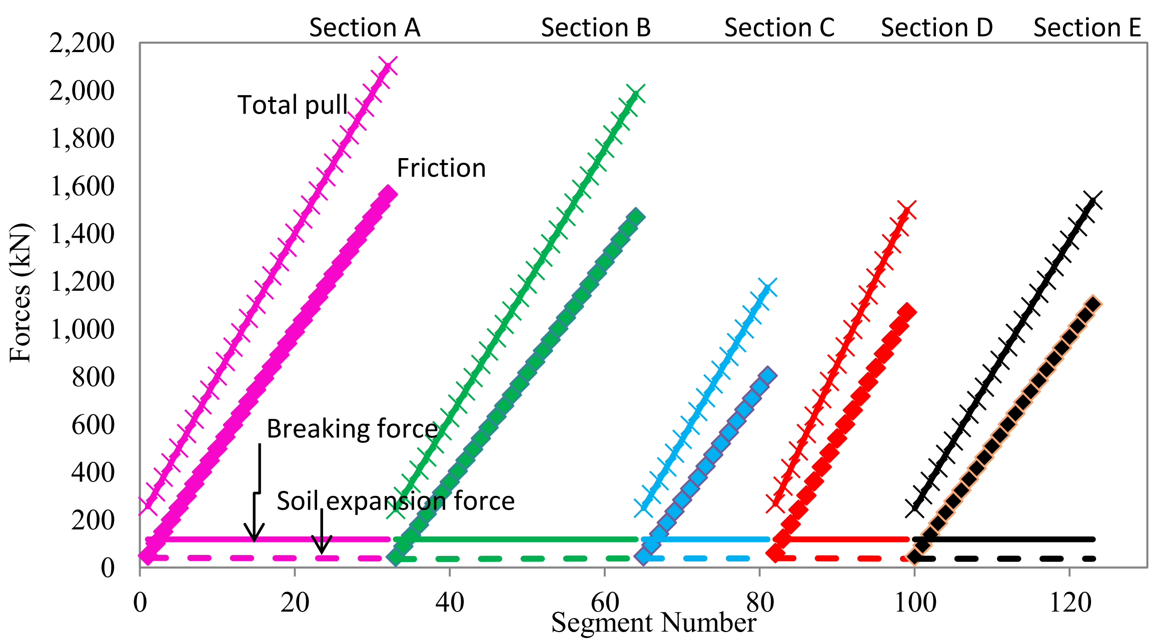

Fig. A4. Decomposition of theoretical pull force with coefficient of friction of 0.2

A5 Conclusions

The field study in collaboration with the City of Edmonton provides us valuable data and measurements to verify the accuracy of the theoretical model of pullback force developed by Ariaratnam and Hahn (2007). The magnitude of the pullback force in this model is a function of three various force components: the friction force, the breaking force, and the soil expansion force. The values of breaking and soil expansion forces are almost constant for all sections. The values of friction force, in contrast, are rapidly increasing as observed by the increase in segment number for all sections. The force governs the pull force in lengthy new pipe installation projects. The numerical model provides a good estimation of predicting experimental maximum pullback force during static pipe bursting. Rational adjustments and proper assumptions are required for the uncertain factors and parameters as discussed above. This can help to minimize uncertainty in the model. The theoretical modal for static pipe bursting can help industry select the proper pulling machine for pipe bursting operations in accordance with maximum theoretical pull force during pre-construction.

References

Ariaratnam, S. T., and Hahn, U. H. (2007). "Simplified model for numerical calculation of pull forces in static pipe-bursting operations." *Tunneling and underground space technology*, 22(5), 644-654.

Ariaratnam, S. T., Lueke, J. S., and Michael, J. K. (2014). "Current trends in pipe bursting for renewal of underground infrastructure systems in North America." *Tunneling and Underground Space Technology*, 39, 41-49.

Atalah, A., Sterling, R., Hadala, P., and Akl, F. (1997). "The effect of pipe bursting on nearby utilities, pavement, and structures." Technical Report, Louisiana Tech University, Ruston, USA.

Bennett, R. D., Khan, S., and Ariaratnam, S. T. (2011). "NASTT Pipe Bursting Good Practices Guidelines Manual - 2011." North American Society for Trenchless Technology, Arlington, USA.

Bennett, R.D., and Wallin, K. (2008). "Step by Step Evaluation of Hydrofracture Risks for HDD Projects." *Proc., 2008 North America No-Dig Conference*, Dallas, USA.

Bigoni, D., and Laudiero, F. (1989). "The quasi-static finite cavity expansion in a non-standard elasto-plastic medium." *International journal of mechanical sciences*, 31(11), 825-837.

Bishop, R. F., Hill, R., and Mott, N. F. (1945). "The theory of indentation and hardness tests." *Proceedings of the Physical Society*, 57(3), 147.

Brachman, R., McLeod, H., Moore, I., and Take, W. (2010). "Three-dimensional ground displacements from static pipe bursting in stiff clay." *Canadian Geotechnical Journal,* 47 (4), 439-450.

Bradley, W. B. (1979). “Failure of inclined boreholes.” *Journal of Energy Resource and Technology*, 101, 232-239.

Caquot, A., and Kerisel, J. (1966). “Traite de Mecanique des Sols.” Gauthier-Villars.

Carter, J. P., Booker, J. R., and Yeung, S. K. (1986). “Cavity expansion in cohesive frictional soils.” *Geotechnique*, 36(3): 349-358.

Chadwick, P. (1959). “The quasi-static expansion of a spherical cavity in metals and ideal soils.” *The Quarterly Journal of Mechanics and Applied Mathematics*, 12(1), 52-71.

Charlez, Ph., and Heugas, O. (1991). “Evaluation of optimal mud weight in soft shale levels.” *Rock Mechanics as a Multidisciplinary Science*, Balkema, 1005-1014.

Chehab, A. G., and Moore, I. (2010). “Pipe-soil shear interaction stiffness in horizontal directional drilling and pipe bursting.” *Geomechanics and Geoengineering: An International Journal*, 5(2), 69-77.

Cholewa, J. A., Brachman, R. W. I., and Moore, I. D. (2009a). “Response of a polyvinyl chloride water pipe when transverse to an underlying pipe replaced by pipe bursting.” *Canadian Geotechnical Journal*, 46(11), 1258-1266.

Cholewa, J. A., Brachman, R. W. I., Moore, I. D., and Take, W. A. (2009b). “Ground displacements from a pipe-bursting experiment in well-graded sand and gravel.” *Journal of Geotechnical and Geoenvironmental Engineering*, 135(11), 1713-1721.

Clarke, B. G. (1995). “Pressuremeter in Geotechnical Design.” Chapman and Hall, London.

DeJong, J., and Harris, M. C. (1971). “Settlements of Two Multistory Buildings in Edmonton.” *Canadian Geotechnical Journal*, 8(2), 217-235.

Detournay, E., and Cheng, A. H. D. (1988). “Poroelastic response of a borehole in a non-hydrostatic stress field.” *International Journal for Rock Mechanics and Mining Sciences*, 25(3), 171-182.

El-Nahhas, F. (1977). “Field measurements in two tunnels in the City of Edmonton.” Master Thesis, Department of Civil Engineering, Univ. of Alberta, Alberta, Canada.

Eisenstein, Z., and Thomson, S. (1978). “Geotechnical performance of a tunnel in till.” *Canadian Geotechnical Journal*, 15(3), 332-345.

Elwood, D., Martin, C. D., and Dafni, J. (2011). “Ground characteristics for the design of the Edmonton North LRT Twin Tunnels.” *Proc., of 14th Pan-American EGS Conference on Soil Mechanics and Geotechnical Engineering*, Toronto, Ontario.

Express Plumbing & Rooter (2013). “Pipe Lining Technology.” Retrieved June 20, 2014, from http://www.expressplumbingandrooter.com/pipeline.html

Fernando, V., and Moore, I. D. (2002). “Use of cavity expansion theory to predict ground displacement during pipe bursting.” *Proceedings of the Pipelines 2002*, American Society of Civil Engineers, Cleveland, USA.

Fraser, R., N. Howell., and R. Torielli. (1992). “Pipe Bursting: The Pipeline Insertion Method.” *Proc., No-Dig International 92*, Washington D.C., North American Society for Trenchless Technology, Arlington, USA.

Hill, R. (1950). “The mathematical theory of plasticity.” Oxford University Press, London.

Howell, N. (1995). “The PE pipe Philosophy for Pipeline Renovation.” *Proceedings of the No-Dig International 95*. The International Society for Trenchless Technology, Dresden, Germany.

Houlsby, G. T. (1991). "How the dilatancy of soils affects their behaviour." *Proceedings of the 10th European Conference on Soil Mechanics and Foundation Engineering*, Florence, Italy.

International Pipe Bursting Association. (2012). "Guideline for Pipe Bursting." International Pipe Bursting Association (IPBA), 1-29.

Kazi, M. R. (2013). "Three Dimensional Numerical Analysis of Static Pipe Bursting." PhD Thesis, Department of Civil Engineering, Queen's University, Kingston, Canada.

Keulen, B. (2001). "Maximum allowable pressures during horizontal directional drillings focused on sand." Delft University of Technology, Delft, Netherlands.

Lapos, B. (2004). "Laboratory study of static pipe bursting: Three-dimensional ground displacements and pull force during installation, and subsequent response of HDPE replacement pipes under surcharge loading." Master Thesis, Department of Civil Engineering, Queen's University, Kingston, Canada.

Lapos, B., Brachman, R. W. I., and Moore, I. D., 2007. "Response to overburden pressure of an HDPE pipe pulled in place using pipe bursting." *Canadian Geotechnical Journal*, 44(8), 957-965.

Leach, G., and Reed, K. (1989). "Observation and assessment of the disturbance caused by displacement methods of trenchless construction." *Proceedings of the 4th International Conference on Trenchless Construction Utilities*, NO-Dig 89, London, United Kingdom.

Lee, H., Najafi, M., & Matthys, J. (2007). "Cost comparison of pipeline asset replacement: open-cut and pipe bursting." *Proceedings of the ASCE International Pipeline 2007 Conference,* Boston, Massachusetts.

Lueke, J. S., and Ariaratnam, S. T. (2001). "Rehabilitation of underground infrastructure utilizing trenchless pipe replacement." *Practice Periodical on Structural Design and Construction,* 6(1), 25-34.

Luger, H. J., and Hergarden, H. J. A. M. (1988). "Directional Drilling in Soft Soil: Influence of Mud Pressures." *Proceedings of the 3rd International Conference on Trenchless Technology – No Dig Conference*, Washington, D.C., United States.

May, R. W., and Thomson, S. (1978). "The geology and geotechnical properties of till and related deposits in the Edmonton, Alberta, area." *Canadian Geotechnical Journal*, 15(3), 362-370.

McLeod, H.A. (2008). "Field measurement of surface displacements from pipe bursting." Master Thesis, Department of Civil Engineering, Queen's University, Kingston, Canada.

Medeiros, L. V., and Eisenstein, Z. (1983). "A deep retaining structure in till and sand. Part I: stress path effects." *Canadian Geotechnical Journal*, 20(1), 120-130.

Najafi, M., Ed. (2007). "Pipe bursting projects." ASCE Manuals and Reports on Engineering Practice 112. American Society of Civil Engineers, Reston, USA.

Ngan, K. H., Rostami, A., Yi, Y. L., and Bayat, A. (2014). "Predicting soil expansion force during static pipe bursting using cavity expansion solutions." International Journal of Geomechanics, submitted.

Nkemitag, M. (2007). "Numerical Investigation of Ground Movements and Pulling Forces during Static Pipe Bursting." PhD Thesis, Department of Civil Engineering, Queen's University, Kingston, Canada.

Nkemitag, M., and Moore, I. D. (2007). "Longitudinal Progression of Burst Head during Pipe Bursting: Calculation of Pulling Force." *Transportation Research Record: Journal of the*

Transportation Research Board, No. 2028, Transportation Research Board of the National Academies, Washington, D.C., 203-210.

Peck, R.B. (1969). “Deep Excavations and Tunneling in Soft Ground: State of the Art Report.” *Proc., of the 7th International Conference on Soil Mechanics and Foundation Engineering*, State of the Art Volume, Mexico.

Peng, L. C. (1978). “Soil- pipe interaction - Stress Analysis Methods for Underground Pipe Lines”, AAA Technology and Specialties Co., Houston, Texas, pp. 67-76.

Plastics Pipe Institute. (2007). “Handbook of Polyethylene Pipe: Second Edition.” Plastics Pipe Institute, 535-583.

Rogers, C. D. F., and Chapman, D. N. (1995). “An experimental study of pipe bursting in sand.” *Geotechnical Engineering*, 113(1), 38-50.

Santarelli, F. J., Brown, E. T., and Maury, V. (1986). “Analysis of borehole stresses using pressure-dependent, linear elasticity.” *International Journal for Rock Mechanics and Mining Sciences*, 23(6), 445-449.

Shi, J., Wang, Y., and Ng, C. W. (2013). “Buried pipeline responses to ground displacements induced by adjacent static pipe bursting.” *Canadian Geotechnical Journal*, 50(5), 481-492.

Simicevic, J., and Sterling, R. L. (2001). “Guidelines for pipe bursting.” US Army Corps of Engineer. Vicksburg, Mississippi. TTC technical report.

Staheli, K., Price, C., and Wetter, L. (2010).” Effectiveness of Hydrofracture Prediction for HDD Design.” *Proceedings of the of 2010 North American No-Dig Conference*, Chicago, USA.

Tatarniuk, C. (2011) “127th Avenue Sanitary Sewer Installation Geotechnical Investigation” Geotechnical Report, the City of Edmonton, Edmonton, Alberta.

Timoshenko, S. P., Goodier, J. N., and Abramson, H. N. (1970). "Theory of elasticity." *Journal of Applied Mechanics*, 37, 888.

Thomson, S., and El-Nahhas, F. (1980). "Field measurements in two tunnels in Edmonton, Alberta." Canadian Geotechnical Journal, 17(1), 20-33.

Thomson, S., and Yacyshyn, R. (1977). "Slope instability in the City of Edmonton." Canadian Geotechnical Journal, 14(1), 1-16.

Vesic, A. S. (1972). "Expansion of cavities in infinite soil mass." *Journal of Soil Mechanics and Foundations Division,* 98, 265-290.

Woodland, D. C. (1990). "Borehole instability in the Western Canadian overthrust belt." *SPE Drilling Engineering*, 27-33.

Wu, B., and Hudson, J. A. (1991). "Stress-induced anisotropy in rock and its influence on wellbore stability." *Rock Mechanics as a Multidisciplinary Science*, Balkema, 941-950.

Yu, H. S. (2000). "Cavity Expansion Methods in Geomechanics." Kluwer Academic Publishers, Norwell, Massachusetts.

Yu, H. S., and Carter, J. P. (2002). "Rigorous similarity solutions for cavity expansion in cohesive friction soils." *International Journal of Geomechanics*, 2(2), 233-258.

Yu, H. S., and Houlsby, G. T. (1991). "Finite cavity expansion in dilatant soil: loading analysis." *Geotechnique*, 41(2), 173-183.

Yu, H. S., and Mitchell, J. K. (1998). "Analysis of cone resistance: review of methods." *Journal of Geotechnical and Geoenvironmental Engineering*, 124(2), 140-149.